Technische Hochschule Brandenburg
University of Applied Sciences

UNIVERSIDAD NACIONAL DE COLOMBIA

Department of Engineering

Bachelor Thesis

Characterization of Physical and Fluid Dynamical Properties of Residual Biomass in Colombia for Gasification in a Fluidized Bed Reactor

Submitted by: Patrick Hartwig

Student No.: 2013 2027

Submitted in Fulfillment of the Requirements
for the Academic Degree

Bachelor of Engineering

(B.Eng.)

First Assessor: Prof. Dr. rer. nat. Reiner Malessa

Second Assessor: Dr.-Ing. Sonia Lucía Rincón Prat

Third Assessor: Dr.-Tech. Diana Carolina Guío Pérez

Brandenburg an der Havel

July 2017

Technische Hochschule Brandenburg
University of Applied Sciences

UNIVERSIDAD NACIONAL DE COLOMBIA

Fachbereich Technik

Bachelorarbeit

Characterization of Physical and Fluid Dynamical Properties of Residual Biomass in Colombia for Gasification in a Fluidized Bed Reactor

vorgelegt von: Patrick Hartwig

Matrikel-Nr.: 2013 2027

zur

Erlangung des akademischen Grades

Bachelor of Engineering

(B.Eng.)

Erstgutachter: Prof. Dr. rer. nat. Reiner Malessa

Zweitgutachter: Dr.-Ing. Sonia Lucía Rincón Prat

Drittgutachter: Dr.-Tech. Diana Carolina Guío Pérez

Brandenburg an der Havel

Juli 2017

Eidesstattliche Erklärung

Hiermit erkläre ich, dass ich die vorliegende Bachelorarbeit selbständig verfasst, keine anderen als die angegebenen Quellen und Hilfsmittel benutzt und die aus fremden Quellen direkt oder indirekt übernommenen Gedanken als solche kenntlich gemacht habe. Die Arbeit habe ich bisher keinem anderen Prüfungsamt in gleicher oder vergleichbarer Form vorgelegt. Sie wurde bisher auch nicht veröffentlicht.

_____ _____

(Ort, Datum) (Unterschrift)

Kurzdarstellung

Kolumbien ist ein agrarwirtschaftlich geprägtes Land, indem eine Vielzahl verschiedener landwirtschaftlicher Produkte, wie zum Beispiel Zuckerrohr, Kaffee oder Reis, angebaut werden. Durch die jährlich anwachsende Menge an produzierten Gütern steigt auch die jährlich produzierte Menge an landwirtschaftlichen Abfällen, welche Anwendung als erneuerbare Energieträger finden können. Aufgrund der Tatsache, dass es in weiten Teilen Kolumbiens, gerade in den ländlichen agrarwirtschaftlich geprägten Gebieten, Probleme mit der Energieversorgung gibt, könnten die landwirtschaftlichen Abfälle genutzt werden, um vor Ort Energie zu erzeugen und die Entwicklung dieser Regionen zu fördern.

Die Forschungsgruppe „Biomass and Optimization of Thermal Systems" (BIOT) der „National University of Colombia" beschäftigt sich mit genau diesem Thema. In dem Projekt „Efficient Use of Alternative Carbonaceous Fuels in the Power Generation in Colombia by Implementation of Fluidized Bed Reactors" ist geplant, eine zirkulierende Wirbelschichtanlage zur Vergasung von Biomassepartikeln zu konstruieren. Wirbelschichtreaktoren besitzen hervorragende Wärmetransporteigenschaften, sowie gute Partikelkontaktraten, welche notwendig für einen thermochemischen Wandlungsprozess sind [1]. Das Ziel des Projektes ist es zu untersuchen, welche der vor Ort anfallenden landwirtschaftlichen Abfälle effizient genutzt werden können, um Energie durch Vergasungsprozesse unter Anwendung einer Wirbelschichtanlage zu produzieren.

Die Auslegung des Wirbelschichtreaktors und die Modellierung des thermochemischen Wandlungsprozesses hängt stark von den physischen und fluiddynamischen Eigenschaften der verwendeten Biomassepartikel ab. Die vorliegende Arbeit beschäftigt sich mit der experimentellen Bestimmung der wesentlichen Eigenschaften der Biomassepartikel. Dazu gehören: die Partikelgrößenverteilung, der mittlere Partikeldurchmesser, die Schütt- und Partikeldichte und der Feuchtigkeitsgehalt. Im Weiteren werden Fluidisierungsversuche mit Mischungen aus Quarzsand, welcher als Bettmaterial dient, und verschiedenen zugeführten Mengen an Biomassepartikeln durchgeführt. Dabei werden die charakteristischen Kenngrößen, wie die Lockerungsgeschwindigkeit, und die Art der Fluidisierung bzw. die Art der sich ausbildenden Schicht experimentell ermittelt, um Erkenntnisse darüber zu erlangen, ob die verschiedenen landwirtschaftlichen Abfälle erfolgreich fluidisiert werden können.

Preface

The present thesis summarizes and evaluates the research work that has been carried out in Bogotá at the National University of Colombia. It has been written in order to fulfill the graduation requirements of the Brandenburg University of Applied Science, which are essential to achieve the academic grade “Bachelor of Engineering”.

I would like to thank Prof. Reiner Malessa and Dr. Sonia Lucía Rincón Prat for offering me the opportunity to undertake an internship in the progressive research group “Biomass and Optimization of Thermal Systems”.

I also thank my co-advisor Dr. Diana Carolina Guío Pérez for her excellent guidance and her support. Furthermore, I would like to thank the entire research group, especially Mr. Louis Edwards Cáceres Martínez for being an excellent colleague and Spanish teacher.

Finally, I gratefully thank my dear family and friends, especially Ms. Nicole Alexandra Cortés Alfred, for their support and encouragement.

Patrick Hartwig

Table of Content

List of Figures

List of Tables

Nomenclature

A_b	Cross-sectional area of the bed	[m²]
A_r	Cross-sectional area of the reactor	[m²]
Ar	Archimedes number	[-]
d_i	Intermediate mesh size between two standard sieves	[m]
$d_{m,i}$	Mesh size of standard sieve	[m]
d_p	Mean particle diameter	[m]
d_p^*	Dimensionless particle diameter	[-]
d_r	Diameter of the reactor	[m²]
g	Gravitational acceleration	[m/s²]
K_i	Particle constant	[-]
L	Bed height	[m]
m_b	Mass of bed	[kg]
m_i	Initial mass	[kg]
$m_{l,i}$	Initial mass of liquid	[kg]
$m_{l,t}$	Terminal mass of liquid	[kg]
m_p	Mass of particles	[kg]
m_{pic}	mass of pycnometer	[kg]
m_t	Terminal mass	[kg]
MC	Moisture content	[%]
p_3	Fraction of particles retained in a standard sieve	[%]
Q_3	Cumulative fraction of particles passing a standard sieve	[%]
Re_p	Particle Reynold number	[-]
$Re_{p,mf}$	Particle Reynold number at minimum fluidization velocity	[-]
U_0	Superficial gas velocity	[m/s]
U_c	Channeling velocity	[m/s]
U_j	Jetting velocity	[m/s]
U_{mf}	Minimum fluidization velocity	[m/s]
U_s	Slugging velocity	[m/s]
U_t	Terminal velocity	[m/s]
u^*	Dimensionless gas velocity	[-]
$\dot{V}_{air}$	Air flow rate	[m³/s]

V_b	Bed volume	[m³]
V_p	Volume of particles	[m³]
V_s	Volume of solids in bed	[m³]
x_i	Fraction of particles with a specific size	[-]

Greek Letters:

Δp	Pressure difference	[mbar]
Δp_c	Pressure difference at channeling velocity	[mbar]
Δp_j	Pressure difference at jetting velocity	[mbar]
Δp_{mf}	Pressure difference at minimum fluidization velocity	[mbar]
Δp_s	Pressure difference at slugging velocity	[mbar]
ε	Void fraction	[-]
ε_0	Void fraction of fixed bed	[-]
ε_{mf}	Void fraction at minimum fluidization velocity	[-]
μ	Dynamic viscosity of gas	[Pa s]
ρ_{bulk}	Bulk density	[kg/m³]
ρ_g	Gas density	[kg/m³]
ρ_l	Density of liquid	[kg/m³]
ρ_p	Particle density	[kg/m³]
φ_s	Mean sphericity of solid particles	[-]

Abbreviations:

BIOT	Biomass and Optimization of Thermal Systems
CFB	Circulating Fluidized Bed
CH-F	Coffee Husk – Finely Ground
CH-R	Coffee Husk – As Received
F	Flotsam
J	Jetsam
OPF-C	Oil Palm Fiber – Coarsely Ground
OPF-F	Oil Palm Fiber – Finely Ground
OPR-C	Oil Palm Rachis – Coarsely Ground
OPR-F	Oil Palm Rachis – Finely Ground
OPS-C	Oil Palm Stone – Coarsely Ground

OPS-R	Oil Palm Stone – As Received
PL-R	Poultry Litter – As Received
RH-F	Rice Husk – Finely Ground
RH-R	Rice Husk – As Received
SCB-C	Sugar Cane Bagasse – Coarsely Ground
SCB-F	Sugar Cane Bagasse – Finely Ground
SCT-C	Sugar Cane Top – Coarsely Ground
SCT-F	Sugar Cane Top – Finely Ground

1 Introduction

Colombia is a country with a wide range of agricultural products such as coffee, sugar, rice and palm oil. The increasing production of agricultural goods has resulted in an increase of agricultural residues, which offer a high potential to be applied as renewable energy sources. Due to the lack of stable electricity supply in vast rural areas throughout Colombia, where most of the residual biomass is available, a power generation technology based on local biomass appears as a suitable solution to boost the development of these areas.

The research group “Biomass and Optimization of Thermal Systems” (BIOT) of the National University of Colombia has brought its attention to this issue. In the project “Efficient Use of Alternative Carbonaceous Fuels in the Power Generation in Colombia by Implementation of Fluidized Bed Reactors”, the design of a small-scale power generation plant is intended. The aim of the project is to figure out, if residual biomass in Colombia can be efficiently used for power generation through thermochemical conversion, such as pyrolysis, gasification and combustion, in a circulating fluidized bed (CFB). A CFB-reactor provides good particle contact rates and heat exchange properties [1], which are favorable for thermochemical conversion of biomass.

The design of the CFB-reactor and the modelling of the thermochemical conversion process highly depend on the physical and fluid dynamical properties of the different biomass particles. The present work elaborates on the main properties of the biomass particles intended to be tested in the CFB unit, such as particle size distribution, mean particle diameter, bulk density, particle density and moisture content. Furthermore, the fluidization properties of bed material/biomass mixtures are investigated. Silica sand was used as bed material and different biomass contents were tested. The minimum fluidization velocity and the fluidization regimes were studied.

2 Types of Biomass

The present investigation is based on a previous selection of biomasses done by the research group BIOT [2], which performed a feasibility evaluation of residual biomass in Colombia. In that study, the theoretical and technical energy potential of 37 types of residual biomass from Colombia was investigated, while taking into consideration accessibility, environmental and social aspects. The result was the selection of the eight most suitable types of residual biomass, which belong to five different agricultural industries.

For a successful thermochemical conversion of biomass particles in a small-scale CFB-reactor, it must be considered that the size of biomass particles, which can be utilized within the process, is restricted. Therefore, a pre-processing, more precisely a grinding, of several types of biomass was necessary. Due to the pre-processing, some of the selected types of biomass are available in different physical states, such as finely and/or coarsely ground and in "as-received" condition. The various physical states of biomass are characterized separately. In total, 15 different samples of the eight pre-selected types of residual biomass are investigated in the present work. A description of each biomass sample is provided below.

2.1 Residues from Coffee Production

The fruit that derives from coffee plants is known as coffee cherry and consists of seven main components that are shown in Figure 2.1. The coffee-beans (f), two of them in most cases, are situated in the center of the coffee cherry and are surrounded by two husks, known as the parchment (d) and the silverskin (e). The silverskin is a very thin and sticky layer that connects the bean to the outer firm parchment. The pulp (c) of the coffee cherry is located around the parchment, which is encased by the outer skin (b).

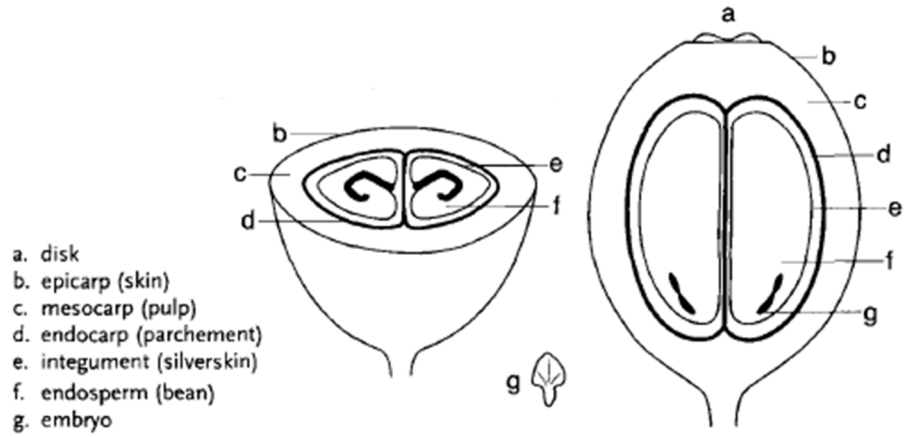

Figure 2.1: Structure of the coffee cherry [3].

After the red coffee cherry is harvested, the pulp is mechanically removed. In that state, the coffee bean is still connected to the parchment via the silverskin. During the drying process the coffee bean loses volume. This forces the firm parchment to break off. The coffee husk, which mainly consists of parchment with traces of silverskin attached to it, illustrated in Figure 2.2, can now get removed and be utilized as biomass fuel.

Figure 2.2: Sample of coffee husk.

Two samples of coffee husk were taken for the physical and fluid dynamical characterization. The first sample is coffee husk in a finely ground state, referred to as CH-F. The second sample is the coffee husk in its "as-received condition" in which it is referred to as CH-R.

2.2 Residues from Palm Oil Production

The fruits of the oil palm grow in dense clusters known as fruit bunches. A fruit bunch, shown in Figure 2.3, is composed of spikelets, fruits and the main stem. The spikelets are connected to the main stem and the fruits are connected and grow on the spikelets.

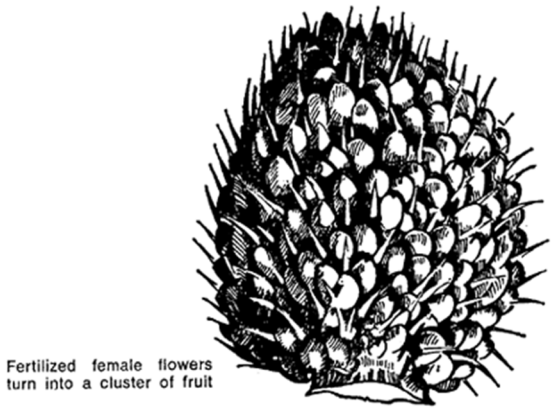

Figure 2.3: Appearance of a fruit bunch [4].

A single fruit of a fruit bunch basically consists of the fibrous pulp that contains the palm oil. The oil palm kernel that contains the palm kernel oil, is situated in the center of the fruit and is surrounded by a hard shell. The structure of a palm oil fruit is illustrated in Figure 2.4.

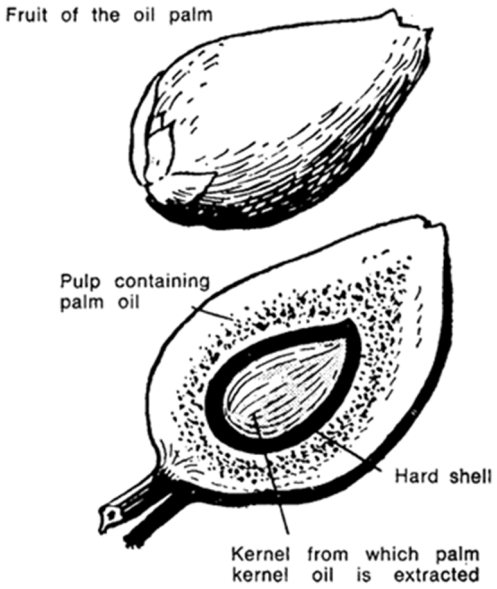

Figure 2.4: Structure of the palm oil fruit [4].

In the harvesting process the entire fresh fruit bunch is cut off the oil palm tree and is sterilized in hot pressure vessels. After this process, the fruits are softened and detached from the bunch. The empty fruit bunch is dislodged, shredded and can be utilized as biomass fuel. The pulp of the softened fruit is mechanically removed from the kernel. The palm oil from the pulp and the palm kernel oil from the kernel are extracted by different crushing processes. Afterwards, the crude oils are purified and clarified and the residues, such as the fibrous mash of the pulp and the press residues of the kernel can also be utilized as biomass fuel.

The production of palm oil generates three different types of residual biomass. The first type that is characterized is the shredded empty fruit bunch, which is referred to as oil palm rachis and shown in Figure 2.5. Samples in two different physical states are available: Coarsely ground oil palm rachis (OPR-C) and finely ground oil palm rachis (OPR-F).

Figure 2.5: Sample of oil palm rachis.

The second type of oil palm residue for the physical and fluid dynamical characterization is the dried fibrous mash, which is referred to as oil palm fiber. Samples in two different physical states are available: Coarsely ground oil palm fiber (OPF-C) and finely ground oil palm fiber (OPF-F). A sample of oil palm fiber is shown in Figure 2.6.

Figure 2.6: Sample of oil palm fiber.

The third type of residual biomass from the palm oil production process are the press residues of the oil palm kernel, which are referred to as oil palm stone and illustrated in Figure 2.7. Samples in two different physical states are available: Coarsely ground oil palm stone (OPS-C) and oil palm stone in “as-received condition” (OPS-R).

Figure 2.7: Sample of oil palm stone.

2.3 Residues from Sugar Production

Every tiller of a sugar cane plant consists of three main elements, as shown in Figure 2.8. The main stem is divided into the lower millable stem and the upper green top. Primarily, the leaves of the sugar cane plant are attached to the entire stem, while the millable stem loses its leaves during the plant growth.

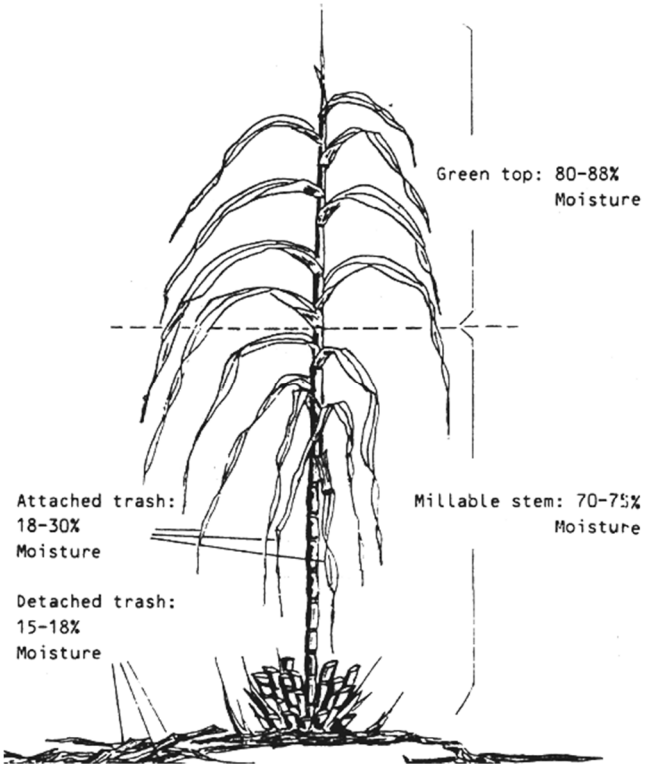

Figure 2.8: Structure of a sugar cane plant [5].

During the harvesting process, the plant's leaves are removed and stay on the cultivated area. The green top of the plant is detached from the main stem and can be utilized as biomass fuel.

The millable stem is washed and cut into shreds, which are crushed by big rollers to extract the sugar cane juice. The press residues, known as bagasse, can be utilized as biomass fuel.

The production of sugar generates two different types of residual biomass. The green top of the sugar cane plant, illustrated in Figure 2.9, is the first type which is investigated for its physical and fluid dynamical properties. Samples in two different physical states are available: Coarsely ground sugar cane top (SCT-C) and finely ground sugar cane top (SCT-F).

Figure 2.9: Sample of sugar cane top.

The second type of residual biomass is the bagasse, shown in Figure 2.10. For this investigation, there are samples in two different physical states available: Coarsely ground sugar cane bagasse (SCB-C) and finely ground sugar can bagasse (SCB-F).

Figure 2.10: Sample of sugar cane bagasse.

2.4 Residues from Rice Production

A rice plant consists of several tillers. Each tiller is composed of the main stem with blades of leaves that are attached to it. Located at the top of a tiller are the flag leaf and the panicle. The rice grains are connected to and grow on the panicle, encased by a rice husk. Figure 2.10 shows the structure of a rice plant.

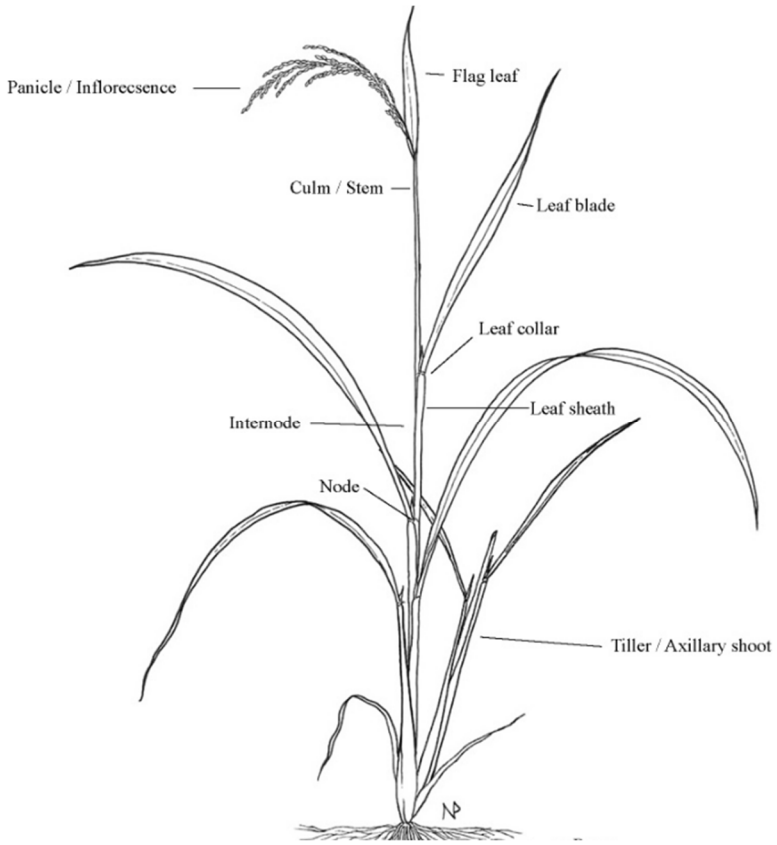

Figure 2.11: Structure of a rice plant [6].

During the harvesting process, the rice plant is cut off and the grains are separated from the stalks. A drying process is necessary before the rice grains are milled in order to remove the husk from the grain. Afterwards the rice is prepared for further processing and the rice husk can be utilized as biomass fuel.

The rice husk is available in two different physical states for its physical and fluid dynamical characterization: Finely ground rice husk (RH-F) and rice husk in “as-received condition” (RH-R). Figure 2.12 shows a sample of rice husk.

Figure 2.12: Sample of rice husk.

2.5 Residues from Poultry Farming

The residue of poultry farming, referred to as poultry litter, is a combination of two components. The first component is the rice husks, which serve as a bedding for the fowl, and the second is the poultry manure.

Due to its high moisture content, a pre-drying of poultry litter is necessary in order to be used as biomass fuel. For the investigation, there is one sample of poultry litter available in "as-received condition", illustrated in Figure 2.13.

Figure 2.13: Sample of poultry litter.

The following table summarizes the samples of residual biomass from the different agricultural sectors of Colombia that were studied in the present work. Furthermore, it gives an overview of the physical states of each sample, made available for both physical and fluid dynamical characterization. The abbreviations that are used to refer to each specific residual biomass type in their available physical states are also provided.

Table 2.1: Overview of studied biomass samples.

Agricultural sector	Residual Biomass Type	Physical State of Sample	Abbreviation
Coffee Production	Coffee Husk	finely ground	CH-F
		as-received	CH-R
Palm Oil Production	Oil Palm Fibre	coarsely ground	OPF-C
		finely ground	OPF-F
	Oil Palm Rachis	coarsely ground	OPR-C
		finely ground	OPR-F
	Oil Palm Stone	coarsely ground	OPS-C
		as-received	OPS-R
Poultry Farming	Poultry Litter	as-received	PL-R
Rice Production	Rice Husk	finely ground	RH-F
		as-received	RH-R
Sugar Production	Sugar Cane Bagasse	coarsely ground	SCB-C
		finely ground	SCB-F
	Sugar Cane Top	coarsely ground	SCT-C
		finely ground	SCT-F

3 Theoretical Background

Following, some concepts and aspects relevant for CFB-applications, will be introduced. The first part (3.1) describes the fluidization process and the parameters, which are necessary to describe the fluidization of a bed of solid particles in a CFB-reactor. The second part (3.2) provides information about the experimental determination of the particle properties, which have an influence on the fluidization.

3.1 Circulating Fluidized Beds

In order to elaborate on the essential characteristics of specific residual biomass particles for a fluidized bed application, some physical fundamentals should be described. Therefore, the principles of the fluidization process, the different fluidization regimes that may occur and the main components of a CFB-plant are presented below. Furthermore, basic calculations for the mathematical description of the fluidization process are given, which are intended to predict the fluidization regimes.

3.1.1 Fluidization Process

Fluidization is the operation in which a bulk of solid particles is turned into a fluid-like state via contact with gas or liquid [7]. In the fluidization process a liquid or gaseous medium flows upwards through a bed of solid particles. Due to this flow, each particle is influenced by three different forces. The first force is gravitational and depends on the mass of the particle. This force is constant and directed downwards. The second is the buoyancy force that is directed upwards and depends on the fluid's density. This force is constant as long, as the temperature is constant. The third force is the drag force, caused by the friction that occurs when the fluid passes through the void spaces of the bed. The drag force is directed upwards, highly depends on the shape and size of the particles and varies with the velocity of the fluid.

With an increase of the superficial gas velocity during the fluidization process, the bed of particles goes through three main states: The fixed bed, the fluidized bed and the pneumatic conveying. The superficial gas velocity is defined as the gas flow rate per cross sectional area of the bed, as if there were no particles in it [8].

When the gas velocity is low, the drag force created by the friction between particles and fluid is insufficient to lift the particles. As a result, the gravitational force dominates and the particles

rest on each other. The void space between the particles, known as porosity, is referred to as void fraction ε_0. In that state, the bed is referred to as fixed bed or packed bed. Figure 3.1 schematically illustrates a fixed bed and the pressure drop Δp developed by frictional forces.

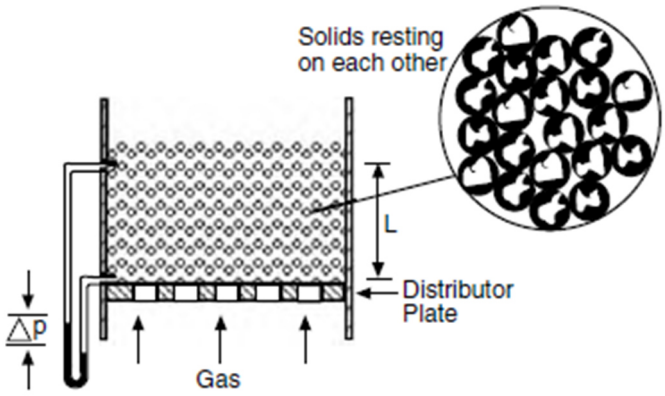

Figure 3.1: Scheme of a fixed bed [7].

The pressure drop per unit of length L of a fixed bed is proportional to the superficial gas velocity until it reaches a critical value, known as minimum fluidization velocity U_{mf} [9].

Once the minimum fluidization velocity is reached, the drag force created by the friction between the gas and the particles is sufficient to compensate the weight of the particles, which is slightly reduced due to the buoyancy force. The fluidized bed begins to expand slightly and the void fraction increases, which enables the bed particles to move. From this point on, the entire bed of fluidized particles exhibits similar behavior to that of liquids. The void fraction of a fluidized bed at the minimum fluidization velocity ε_{mf}, is slightly larger than the void fraction of a fixed bed, which facilitates the flow of the gas through the particles [8].

After reaching the minimum fluidization velocity, different fluidization regimes can occur with a further increase of the gas velocity. The occurring regimes depend on the characteristics of the particles and will be introduced below. The next critical value reached by the gas velocity is referred to as terminal velocity U_t. At this point, the drag force acting on the particles dominates and the particles begin to be entrained from the fluidized bed. This state is known as pneumatic conveying. Since more energy is expended to lift the particles, the pressure difference throughout the bed increases as long as the total mass of particles remains constant. Due to the entrainment and the wide dispersion of the particles, the void fraction sharply increases [8].

Figure 3.2 shows the typical development of the total pressure drop as a function of the superficial gas velocity and the corresponding change of the void fraction. Furthermore, it illustrates the critical velocities U_{mf} and U_t, which are the transition points of the three main states of the bed within the fluidization process. The information provided in Figure 3.2 is valid for a homogeneous bed of equal-sized and perfectly spherical particles.

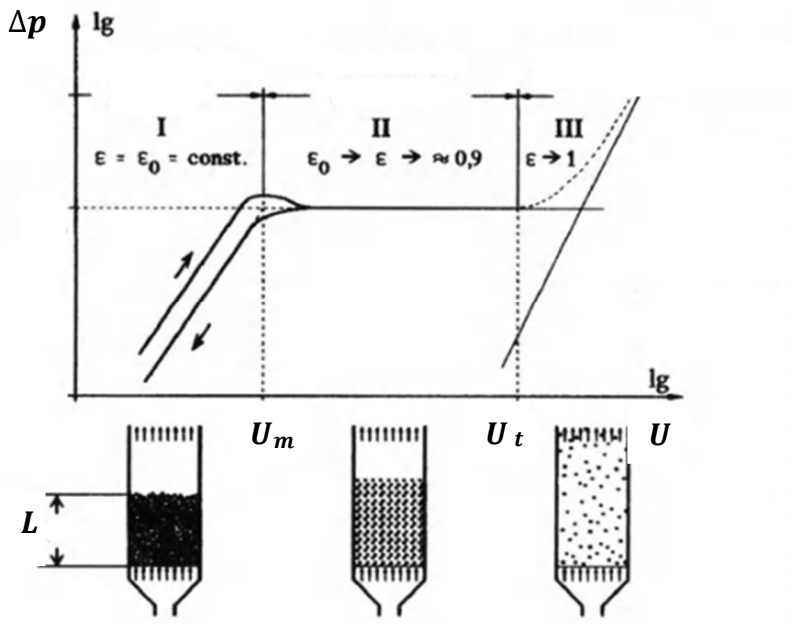

Figure 3.2: Total pressure drop for different bed states (modified) [8].

The characteristics of a real fluidized bed with nonhomogeneous particles do not depend exclusively on the gas velocity. Even though it is the most important variable, the influence of the particle properties such as the size distribution and different particle densities must also be considered.

In a real application of fluidized beds several distinctions can be observed; for instance, the transition from a fixed bed to a fluidized bed tends to be smooth, over a larger gas velocity range and not as sharp as shown in Figure 3.2. Due to the liquid-like behavior of a fluidized bed, denser particles tend to sink while lighter particles tend to move towards the top of the bed, resulting in an irregular distribution of the particles, which is referred to as “segregation” [9] and an uneven expansion of the bed.

The total pressure drop of a fluidized bed can increase due to the friction between the gas and the wall, in addition to the movement of the particle, which expend energy. If there is a wide

size distribution of the particles and/or particles with different densities, the terminal velocity of the particles varies. Thus, smaller and/or lighter particles are entrained at lower gas velocities. If that is the case for a mentionable fraction of particles, the total mass of the bed and therefore, the pressure drop through the bed can also decrease within the fluidization. Depending on the particle characteristics, the fluidized bed also develops different regimes of fluidization.

3.1.2 Regimes of Fluidization

The regimes of fluidization that arise after exceeding the minimum fluidization velocity, mainly depend on the particle characteristics, the gas properties and the gas velocity. Figure 3.3 illustrates various types of fluidization such as the bubbling and turbulent fluidization and other types of particle contacting that can appear during the fluidization process.

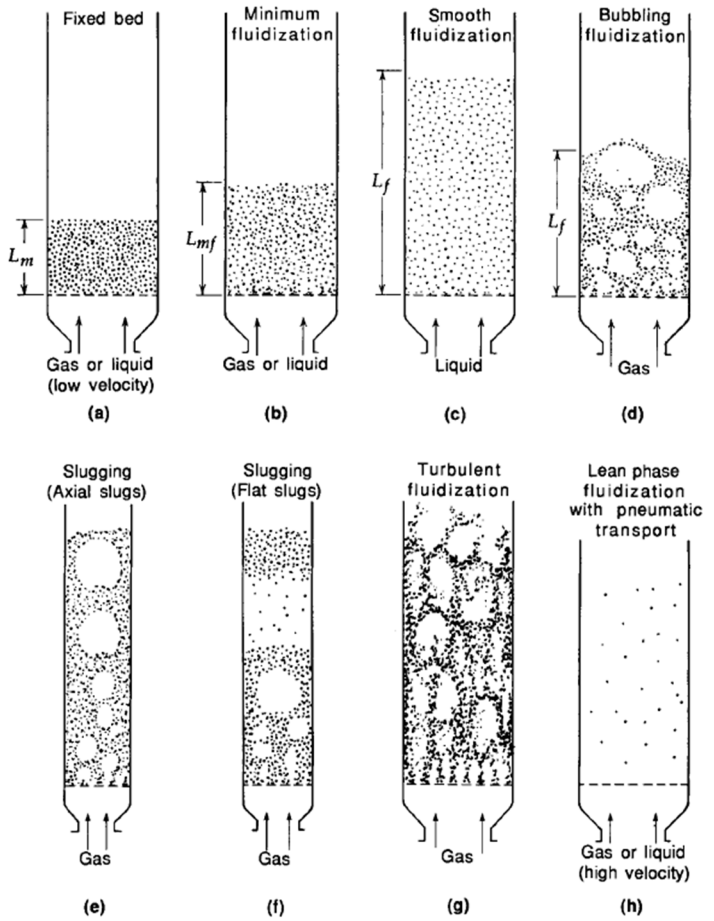

Figure 3.3: Types of fluidization and particle contacting [10].

In a bubbling regime, the agitation of the particles increases and bubbles appear at the bottom of the fluidized bed at gas velocities, which are slightly higher than the minimum fluidization

velocity. While rising through the bed, the bubbles grow and begin to coalesce. The bubbles burst at the top of the fluidized bed and particles get thrown up. A bubbling fluidization regime, as it is illustrated in Figure 3.3 (d), shows a better mixing behavior of the solid particles in the bed in contrast to a homogenous fluidization.

If a bed of particles is deep enough, the rising bubbles can grow up to sizes, which are as large, as the entire cross-sectional area of the fluidized bed. This phenomenon is referred to as "slugging" and likely occurs in small-diameter beds. Kunii et al. [10] describes two different types of slugs: "axial slugs" and "fat slugs".

As shown in Figure 3.3 (e), the "axial slugs" grow to a size that is nearly but not as large as the entire bed. When axial slugs occur, the bed expands. Large parts of the bed are lifted and particles fall back down at the sides of the bed. Another type of slugs are the so-called "fat slugs", shown in Figure 3.3 (f). Here, the rising bubbles reach the size of the entire superficial area of the bed and large parts of the bed, in some cases the entire bed, can be lifted. The lifted portion of the bed is unstable and can easily fall apart [10, 11].

Due to the fact, that the parts of the bed, which get lifted by slugs, do not show a steady behavior, an even mixing of the bed particles and an even heat exchange are not provided. Therefore, slugging is considered to be a malfunction of the bed that is nonconstructive for practical applications of fluidized beds.

In the turbulent fluidization regime, which occurs when the gas velocity reaches the terminal velocity of the particles, the rising gas forms bubbles, which grow very fast and push the solid particles upward. The entire bed is highly expanded and nonuniform. As illustrated in Figure 3.3 (g) the entire turbulent fluidized bed is a diffuse composition of solid particle clusters and spaces with a high voidage. Referring to the turbulent motion of the entire bed, the gas-solid mixing properties and the heat exchange of a turbulent fluidization regime are excellent [10, 11].

When a fixed bed consists of fine powder-like particles, the void fraction of the bed is very low and the cohesive forces between the particles have a higher influence on the behavior of the bed. Therefore, the fine particles tend to agglomerate. At low superficial gas velocities, the drag force caused by the friction between the rising gas and the particles, does not offset the cohesive

forces between the particles of the agglomerates and a suspension of the particles is not given. To achieve a gas flow through the bed, channels arise around the agglomerates of the bed [8].

Channeling can begin to appear at gas velocities, which are lower than the minimum fluidization velocity, while most of the gas passes the bed through the channels and only small fractions of the bed are fluidized. Figure 3.4 illustrates a channeling regime of a bed of particles. Due to the fact that the upstreaming gas can pass through the channels, the gas flow resistance caused by the bed of particles is lower, which results in a lower pressure drop through the bed. Since the gas velocity within the channels is a multiple of the superficial gas velocity, the entrainment of a small fraction of particles can occur. When a considerable amount of particles are entrained from the bed through the channels, the state of the bed is referred to as “jetting”. Channeling and jetting is also considered to be a malfunction of a fluidized bed.

Figure 3.4: Channeling of rising gas [8].

Another phenomenon that can occur during the fluidization process is the earlier mentioned segregation of the bed, which denotes the separation of a bed that consists of particles with different sizes and/or densities, for instance a bed that mainly consists of silica sand as a bed material with a small amount of an added component, such as biomass particles. Kunii et al. [12] describes two different types of segregation: “Jetsam” (J) and “Flotsam” (F). Jetsam describes the separated bed of particles when the added component sinks to the ground and jetsam describes the opposite, the state when the added component rises and “floats” on the bed.

3.1.3 Components of a CFB-Plant

As shown in Figure 3.5, a basic CFB-plant consists of four main components; the reactor (riser), the cyclone, the standpipe and the loop seal. Inside the plant, a specific amount of bed material circulates in order to retain the heat within the plant in addition to improving the contact rate of the added reactants with the bed material. Furthermore, a constant amount of solid bed material enables a uniform circulation that is necessary for a steady operation of the plant. For gasification processes of biomass, silica sand is often used as bed material due to its chemical stability [13].

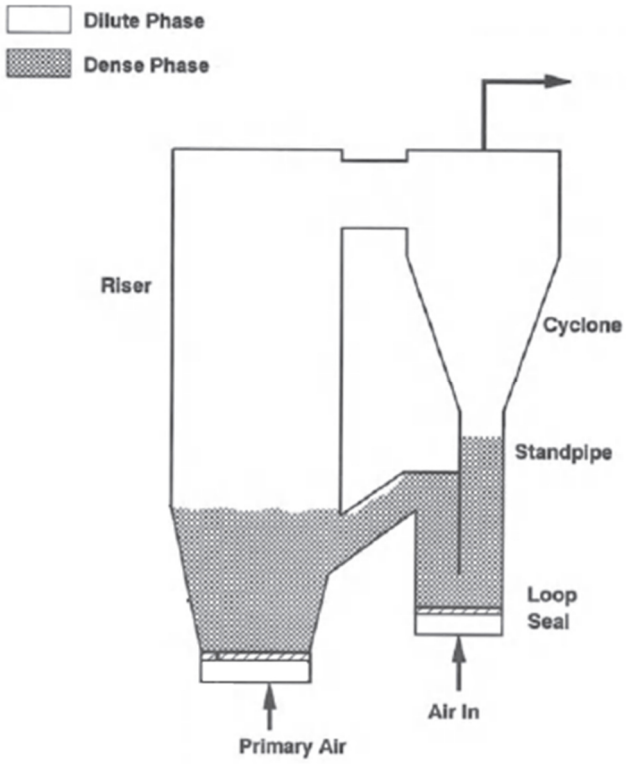

Figure 3.5: Components of a CFB-plant (modified) [14].

The most important component of a CFB-plant for a gasification process of biomass is the reactor that is filled with a fixed amount of bed material, which usually has a mean particle diameter between 100 and 300 µm [15]. In the lower area of the reactor, biomass is constantly fed through a screw feeder. The amount of the biomass feed in the reactor is in a range between 1 - 3 % of the total mass of the bed material. At the bottom of the reactor, a gas distributor, which can be a simple perforated plate, pipe spargers or more complicated nozzles or caps [16], is located that enables a uniform gas flow throughout the entire cross-sectional area of the reactor. In a gasification process, air, oxygen or steam (or mixtures) can be utilized as a fluidization and gasification medium.

During fluidization, bed material and not entirely gasified biomass particles are entrained from the reactor into the cyclone. The incoming solid particles are directed into a rotating motion along the sidewalls of the cyclone. The gravitational and the centrifugal forces separate the incoming gas from the solid particles. The solids are discharged at the bottom of the cyclone into the standpipe and the gas escapes through the upper outlet. Figure 3.6 illustrates the solid particle flow inside a CFB-plant [17].

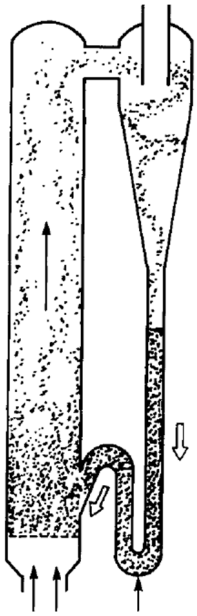

Figure 3.6: Circulation of solid particles in a CFB-plant (modified) [10].

The standpipe is usually a vertical pipe that connects the cyclone with the loop-seal. In a standpipe, solid particles can be transferred by gravity from an area with lower pressure (outlet of cyclone) into an area with higher pressure (bottom of the riser). When the particles fall from the cyclone into the standpipe and move downwards against the upwards directed gas flow, the gas-solid relative velocity is higher, the frictional pressure drop increases and the standpipe can provide the required sealing pressure drop. Hence, the standpipe has the function of a seal and ensures that the upstream of gas in the reactor does not flow into the loop seal, which would disturb the circulation of the solids and result in the inability to operate properly [18].

Loop seals are available in various forms. A typical loop seal is a syphon-shaped pipe that is filled with bed material. At the bottom of a loop seal is a gas inlet that enables the fluidization of the particles inside. The fluidized particles show similar behavior to that of liquids and the loop seal operates according to the principle of communicating vessels, which enables an even return flow of bed material into the reactor [19].

3.1.4 Mathematical Description of the Fluidization Process

The frictional pressure drop per length of a fixed bed of equal sized particles can be elaborated with the Ergun-equation [20]. An approximation of the pressure drop per length of a fixed bed with unequal sized particles can be made by using the mean particle diameter d_p, as shown in Equation 3.1, where μ and ρ_g are the dynamical viscosity and the density of the gas, while φ_s stands for the sphericity of the particles.

$$\frac{\Delta p}{L} = 150 \frac{(1-\varepsilon_0)^2}{\varepsilon_0^3} \frac{\mu\, U_0}{(\varphi_s\, d_p)^2} + 1.75 \frac{1-\varepsilon_0}{\varepsilon_0^3} \frac{\rho_g\, U_0^2}{\varphi_s\, d_p} \qquad \text{(Equation 3.1)}$$

In a fluidized bed at minimum fluidization velocity, the upward directed frictional force at the particles is in equilibrium with the downward directed weight force that is reduced by the buoyancy. The frictional forces can be described as the pressure drop multiplied with the cross-sectional area A_b of the bed. The weight force of the particles reduced by their buoyancy, is described by the product of the difference of the particle density ρ_p and the gas density ρ_g, the volume of solid particles in the bed V_s and the gravitational acceleration g. Equation 3.2 illustrates the equilibrium of forces.

$$\Delta p\, A_b = (\rho_p - \rho_g)\, V_s\, g \qquad \text{(Equation 3.2)}$$

The volume of the solid particles in the bed is correlated to the volume of the entire bed V_b by the void fraction. The correlation at minimum fluidization is described by Equation 3.3.

$$V_s = (1-\varepsilon_{mf})\, V_b = (1-\varepsilon_{mf})\, A_b\, L \qquad \text{(Equation 3.3)}$$

By combining and rearranging Equation 3.2 and 3.3, the so-called minimum fluidization condition is given, illustrated by Equation 3.4 [20].

$$\frac{\Delta p}{L} = (1-\varepsilon_{mf})\,(\rho_p - \rho_g)\, g \qquad \text{(Equation 3.4)}$$

The minimum fluidizing condition can be utilized for an experimental determination of the void fraction of particles at minimum fluidization velocity.

By combining Equation 3.1 and 3.4, an expression of the superficial gas velocity at minimum fluidization conditions is given, while the void fraction and the superficial gas velocity of

Equation 3.1 must be replaced by the specific values at minimum fluidization. The result is Equation 3.5.

$$(1-\varepsilon_{mf})\,(\rho_p-\rho_g)\,g = 150\frac{(1-\varepsilon_{mf})^2}{\varepsilon_{mf}^3}\frac{\mu\,U_{mf}}{(\varphi_s\,d_p)^2} + 1.75\frac{1-\varepsilon_{mf}}{\varepsilon_{mf}^3}\frac{\rho_g\,U_{mf}^2}{\varphi_s\,d_p} \qquad \text{(Equation 3.5)}$$

By adding the following term to both sides of the Equation 3.5, the equation can be arranged as shown in Equation 3.6.

$$\frac{d_p^3\,\rho_g}{\mu^2}$$

$$\frac{d_p^3\,\rho_g\,(\rho_p-\rho_g)\,g}{\mu^2} = \frac{150\,(1-\varepsilon_{mf})}{\varepsilon_{mf}^3\,\varphi_s^2}\left(\frac{d_p\,U_{mf}\,\rho_g}{\mu}\right) + \frac{1.75}{\varepsilon_{mf}^3\,\varphi_s}\left(\frac{d_p\,U_{mf}\,\rho_g}{\mu}\right)^2 \qquad \text{(Equation 3.6)}$$

This arrangement enables a replacement of several terms with dimensionless numbers, such as the Archimedes and the Reynold number. The replacement shown in Equation 3.7 enables an up- or downscaling of the reactor or accordingly the entire CFB-plant [20].

$$Ar = \frac{150\,(1-\varepsilon_{mf})}{\varepsilon_{mf}^3\,\varphi_s^2}\,Re_{p,mf} + \frac{1.75}{\varepsilon_{mf}^3\,\varphi_s}\,Re_{p,mf}^2 \qquad \text{(Equation 3.7)}$$

The Archimedes' and the Reynold's numbers contain parameters, which describe particle characteristics and are decisive for the operation of a CFB-reactor in a gasification process, such as the dynamical viscosity and the density of the utilized gasification medium. The terms, which contain the sphericity of the particles and the void fraction of the bed can be summarized to particle constants K_i, shown in Equation 3.8.

$$Ar = K_2\,Re_{p,mf} + K_1\,Re_{p,mf}^2 \qquad \text{(Equation 3.8)}$$

For a prediction of the critical gas velocities and the fluidization regime of specific particles at a specific gas velocity, two quantities are introduced; the dimensionless particle diameter d_p^*, described by Equation 3.9 and the dimensionless gas velocity u^*, described by Equation 3.10 [20].

$$d_p^* = Ar^{1/3} \qquad \text{(Equation 3.9)}$$

$$u^* = \frac{Re_p}{Ar^{1/3}} \qquad \text{(Equation 3.10)}$$

When the dimensionless particle diameter and gas velocity are estimated, the critical velocities and the fluidization regime can be approximated with a flow regime diagram, as illustrated in Figure 3.7, where the letters A, B and D refer to the "Geldart classification of particles", which is introduced in section 3.2.3.

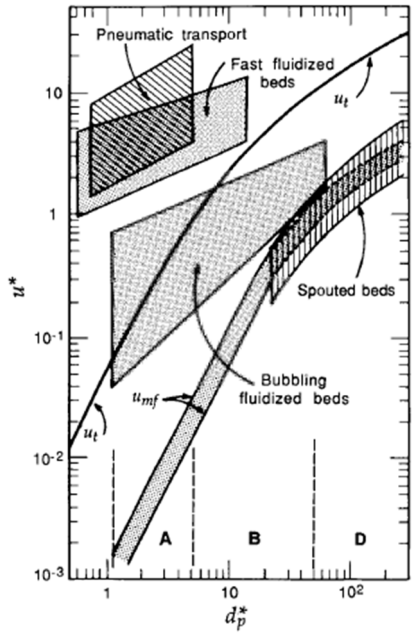

Figure 3.7: Flow regime diagram [21].

3.2 Particle Characteristics

Since the particle characteristics highly influence the fluidization process, an experimental determination of the characteristics is necessary in order to predict the behavior of the biomass particles for a successful design of a CFB-plant. The particle properties of interest are the mean particle diameter, the bulk and particle density and the corresponding moisture content. Moreover, the "Geldart classification of particles", which is based on the particle characteristics, is explained in detail.

The experiments used to determine the particle properties are explained in section 4. In the following, the above mentioned particle characteristics and the basic calculations to evaluate the results of the experiments are provided.

3.2.1 Granulometry

Granulometry is the particle size analysis of granular solid material. The aims of this analysis are, to create a plot of the particle size distribution and to calculate the mean particle diameter.

Several different methods, such as photo analysis or sedimentation techniques, are applicable to determine the distribution of different sized particles. For granular air-dry biomass particles, the most commonly used method is the sieve analysis. This method requires the utilization of stacks of sieves with various mesh sizes. A stack usually consists of six single sieves, a bottom plate and a top cover. The upper sieve, in which the granular material is placed, has the largest aperture size, while the mesh of every adjacent sieve is smaller than the one on top of it. The sieving procedure can be done by hand or by a mechanical sieve shaker [22].

For the graphic illustration of the particle size distribution, the following quantities are introduced; Q_3, the cumulative mass fraction of particles, which pass a standard sieve and p_3, the absolute mass fraction of particles, which are retained in a single standard sieve [23].

As shown in part 3.1.4, the mean particle diameter is a decisive quantity within the process of fluidization. When the particle size distribution is known, the Equation 3.11 can be utilized to calculate the mean particle diameter of mixed-sized particles [24], where d_i is the intermediate mesh size between two adjacent sieves and x_i the mass fraction of particles, which remain between two adjacent sieves.

$$d_p = \frac{1}{\sum\left(\frac{x_i}{d_i}\right)} \qquad \text{(Equation 3.11)}$$

The intermediate mesh size of two adjacent standard sieves is calculated with the Equation 3.12, where $d_{m,i}$ is the mesh size of each specific standard sieve.

$$d_i = \frac{\left(d_{m,i} + d_{m,i+1}\right)}{2} \qquad \text{(Equation 3.12)}$$

3.2.2 Bulk and Particle Density

The bulk density ρ_{bulk} is the mass of a bed of solid granular particles m_b per unit of bed volume, which includes the void spaces between the particles. The Equation 3.13 can be used to calculate the bulk density [25].

$$\rho_{bulk} = \frac{m_b}{V_b} \qquad \text{(Equation 3.13)}$$

The particle density ρ_p is the mass of a bed of solid particles per unit of particle volume V_p. Since the void spaces are not included in the volume, the particle density is higher than the bulk

density. As shown in Equation 3.14 the particle density is correlated to the bulk density by the void fraction [25].

$$\rho_{bulk} = \rho_p \, (1 - \varepsilon) \qquad \text{(Equation 3.14)}$$

For mixed-sized biomass particles, the determination of the exact volume of the particles is not as simple as the determination of the bed volume. Due to the wide range of sizes and irregular shapes, the possibility of measuring specific lengths for volume calculations is not given. Therefore, a pycnometer for solid particles can be utilized to determine the density of biomass particles.

A pycnometer is a small flask-like bottle with a volume capacity that is exactly known. The glass stopper that closes the pycnometer is ground to ensure that it always stays in the same position. An axial capillary bore is located in the center of the glass hopper [26]. When the pycnometer is filled by a liquid, the surplus liquid is discharged through the capillary bore while placing the glass stopper on the pycnometer. Since the inner volume of the pycnometer is known and the weight of the empty and filled pycnometer can be measured very accurately, the density of the liquid inside can be calculated. Figure 3.8 illustrates the composition of a pycnometer.

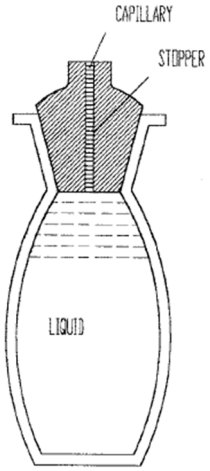

Figure 3.8: Composition of a pycnometer [26].

Since the density of the test liquid is known, the pycnometer can be utilized to determine the density of solid particles as well. When the pycnometer is completely full with the test liquid and solid particles are added, the volume of test liquid that is identical to the total volume of solid particles is discharged through the capillary bore, while closing the stopper. The mass difference of the pycnometer filled only with the test liquid and the pycnometer filled with the

test liquid and solid particles can be measured. For computation of the particle density, the following equations can be used.

The Equation 3.15 summarizes the initial mass m_i that includes the mass of the sample of solid particles m_p, the mass of the empty pycnometer m_{pic} and the initial mass of the test liquid $m_{l,i}$.

$$m_i = m_p + m_{pic} + m_{l,i} \quad \text{(Equation 3.15)}$$

To calculate the terminal mass m_t the Equation 3.16 can be utilized. The equation includes the mass of the empty pycnometer and the mass of the added solid particles under consideration of the buoyancy that is described by the product of the total volume of the solid particles V_p and the density of the test liquid ρ_l. The terminal mass of the test liquid $m_{l,t}$, which is reduced by the identical total volume of the particles times the density of the test liquid, is also included.

$$m_t = m_p - V_p\,\rho_l + m_{pic} + m_{l,t} \quad \text{(Equation 3.16)}$$

Since the mass of a sample of solid particles can be easily measured before it is added to the pycnometer and the initial and terminal mass are known, the Equation 3.17 that is adapted from the equation found in the "Encyclopedia of soil science" [27], can be used to determine the particle density.

$$\rho_p = \frac{m_p}{V_p} = \frac{m_p}{m_i - m_t}\rho_l \quad \text{(Equation 3.17)}$$

3.2.3 Geldart Classification of Particles

The above mentioned "Geldart classification of particles" indicates the particle behavior in a fluidized bed. Therefore, solid particles are divided into four groups. From the smallest to the largest particle size, the groups are referred to as C, A, B and D and depend on the mean particle diameter and the particle density. An overview of the four different Geldart groups is given by Figure 3.9, where the difference between the particle density and the density of the fluidization gas is plotted over the range of the mean particle diameter. The limits of size ranges of each group of particles are not strict but indicative, while the range of the particles density of each group varies with the size of the particles [28, 29].

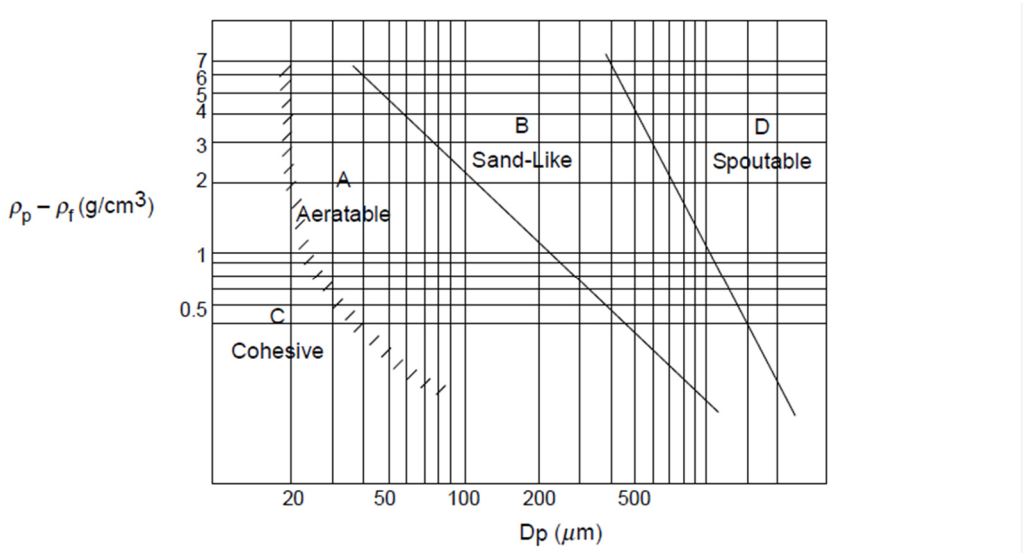

Figure 3.9: Overview of the Geldart groups [29].

Group C involves particles which are very fine and powder-like. The mean particle diameter is usually smaller than 30 µm. Due to the high cohesive forces between the particles and the agglomeration, an even fluidization is extremely difficult to reach. The fluidization regime of "Geldart C particles" depends on the diameter of the bed and respectively on the diameter of the reactor. In small-diameter reactors, the bed of "Geldart C particles" tends to create axial slugs, while channeling tends to occur within reactors of larger diameters [28, 29].

Group A includes small-sized particles with a mean particle diameter, that is normally within a range of 30 µm to 100 µm and/or a particle density that lower than 1.4 g/cm³. The solid particles of the bed fluidize easily and show a so-called "areatable" behavior. When the minimum fluidization velocity is reached, a bed of "Geldart A particles" notably starts to expand with a further increase of the gas velocity before bubbling occurs. Furthermore, there is a maximum bubble size that is typically less than 10 cm and independent of the diameter of the bed. Due to that fact, axial slugging can occur in small-diameter reactors [28, 29].

Group B involves sand-like particles with a mean diameter between 40 and 500 µm and a particle density in a range of 1.4 to 4 g/cm³. "Geldart B particles" fluidize well, while the bed of solids immediately begins to create a bubbling fluidization regime when the minimum fluidization velocity is reached. The bubble size is almost independent of the mean particle diameter, while increasing approximately linear to the distance from the bottom of the bed [28, 29].

Group D involves large and/or dense particles with a mean particle diameter that is usually larger than 500 µm. Deep beds of "Geldart D particles" require high superficial gas velocities to fluidizes the particles. The bubbles, which occur after the gas reaches the minimum fluidization velocity, merge rapidly and grow to large sizes while rising more slowly than the rest of the rising gas. While reaching the top of the bed, the large bubbles burst and spout solid material upward. It is also observed that large bubbles are able to cause channeling of the gas through the bed. In small-diameter beds, axial slugs can occur [28, 29].

3.2.4 Moisture Content

The moisture content of solid material is the perceptual weight fraction of water included in the material. The oven-drying process is a simple method used to determine the moisture content of a solid material. The mass of a sample of the material of interest can be measured before and after oven-drying. As shown in Equation 3.18, which is adapted from the equation given in the German Norm "DIN 51718:2002:06" [30], the moisture content MC is described by the mass difference of the initial and terminal mass in relation to the initial mass.

$$MC = \frac{m_i - m_t}{m_i} \, 100\ \% \qquad \text{(Equation 3.18)}$$

Furthermore, the duration of the oven-drying process is highly influenced by the drying temperature. The appropriate temperature depends on the content of volatile matter of the specific material and their volatilization temperature. In addition, the duration of the drying process depends on the form and size of the particles, more specifically on the ratio of the superficial area to the volume; the larger the ratio, the longer the drying process takes. During the oven-drying, the mass of the sample can be measured on a regular basis, for instance every couple of hours until the mass does not significantly change. At this point, the constancy of mass is reached and the drying process is finished.

4 Experimental Determination of the Properties of the Biomass Particles

In the following, the experiments used to determine the physical and fluid dynamical properties of each residual biomass type are described. The utilized equipment is introduced and the experimental procedures are explained in detail.

Since the fluid dynamical behavior (minimum fluidization velocity and occurring fluidization regime), depends on the physical properties of the biomass particles, the physical properties including the particle size distribution, the mean particle diameter, the bulk and particle density and the moisture content are investigated at first. Next, the classification according to Geldart is carried out and finally, the fluidization experiments are performed.

In total, 15 samples of eight residual biomass types (as presented in section 2) from five agricultural sectors in Colombia are investigated. The experimental determination of some properties including the particle size distribution, the minimum fluidization velocity and the observed fluidization regimes, are explained based on selected samples. An extended overview of all results can be found in the appendix.

4.1 Determination of Particle Size Distribution

Since the previously dried and ground biomass samples are stored and transported in bags, the different sized particles are not evenly distributed inside the bags; also, biomasses of low density are stored in different bags. Hence, extraction of representative samples cannot be assured. To ensure that the particle size analysis is representative, the entire amount available for each sample was sieved. The available mass of each biomass sample varies between approximately 100 g, for instance of OPR-F, and 7 kg of PL-R.

According to Basu [24], the sieve analysis is recommended to measure particle sizes of solid granular particles. For the sieving procedure, different sets of standardized test sieves of the "U.S. Standard Sieve Series" are used. A stack of six standardized sieves and the used "Ro-Tap Testing Sieve Shaker" are illustrated in Figure 4.1.

Figure 4.1: Testing sieve shaker.

Due to the wide size distribution of the investigated biomass particles and in order to generate accurate measurements, a large number of test sieves are used. Sieves with aperture sizes in the range of 45 µm and 9500 µm were used. An overview of the used sieves of the "U.S. Standard Sieve Series" and the corresponding mesh size in micrometers are provided in Table 4.1.

Table 4.1: Mesh size of utilized U.S. standards sieves.

Mesh Size of U.S. Standard Sieves					
Sieve Number	Mesh Size [µm]	Sieve Number	Mesh Size [µm]	Sieve Number	Mesh Size [µm]
3/8	9500	16	1180	60	250
1/4	6300	18	1000	80	180
4	4760	20	850	100	150
6	3350	25	710	120	125
8	2360	30	600	140	106
10	2000	35	500	170	90
12	1700	40	425	270	53
14	1400	50	300	325	45

For the sieving procedure, every sample of biomass is divided into smaller portions of 100 to 200 g and sieved separately. The duration of the sieving process of each portion depends on the particles sizes, which can be roughly assessed before the sieving. A bulk of particles including only a small amount (of about 10 %) of fine powder-like particles is considered to be an "easy-to-screen" material. For these materials, sieving times of 5 to 10 min for sieves with a mesh size above 160 µm and sieving times of 10 to 30 min for sieves with a mesh size below 160 µm are required. In turn, for a "difficult-to-screen" bulk of particles with a content of powder-like particles notably higher than 10 %, sieving times of up to 1 h are required [22].

A practical approach to find an appropriate sieving time is to inspect the sieves on a regular basis in order to ensure that the sieves are not clogged. Also, after 10 to 15 min of sieving, the sieve can be shaken by hand over a plain and clean surface to make sure that no more finer particles are passing the sieve.

After the sieving procedure, the particles retained in each sieve, are packaged separately and weighted to calculate the mass fraction in relation to the entire mass of the sample. To illustrate the particle size distribution, a diagram as it is exemplarily shown in Figure 4.2 is used.

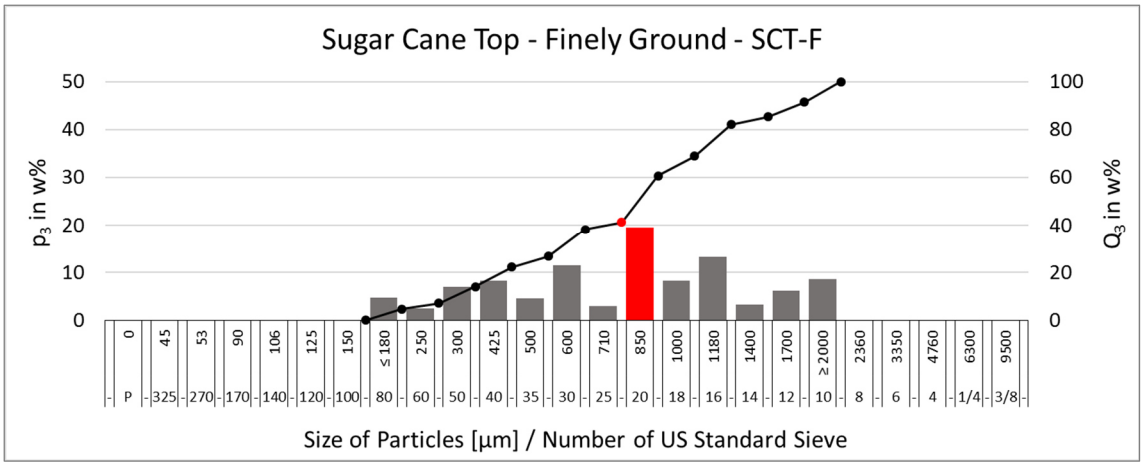

Figure 4.2: Exemplary illustration of the particle size distribution.

The bars in the diagram show the mass fraction p_3 of the particles retained in each single standard sieve. The red bar in Figure 4.2 for instance, states that 20 % of the particles have passed the sieve number 18 (100 µm aperture size) but are retained in the sieve number 20 (850 µm aperture size). Accordingly, 20 % of the particles have a size between 850 and 1000 µm.

The points in the diagram illustrate the cumulative mass fraction Q_3 of particles, which pass each standard sieve. The red point for instance states that 40 % of the particles pass the sieve number 20 and therefore, 40 % of the particles are smaller than 850 µm.

The abscissa of the diagram includes all sieves utilized for the screening of the different biomass samples. Even though, not every single sieve was utilized for every sample, the diagram shows the entire range of sieves to achieve an identical layout of the particle size distribution for all samples. This form of presentation is chosen to facilitate the comparison of the particle size distribution of the different biomass samples.

The particles size distribution of SCT-F in Figure 4.2 is used to explain the form of the graphical illustration. The diagrams of the particles size distribution of all the 15 investigated biomass samples are provided in the appendix (A1).

4.2 Determination of Mean Particle Diameter

Since the masses of particles retained in each sieve, are measured, the mean particle diameter can be calculated using Equations 3.11 and 3.12. The measured values necessary for an exemplary calculation of the mean particle diameter of OPR-F are shown in Table 4.2.

Table 4.2: Measured values and exemplary calculation of the mean particle diameter.

Sieve			Oil Palm Rachis - Finely Ground - OPR-F		
Sieve No.	Mesh Size $d_{m,i}$	Intermediate Mesh Size d_i	Mass Retained in Sieve	Mass Fraction Retained in Sieve x_i	x_i / d_i
#	in µm	in µm	in g	-	in µm
Plate	0	45	23,86	0,036	0,000797
170	90	98	6,06	0,009	0,000093
140	106	115,5	8,85	0,013	0,000115
120	125	137,5	9,14	0,014	0,000100
100	150	165	26,50	0,040	0,000241
80	180	215	30,94	0,046	0,000216
60	250	275	16,31	0,025	0,000089
50	300	362,5	93,10	0,140	0,000386
40	425	462,5	62,77	0,094	0,000204
35	500	550	28,34	0,043	0,000077
30	600	655	70,12	0,105	0,000161
25	710	780	29,10	0,044	0,000056
20	850	925	51,54	0,077	0,000084
18	1000	1090	33,54	0,050	0,000046
16	1180	1290	58,48	0,088	0,000068
14	1400	1550	7,31	0,011	0,000007
12	1700	1850	46,66	0,070	0,000038
10	2000	2180	62,95	0,095	0,000043
8	2360	-	0,00	-	-
		Total Mass:	665,55	d_p in µm:	354

Table 4.2 is divided into two parts. The left side provides information about the utilized standard test sieves, while the right side shows the computation of the mean particle diameter. In the first two columns, the utilized sieves and the corresponding mesh sizes $d_{m,i}$ are listed. The third column shows the intermediate mesh size d_i that is calculated using the Equation 3.12. The mass of particles retained in each sieve is measured after the sieving process (forth column) and the mass fraction x_i is calculated and presented in the fifth column. In the last column, the relation of the retained mass fraction to the intermediate mesh size is given. At the bottom of the table, the mean particle diameter d_p is calculated using Equation 3.11.

During computation, the fact that the intermediate mesh size of the bottom plate depends upon the mesh size of the smallest utilized sieve must be considered. For example in Table 4.2, the intermediate mesh size of the bottom plate is 45 µm, which is the arithmetic value of the smallest utilized sieve with a mesh size of 90 µm and the mesh size of the bottom plate, which is zero. Hence, there is low certainty that the particles in the bottom plate have an intermediate size of 45 µm, which results in an error in calculation. To minimize this error, the sieving of the particles retained in the bottom plate is repeated with smaller sieves until the mass of the particles that are retained in the bottom plate is less than 10 % of the total mass of the sample. The same error can occur while calculating the intermediate particle size of the largest utilized sieve. The minimization of this error is carried out analogously.

Figure 4.3 illustrates the calculated mean particle diameters of the investigated biomass samples.

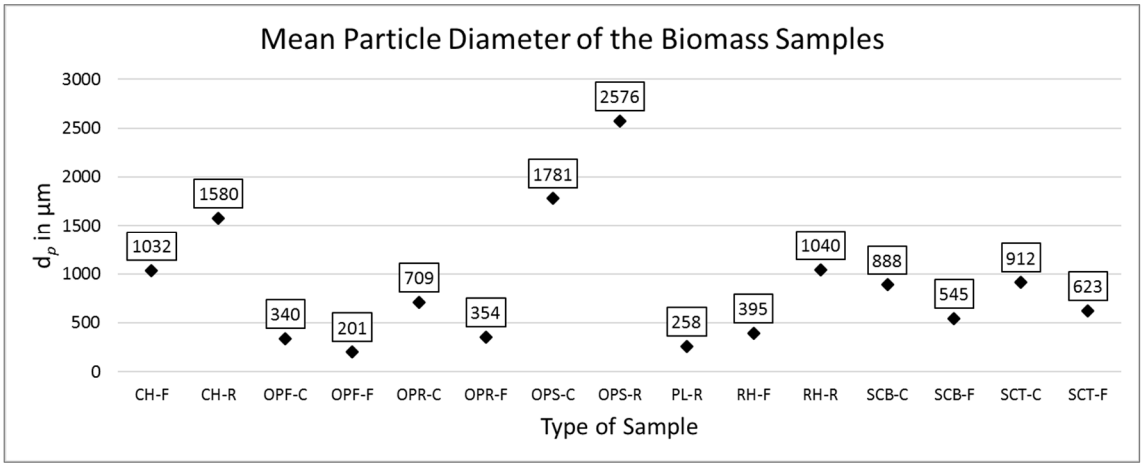

Figure 4.3: Mean particle diameter of the biomass samples.

4.3 Determination of Moisture Content

To determine the moisture content, the oven-drying method is used. The principle of this method is to dry the sample until the mass remains constant in order to determine the total mass difference for the sample before and after the drying. The mass difference is used to calculate the moisture content.

For the practical application of the oven-drying method, from all 15 different biomass samples, three drying-samples of 5 g were taken. Special attention was given to the fact that the drying-samples should have the same particle size distribution as the original samples, therefore, sieving fractions were used to prepare the drying-samples accurately. The drying-samples are placed in small aluminun bowls as shown in Figure 4.4.

Figure 4.4: Drying-sample of OPS-C.

The norm “ASTM-D 4442-07” [31] recommends a drying temperature of 103±2 °C for wood and wood-based material. The norm “DIN 51718” [30] recommends a drying temperature of 106±5 °C for solid fuels such as lignite, charcoal and briquets. Based on the provided information, the drying-process of the biomass samples was performed in a forced-convection oven with a constant temperature of 105 °C.

To determine an appropriate drying time, the weight loss of the samples is measured after 18, 24 and 28 h of drying. The difference in weight between 18 and 24 h of drying is notable while the mass does not change significantly between 24 and 28 h of drying. Consequently, a drying time of 24 h is suitable to determine the moisture content of the samples.

For computation of the moisture content MC, the Equation 3.18 is used, where the initial mass m_i is the mass of the sample before the drying-process and the terminal mass m_t is the mass of the sample after the drying-process. The results are illustrated in Figure 4.5.

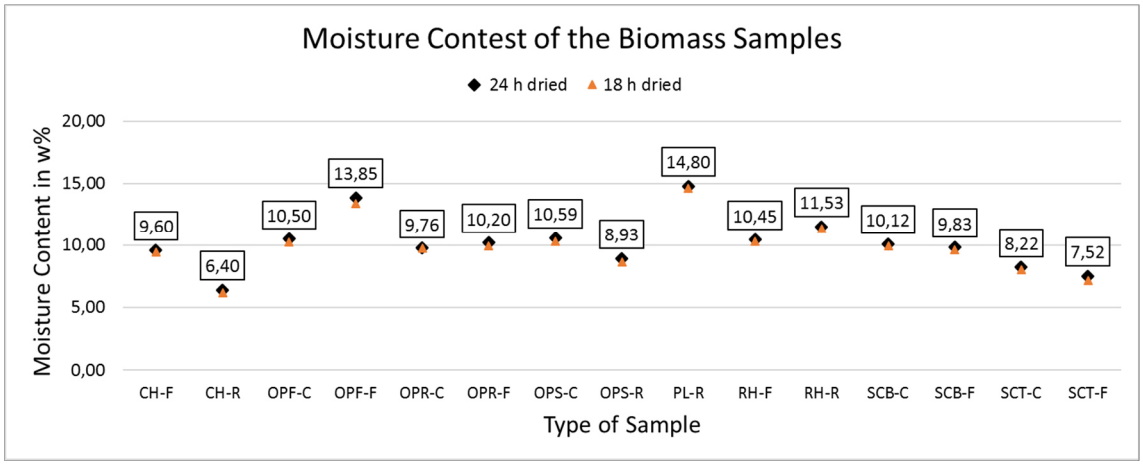

Figure 4.5: Moisture content of the biomass samples.

4.4 Determination of Bulk Density

The bulk density is the mass of a bed of granular material per unit of bed volume, which includes the voidage between the particles. The bulk density can be determined by measuring the weight of a specific volume of particles, which is filled in a graduated cylinder. For a repeatable measurement, the norm “ASTM-D 2854-09” [32] recommends a smooth filling of a graduated cylinder by a free fall of particles at flow rate of 1 ml/s, which ensures that the bed of particles is not compressed. Also, the diameter of the graduated cylinder must be at least ten times as large as the mean particle diameter of the sample and the minimum test volume must be 100 ml. For a practical determination of the bulk density, the norm “ASTM-D 2854-09” recommends an experimental assembly as it is shown in Figure 4.6.

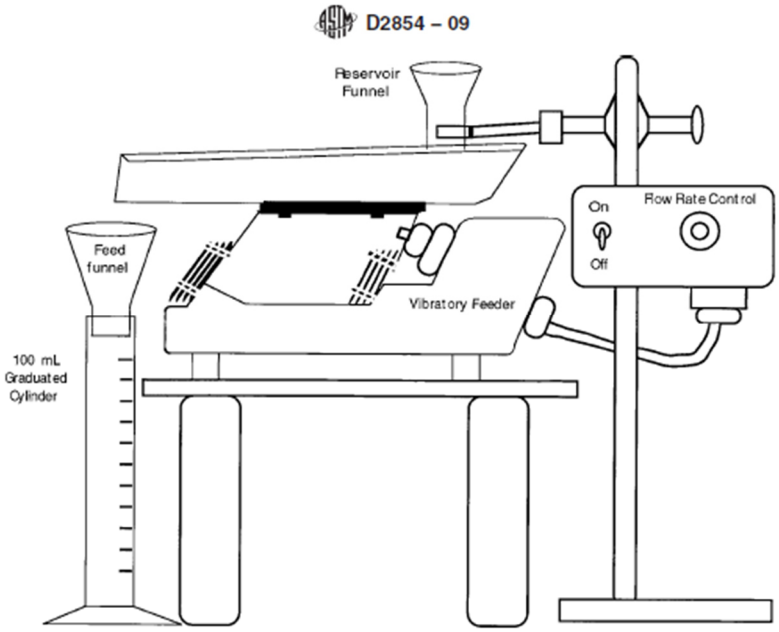

Figure 4.6: Experimental assembly for bulk density determination [32].

The main component of this apparatus is a vibratory feeder, which is adjustable to enable the controlling of the flow rate of the particles being added through a reservoir funnel. A graduated cylinder is placed at the open end of the vibratory feeder to capture the falling particles and to measure the total volume.

The actual experimental assembly used for measuring the bulk density of the available biomass samples was adapted from the apparatus shown in Figure 4.6 and consists of three parts. The first part is a horizontal cylinder that serves as a reservoir for a test sample of biomass particles. The cylinder is connected to a tripod with a set of utility clamps, which enables an adjustment of the angle of the cylinder with respect to the horizontal. The second part is a sieve shaker with another set of utility clamps attached to it. The clamps are attached in a way that they constantly and slightly tap the horizontal cylinder when the sieve shaker is turned on. The result is a smooth vibration of the cylinder and a movement of the particles inside towards the open end. The third part is a graduated cylinder that captures the falling particles. For an instant measurement of the weight, the graduated cylinder is placed on a scale. The utilized experimental setup is shown in Figure 4.7.

Figure 4.7: Experimental setup used for bulk density determination.

Since the angle of the horizontal cylinder can be adjusted, the possibility to regulate the flow rate of the particles is given. For different sized and shaped biomass particles, the angle of the cylinder that enables the required flow rate of 1 ml/s varies and must be determined previous to the execution of the experiment.

For the experimental determination of the bulk density, a test sample of each type of the available biomasses is used, taking under consideration that each test sample should have the same particle size distribution as the original sample. During the experiment, the amount of particles, which freely fall into the graduated cylinder, is measured. The experiment is stopped once the bed of particles in the graduated cylinder reaches a volume of 100 ml. Afterwards, the weight is measured and the bulk density is calculated using the Equation 3.13. For each test sample, the experiment was carried out three times and the arithmetic value of the bulk density was calculated. The results are illustrated in Figure 4.8.

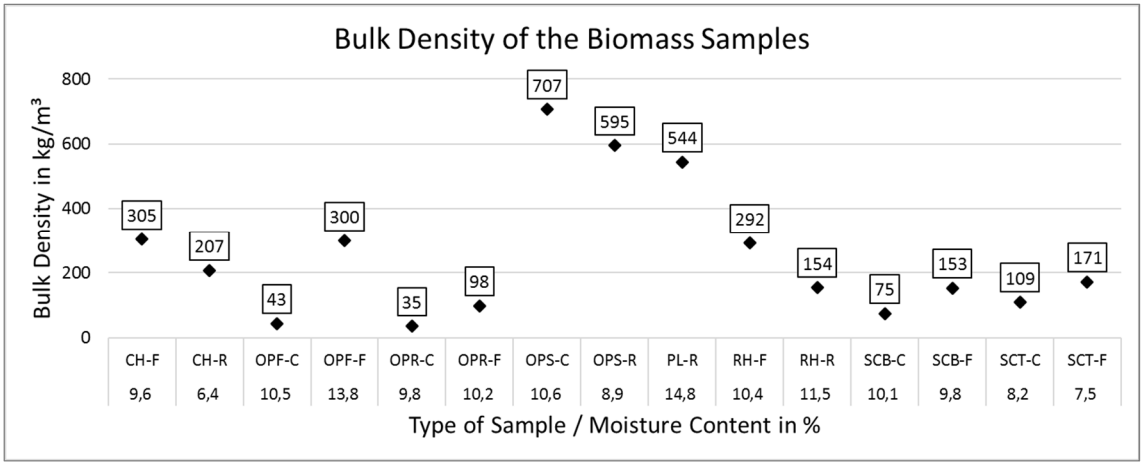

Figure 4.8: Bulk density of biomass samples.

4.5 Determination of Particle Density

Particle density is the mass of a solid granular material per unit of particle volume, including pores and air or gas inclusions inside the particles. To find the particle density, a 25 ml pycnometer was used. The test liquid that is normally used for the density determination of solid particles is water, but, since biomass particles tend to absorb water, the utilization of paraffin as a test liquid is recommended by the norm "UNE-EN 993-1" [33]. The utilized pycnometer is shown in Figure 4.9.

Figure 4.9: Utilized pycnometer (25 ml) and scale.

For each type of biomass, three test samples with a mass between 0.3 and 0.5 g were taken. Due to the restricted opening size of the pycnometer and the small quantity of the test samples, an assembling of a test sample with the same particle size distribution as the original biomass

sample was not possible; therefore, the test samples were taken from the most representative particle size fractions of each biomass sample.

Before the experiments were carried out, the density of the paraffin at ambient temperature was verified. For this reason, the mass of the empty pycnometer and the mass of the pycnometer filled with paraffin is measured. The mass difference is divided by the known volume of exactly 25 ml. The utilized paraffin has a density of 0.81 g/cm³.

The experiments were carried out in three steps. At first, the initial mass as explained by Equation 3.15 was measured. Secondly, the test sample is added to the pycnometer and the terminal mass as explained by Equation 3.16 is measured. Lastly, the Equation 3.17 is used to compute the particle density of each test sample.

Three test samples of each type of biomass are tested. In order to determine if there is a biomass type that absorbs a notable amount of the test liquid, which may significantly affect the measurement, the experiments are carried out as follows. When the first of the three test samples is added to the pycnometer and the initial and terminal masses are measured to calculate the density, the first test sample stays in the pycnometer while the second test sample is added. Thus, the terminal mass of the pycnometer with the first test sample becomes part of the initial mass of the pycnometer for the second test sample. When the first test sample absorbs a notable amount of the test liquid, less of the test liquid is discharged from the pycnometer when the second sample is added. Hence, the terminal mass of the pycnometer with the second test sample is proportionally higher than the terminal mass of the pycnometer with the first sample, which results in an increase of the calculated particle density. This effect is even higher when the third test sample is added.

When a significant increase of the calculated particle density between the three test sample of each biomass type is not observed, the influence of absorption can be neglected. The arithmetic value of the determined particle densities of the test samples is illustrated in Figure 4.10.

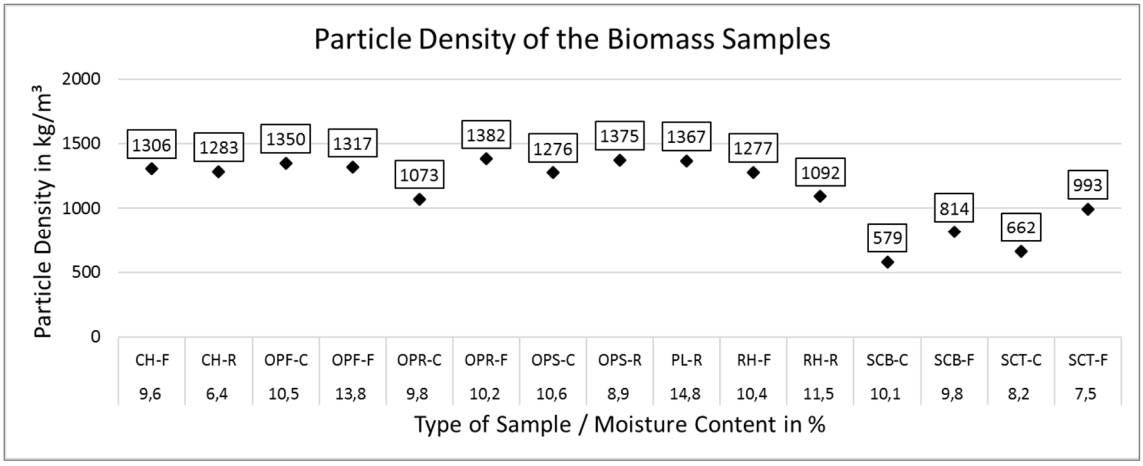

Figure 4.10: Particle density of the biomass samples.

4.6 Geldart Classification

In order to approximate the behavior of the particles, the Geldart classification is applied. According to the mean particle diameter and the particle density, the different biomass samples were categorized into one of the four Geldart groups; this is done by plotting the particle density of each biomass sample over its mean particle diameter. The fluidization medium assumed for this purpose was air. Since the density of air in relation to the particle density of the biomass samples is very low, the influence of the air density is neglected in the plot. An overview of the Geldart group of all biomass samples is provided in Figure 4.11.

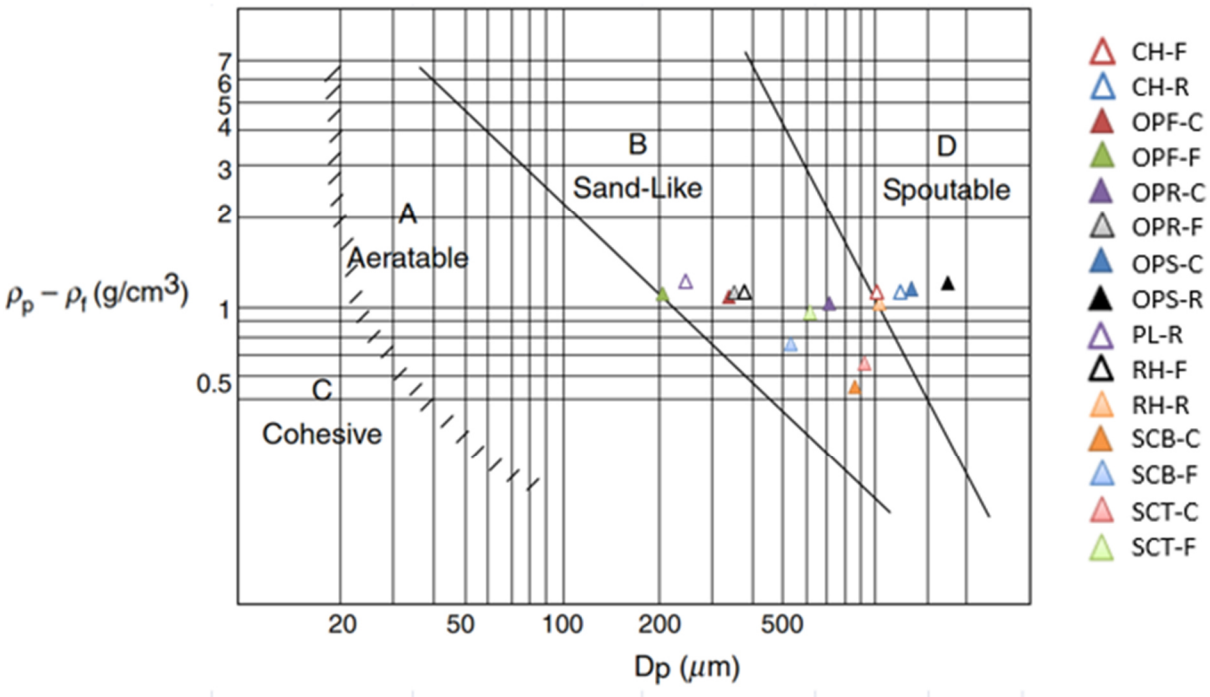

Figure 4.11: Geldart's classification chart indicating the biomass samples (modified) [29].

As illustrated in Figure 4.11, about two thirds of the investigated biomass samples are categorized as “Geldart B particles”. Three samples are categorized as “Geldart D particles” and another three samples are plotted at the transitions line between A and D groups. The samples belonging to group B are expected to fluidize well and form a bubbling fluidization regime in a CFB-reactor while the group D samples are likely to show an erratic behavior that could result in channeling or slugging. The actual fluidization regimes exhibited by each biomass sample are verified through practical fluidization experiments, which are explained in the following chapter.

4.7 Determination of Minimum Fluidization Velocity and Fluidization Regimes

The experimental assembly used to determine the minimum fluidization velocity and the corresponding fluidization regime of the different biomass samples consists of two basic components.

The first component is the cold-flow fluidized bed riser, which is referred to as the reactor. The reactor is a 70 cm long transparent pipe made of acrylic glass with a circular cross section and an inner diameter of 13.5 cm. Flanges at the top and bottom end of the reactor allow the connection of the reactor with other parts of the experimental plant such as the air distributor located at the bottom. The distributor consists of a perforated plate with an aperture size of about 1 mm, which enables an evenly distributed gas flow. The distributor plate is covered with a synthetic fabric that is permeable to air and prevents the powder-like particles of biomass or bed material to pass through or clog the distributor. Compressed air is used as fluidization medium and the flow rate can be adjusted with a variable area flow meter. As shown in Figure 4.12, there are seven sensing points integrated at the back of the vertical installed reactor, which enable measurements of the internal pressure at different positions. In addition, strips of copper tape are placed on the reactor walls, which enable an earthing of the acrylic glass pipe and prevent electrostatic charging during the fluidization experiments.

Figure 4.12: Experimental setup for the fluidization of the biomass samples.

The second component of the unit is the gas cyclone that separates the solid particles from the gas. At the bottom of the cyclone, an exhaust hose connects the solid particle outlet of the cyclone with a reservoir that captures the separated solid particles. At the top of the cyclone another exhaust hose connects the gas outlet with an air filter. The air filter was found to influence the air flow within the entire plant since it creates a flow resistance and increases the exit pressure depending on the particles load in the exhaust gas. Therefore, the filter is detached from the plant, while the fluidization experiments are executed.

During the fluidization experiments, the superficial velocity inside the reactor and the pressure drop through the bed were determined. The air flow rate was adjusted using a rotameter that is connected to the compressed air supply. The superficial velocity of the air inside the reactor can be found by dividing air flow rate $\dot{V}_{air}$ by the cross-sectional area of the reactor A_r, as shown in Equation 4.1.

$$U_0 = \frac{\dot{V}_{air}}{A_r} = \frac{4}{\pi}\frac{\dot{V}_{air}}{d_r^2} \qquad \text{(Equation 4.1)}$$

In order to determine the pressure drop through the bed of particles, pressure sensors were connected with the sensing points; seven on the reactor and one below the distributor plate. Consequently, the total measured pressure difference is the sum of the pressure drop caused by the distributor plate and the pressure drop caused by the bed of particles. To calculate the pressure drop through the bed at a certain superficial gas velocity, the total measured pressure drop must be diminished by the pressure drop caused by the distributor plate at given superficial gas velocity. For this reason, the pressure drop of the distributor plate at different superficial gas velocities is determined by running the plant without any bed of particles inside. Due to the low superficial gas velocities, the pressure drop caused by the air friction at the walls of the reactor can be neglected.

A variety of fluidization experiments were conducted. In the first experiments, a bed consisting of biomass particles only is fluidized in order to observe the particle behavior of each biomass sample and to determine the critical gas velocities. The second fluidization experiments campaign was conducted using a bed of silica sand mixed with small amount of the biomass samples.

4.7.1 Fluidization of a Bed of Biomass Particles

For the first group of experiments, representative fluidization samples with the same particle size distributions as the original sample were utilized. The height of the bed of particles is about 10 cm while the weight of each bed varies depending on the specific bulk density of each biomass sample. During the experimental procedure, the superficial gas velocity is slowly increased, while the pressure difference through the bed is measured. The aim of the fluidization test is to plot the total pressure drop as a function of the superficial gas velocity; this is exemplarily shown in Figure 4.13.

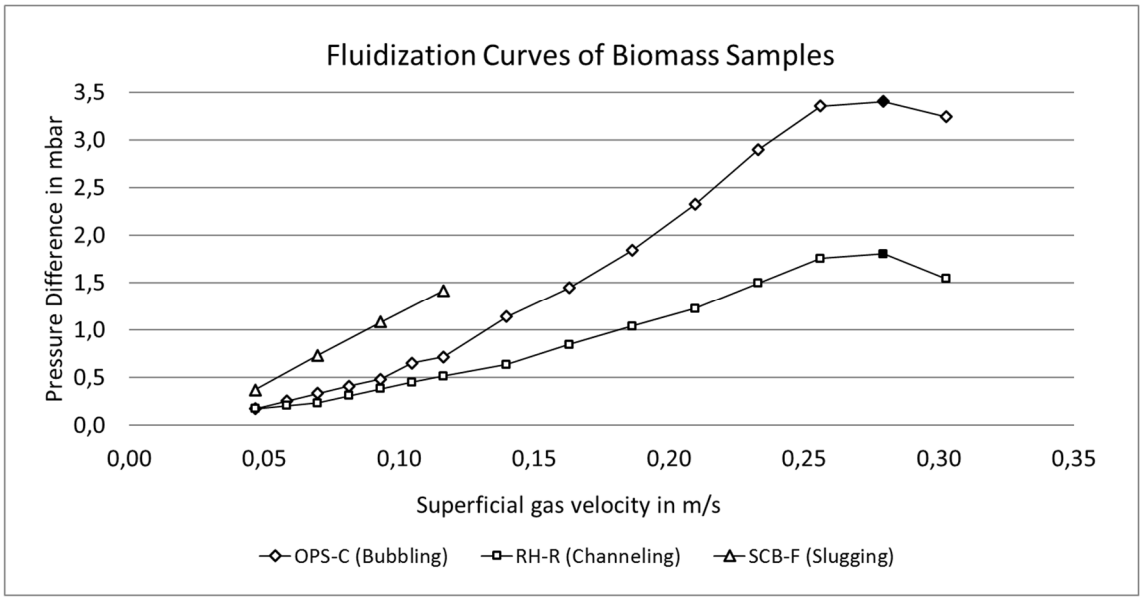

Figure 4.13: Exemplary fluidization curves of biomass samples.

The three plotted curves in Figure 4.13 are selected to demonstrate the development of the pressure drop in a bubbling fluidization regime, in a channeling bed and in a slugging bed.

The curve of OPS-C particles shows a regular development of the pressure drop within the bed of particles that creates a bubbling fluidization regime. The pressure drop within the fixed bed increases approximately linearly with the increase of the gas velocity until it reaches the minimum fluidization velocity, which is marked by a full dot in the diagram. At this point, the bed begins to create a bubbling regime and the pressure drop remains almost constant.

The curve of RH-R particles also shows a regular development of the pressure drop. Compared to OPS-C particles, the linear increase of the pressure drop is lower. However, during fluidization, it is observed that the bed of particles creates channels. When channels occur (marked by a full dot on the plot), the resistance of the bed to the airflow is comparatively lower and the pressure drop does not increase further. Due to the fact that the majority of the upstreaming air passes the bed through the channels, an even fluidization of the entire bed is not reached.

The fluidization curve of SCB-F particles does not show a regular development of the pressure drop. Even though the pressure difference through the bed increases linearly at the beginning, slugging occurs at low gas velocities and an even fluidization of the bed is not reached. Due to

slugging, the majority of the bed is lifted by the upstreaming air. A measurement of the pressure drop is not possible and the experiment must be stopped.

The three fluidization curves were selected to describe the diverse fluidization regimes, which were observed during the experimentation. The fluidization curves of all the biomass samples can be found in the appendix (A2).

Since several beds of particles of some of the biomass samples create channels and slugs, stable fluidization is not reached and a minimum fluidization velocity is impossible to determine. Table 4.3 illustrates, for all studied samples, the ascertained results of the fluidization tests, providing the minimum fluidization velocity U_{mf}, the channeling velocity U_c, the slugging velocity U_s according with the observed phenomena and the corresponding total pressure drop at that velocity.

Table 4.3: Results of the fluidization of different biomass samples.

Biomass	Sample	Fluidization Regime	U_{mf}	Δp_{mf}	U_c	Δp_c	U_s	Δp_s
-	-	-	in m/s	in mbar	in m/s	in mbar	in m/s	in mbar
Coffee Husk	CH-F	Channeling	-	-	0,14	1,24	-	-
	CH-R	Channeling	-	-	0,56	1,55	-	-
Oil Palm Fiber	OPF-C	Slugging	-	-	-	-	0,33	0,37
	OPF-F	Slugging	-	-	-	-	0,30	0,74
Oil Palm Rachis	OPR-C	Slugging	-	-	-	-	0,35	0,39
	OPR-F	Slugging	-	-	-	-	0,29	N/A
Oil Palm Stone	OPS-C	Bubbling	0,28	3,40	-	-	-	-
	OPS-R	Bubbling	0,23	2,59	-	-	-	-
Poultry Litter	PL-R	Bubbling	0,14	2,74	-	-	-	-
Rice Husk	RH-F	Channeling	-	-	0,14	1,14	-	-
	RH-R	Channeling	-	-	0,28	1,80	-	-
Sugar Cane Bagasse	SCB-C	Slugging	-	-	-	-	0,19	N/A
	SCB-F	Slugging	-	-	-	-	0,14	N/A
Sugar Cane Top	SCT-C	Slugging	-	-	-	-	0,23	N/A
	SCT-F	Slugging	-	-	-	-	0,14	N/A

In Table 4.3, the description “N/A” is used when the occurring slugs lift the bed of particles to the top of the reactor. In that case, the experiment must be stopped and the pressure drop cannot be measured.

4.7.2 Fluidization of a Bed of Silica Sand mixed with Biomass Particles

For the second set of fluidization experiments, silica sand was used as bed material, which is mixed with different amounts of biomass particles. The experiment has two major aims; the first is to find out if the fluidization behavior of the different biomass samples can be improved while mixing it with silica sand; the second is to determine if an even mixing of the particles (necessary for a successful thermochemical conversion), can be reached during the fluidization.

The silica sand is available from a local supplier and has a mean particle diameter of 138 µm. The particle size distribution of the sand, determined by a sieve analysis, is illustrated in Figure 4.14.

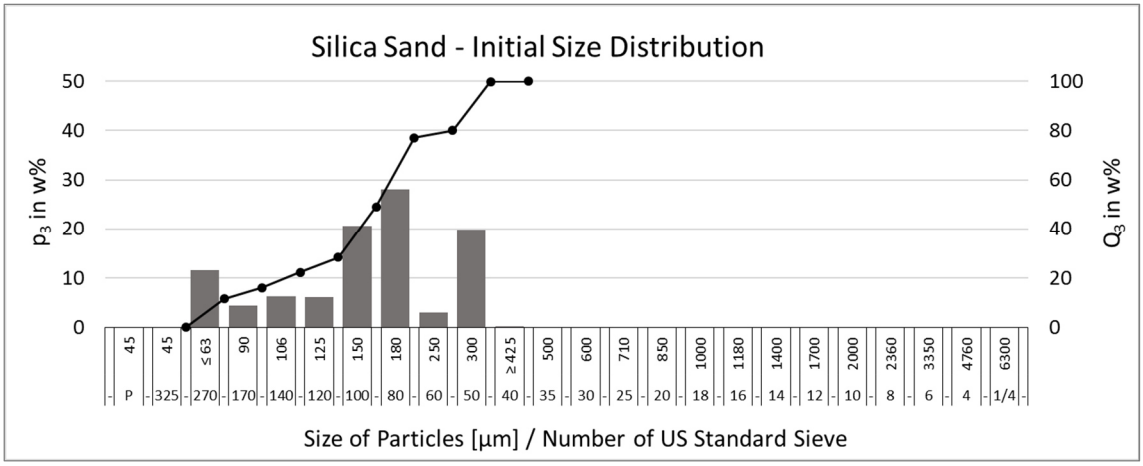

Figure 4.14: Initial particle size distribution of the silica sand.

According to Basu, for a gasification process in a CFB-plant, the mean particle diameter of the bed material is usually in a range between 100 and 300 µm [7]. Therefore, the sand for the experiments was selected to have a mean particle diameter of 200 µm. The fraction of fines in the original sand had to be separated in order to achieve the desired mean particle diameter of 200 µm, all the available silica sand is sieved in order to separate smaller sized particles (200 µm). Equation 3.11 can be utilized to calculate the mean particle diameter and to determine a particle size distribution with a wanted mean particle diameter of 200 µm. The particle size distribution of the actually used silica sand is shown in Figure 4.15.

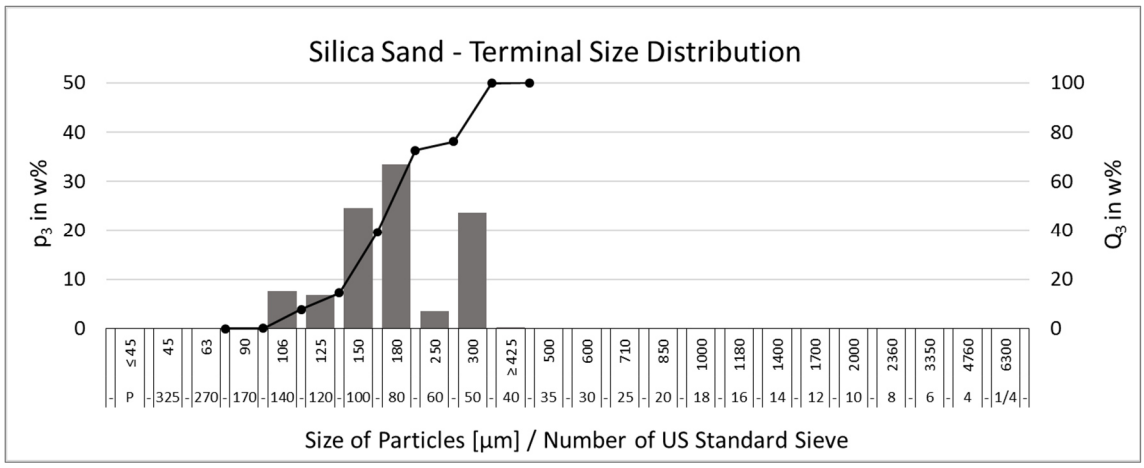

Figure 4.15: Terminal particle size distribution of the silica sand.

The particle density of silica sand is about 2600 kg/m³ [34], and hence, silica sand particles with a mean particle diameter of 200 µm can be classified as "Geldart B particles". A bed of "Geldart B particles" is likely to forms a bubbling fluidization regime when the minimum fluidization velocity is reached. Fluidization of a bed of 2 kg of silica sand allowed verifying the appearance of the bubbling fluidization regime as it was expected. The regular fluidization curve of the utilized silica sand with a mean particle diameter of 200 µm is shown in Figure 4.16. The measured minimum fluidization velocity was 0.026 m/s.

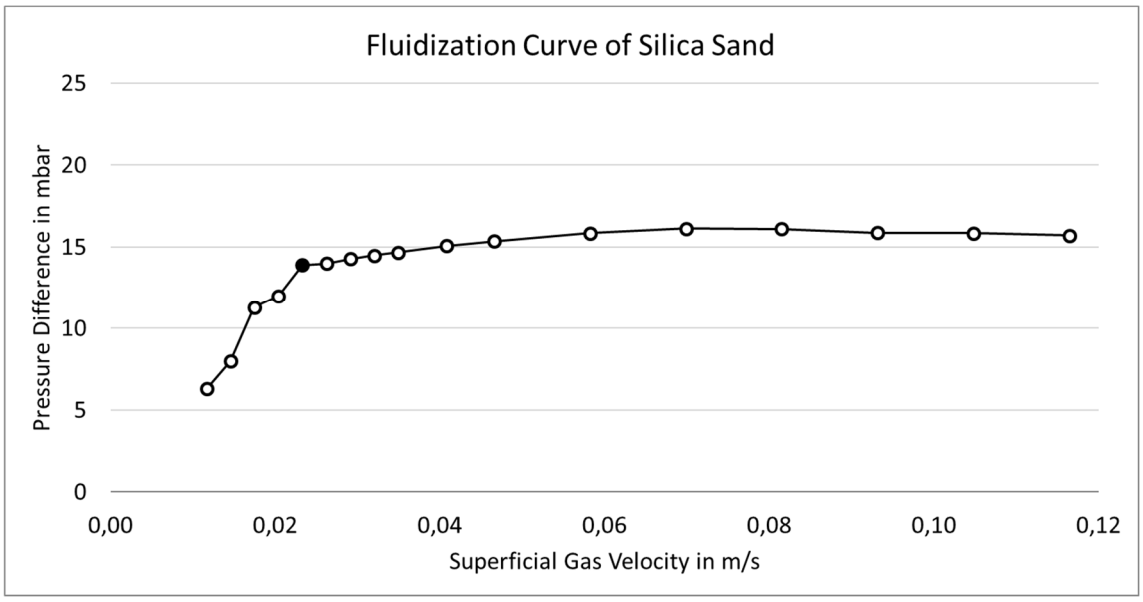

Figure 4.16: Fluidization curve for the silica sand.

For each biomass sample, four fluidization experiments were carried out. The investigated beds of particles have a total mass of 2 kg and consist of a binary mixture of silica sand and biomass with different weight fractions, 3 %, 5 %, 7 % or 10 % of biomass particles. The added amounts

of biomass particles are representative samples with the same particle size distributions as the original sample. Due to the restricted amount of OPF-C, OPF-F, OPR-C and OPR-F particles, the fluidization of these biomass samples was carried out using only bed mixtures with a content of 3 % and 5 % of biomass particles. The experimental procedure is carried out analogously to the first fluidization experiment (see section 4.7.1).

In order to evaluate the results of the fluidization experiments, the occurring fluidization regimes observed during the experiments and the plotted fluidization curves, which show the pressure drop through the bed as a function of the superficial gas velocity, are analyzed simultaneously. The evaluation and the interpretation of the results from the experiments are exemplarily shown in the following, by using the ascertained results of the two different rice husk samples: RH-F and RH-R. Table 4.4 gives an overview of the occurring fluidization regimes of the investigated samples. In addition, the critical gas velocities and the corresponding pressure differences through the bed of particles are given.

Table 4.4: Occurring fluidization regimes of RH-F and RH-R.

Biomass	Sample	Biomass Content in Bed	Fluidization Regime	U_{mf}	Δp_{mf}	U_c	Δp_c	U_j	Δp_j	U_s	Δp_s
-	-	in %	-	in m/s	in mbar	in m/s	in mbar	in m/s	in mbar	in m/s	in mbar
Rice Husk	RH-F	3	Bubbling	0,041	16,1	-	-	-	-	-	-
		5	Bubbling	0,041	16	-	-	-	-	-	-
		7	Channeling	-	-	0,035	16,1	-	-	-	-
		10	Segregation (J)	-	-	-	-	-	-	-	-
	RH-R	3	Bubbling	0,029	16,1	-	-	-	-	-	-
		5	Bubbling	0,041	15,4	-	-	-	-	-	-
		7	Segregation (J)	-	-	-	-	-	-	-	-
		10	Segregation (J)	-	-	-	-	-	-	-	-

As shown in Table 4.4, the fluidization of the bed material with biomass contents of 3 % and 5 % create a bubbling fluidization regime that results in a homogeneous mixing of the entire bed. The fluidization of the bed material with biomass contents of 7 % and 10 % results in the appearance of channels or in the segregation of the bed. Such results do not allow an even mixing of the particles. Accordingly, it can be presumed that a successful thermochemical conversion of rice husk particles (with similar properties as in the present study) is possible as long as the instantaneous content of rice husk particles inside the bed does not exceed 5 %. The fluidization curves of the different bed mixtures with RH-R and RH-F particles are illustrated in Figure 4.17 and Figure 4.18.

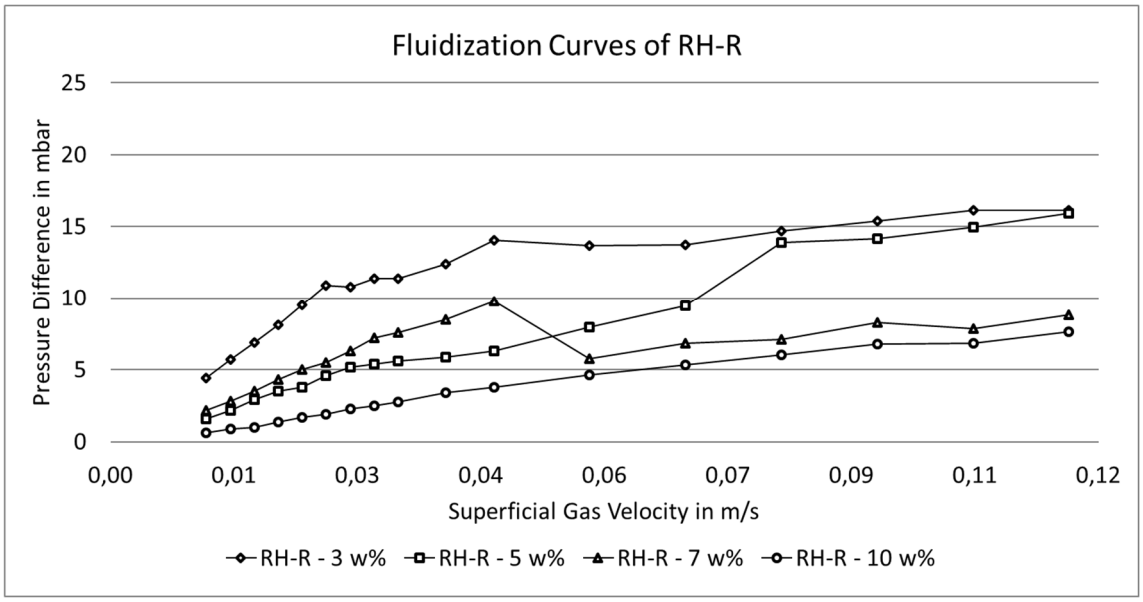

Figure 4.17: Fluidization curves of RH-R.

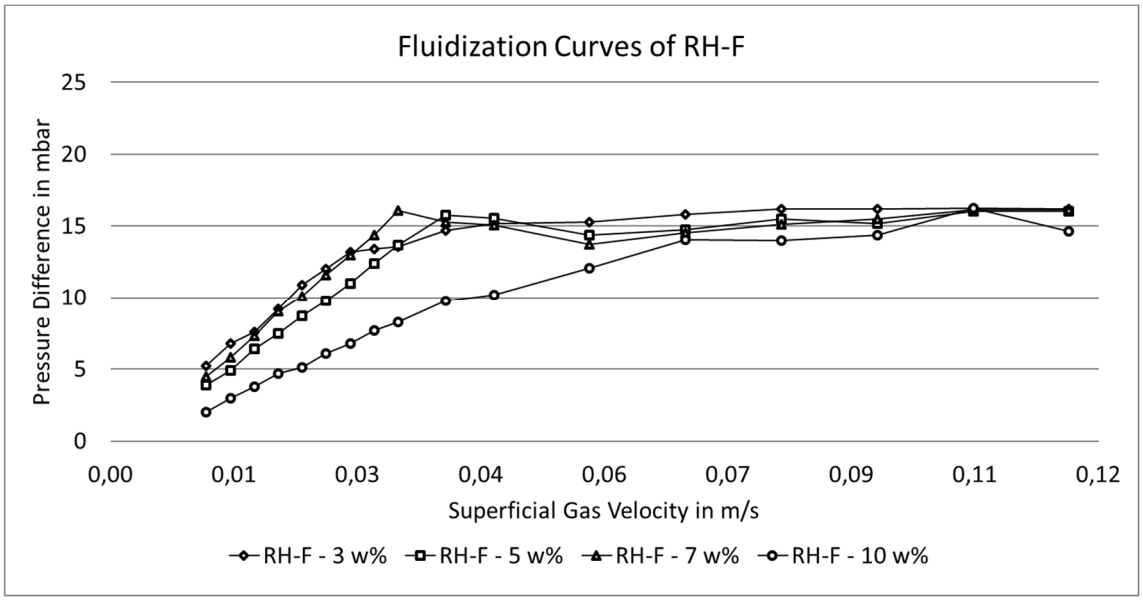

Figure 4.18: Fluidization curves of RH-F.

By comparing the fluidization curves of the RH-R bed mixtures in Figure 4.17, it is notable that with a decrease of the RH-R content in the bed, the fluidization curves appear more regular and more similar to the ideal fluidization curve that is for instance shown in Figure 3.2. While the curve “RH-R - 7 w%” in Figure 4.17 shows a linear increase of the pressure drop at lower gas velocities, it could be observed that a segregation of the bed took place and a regular fluidization with an even mixing of the particles was not given.

The fluidization curves in Figure 4.18 also show that the bed mixtures with RH-F particles fluidize more regularly with a decrease of the RH-F content in the bed. The curve "RH-F - 7 w%" looks like a fluidization curve of a bed of particles that creates a bubbling fluidization regime, but considering that this bed showed occurrence of channels, an even mixing was not given during the fluidization.

Since the rice husk is available in two different physical states, namely in "as-received condition" and "finely ground", the influence of the pre-processing can be investigated as well by comparing the plotted fluidization curves in Figure 4.17 (as received) with the curves in Figure 4.18 (finely ground). It is notable that all the fluidization curves of the finely ground particle mixtures are closer to the ideal curve than the curves of the mixtures with the particles in "as-received condition". In order to get a closer look at the curves of the bed mixtures, which create an actual bubbling regime and had the ability to provide an even mixing of the particles, a direct comparison of the fluidization curves of the 3 % and the 5 % mixtures of both kinds of particles is illustrated below. Figure 4.19 shows the fluidization curves of the bed mixtures with 3 % and Figure 4.20 provides the fluidization curves of the bed mixtures with 5 % of rice husk particles.

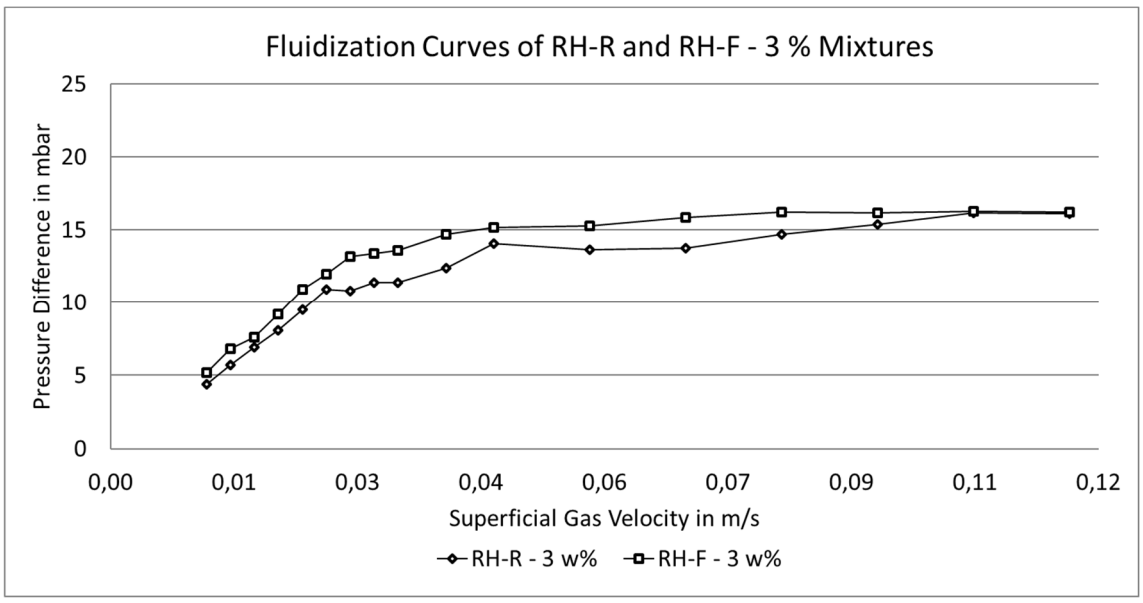

Figure 4.19: Fluidization curves of mixtures with 3 w% RH-R and RH-F particles.

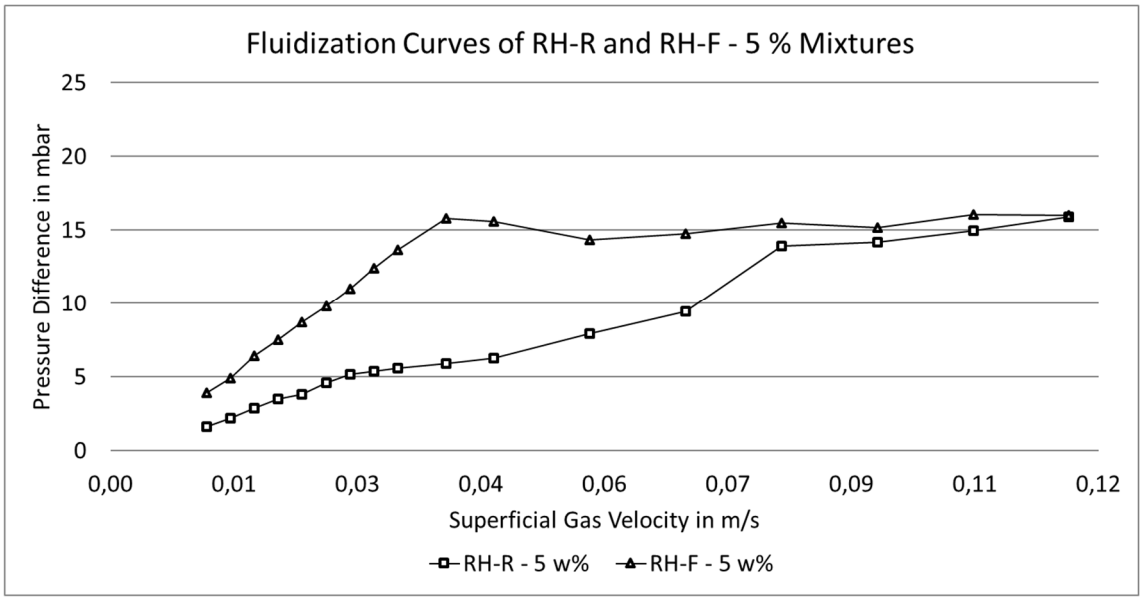

Figure 4.20: Fluidization Curves of mixtures with 5 w% RH-R and RH-F particles.

The difference between the fluidization curves “RH-F - 3 w%” and “RH-R - 3 w%”, illustrated in Figure 4.19, is only marginal. The curve “RH-F - 3 w%” shows a smooth transition from the fixed bed state to the fluidized bed state, while reaching the minimum fluidization at a superficial gas velocity of 0.041 m/s. With a further increase of the gas velocity the pressure difference over the bed of particles increases slightly. The curve “RH-R - 3 w%” shows a pressure drop that increases linearly with respect to the superficial gas velocity until it reaches the minimum fluidization velocity at 0.029 m/s. Afterwards, the pressure drop increases more rapidly and unevenly.

The difference between the fluidization curves in Figure 4.20 is more noticeable. The curve “RH-F - 5 w%” develops nearly ideally; the pressure difference through the fixed bed state increases linearly with respect to the superficial gas velocity and after reaching the minimum fluidization velocity at 0.041 m/s the pressure drop stays almost constant. The curve “RH-R - 5 w%” also shows a linear increase of the pressure difference in the fixed bed state, which is much lower than the increase of the “RH-F - 5 w%” curve. The minimum fluidization velocity of the sample in “as-received condition” is equal to the one of the “finely ground” sample but after reaching the velocity the pressure drop through the bed highly increases with a further increase of the gas velocity.

In conclusion, the analysis of the ascertained results of the fluidization experiments with mixtures of silica sand and rice husk particles (in different fractions and in different physical

states) show that a thermochemical conversion of rice husk in a CFB-reactor is possible, while taking into consideration the physical and fluid dynamical properties of the rice husk particles. The experiments prove that an even mixing of the particles inside the bed is given, as long as the content of rice husk particle does not exceed 5 % of the total mass. Furthermore, the comparison of the fluidization experiment of rice husk particles in different physical states shows that a pre-processing, particularly a grinding can improve the regularity of the fluidization process, which is necessary for the design of the gasification process and the applied CFB-reactor.

The analysis of the results of the fluidization experiment with rice husk particles is exemplarily made in detail. 15 different biomass samples were investigated. Due to the high amount, not every analysis can be explained in detail. The fluidization curves of all the investigated biomass samples are provided in the Appendix (A3). Table 4.5 provided below, illustrates the observations made during the fluidization experiments. In the next section, the evaluation of all the experiments including the fluidization experiment and their results, is given.

Table 4.5: Occurring fluidization regimes of the biomass samples.

Biomass	Sample	Biomass Content in Bed	Fluidization Regime	U_{mf}	Δp_{mf}	U_c	Δp_c	U_j	Δp_j	U_s	Δp_s
-	-	in %	-	in m/s	in mbar	in m/s	in mbar	in m/s	in mbar	in m/s	in mbar
Coffee Husk	CH-F	3	Bubbling	0,032	16	-	-	-	-	-	-
		5	Bubbling	0,032	16	-	-	-	-	-	-
		7	Slugging	-	-	-	-	-	-	0,058	18
		10	Segregation (J)	-	-	-	-	-	-	-	-
	CH-R	3	Bubbling	0,035	15,5	-	-	-	-	-	-
		5	Jetting	-	-	-	-	0,058	6,2	-	-
		7	Jetting	-	-	-	-	0,116	7,9	-	-
		10	Segregation (J)	-	-	-	-	-	-	-	-
Oil Palm Fiber	OPF-C	3	Slugging	-	-	-	-	-	-	0,058	17,8
		5	Jetting	-	-	-	-	0,116	7,7	-	-
	OPF-F	3	Bubbling	0,041	16	-	-	-	-	-	-
		5	Bubbling	0,041	15,2	-	-	-	-	-	-
Oil Palm Rachis	OPR-C	3	Channeling	-	-	0,058	9,1	-	-	-	-
		5	Segregation (F)	-	-	-	-			-	-
	OPR-F	3	Jetting	-	-	-	-	0,058	7,4	-	-
		5	Channeling	-	-	0,047	5,4	-	-	-	-
Oil Palm Stone	OPS-C	3	Bubbling	0,032	16,2	-	-	-	-	-	-
		5	Bubbling	0,029	16,2	-	-	-	-	-	-
		7	Bubbling	0,026	16	-	-	-	-	-	-
		10	Bubbling	0,032	16	-	-	-	-	-	-
	OPS-R	3	Bubbling	0,035	16	-	-	-	-	-	-
		5	Bubbling	0,035	15,9	-	-	-	-	-	-
		7	Bubbling	0,032	16,1	-	-	-	-	-	-
		10	Bubbling	0,035	15,4	-	-	-	-	-	-
Poultry Litter	PL-R	3	Bubbling	0,35	16,1	-	-	-	-	-	-
		5	Bubbling	0,29	16,1	-	-	-	-	-	-
		7	Bubbling	0,29	16,1	-	-	-	-	-	-
		10	Bubbling	0,29	16,1	-	-	-	-	-	-
Rice Husk	RH-F	3	Bubbling	0,041	16,1	-	-	-	-	-	-
		5	Bubbling	0,041	16	-	-	-	-	-	-
		7	Channeling	-	-	0,035	16,1	-	-	-	-
		10	Segregation (J)	-	-	-	-	-	-	-	-
	RH-R	3	Bubbling	0,029	16,1	-	-	-	-	-	-
		5	Bubbling	0,041	15,4	-	-	-	-	-	-
		7	Segregation (J)	-	-	-	-	-	-	-	-
		10	Segregation (J)	-	-	-	-	-	-	-	-
Sugar Cane Bagasse	SCB-C	3	Segregation (J)	-	-	-	-	-	-	-	-
		5	Slugging	-	-	-	-	-	-	0,082	15,9
		7	N/A	-	-	-	-	-	-	-	-
		10	Jetting	-	-	-	-	0,116	8,9	-	-
	SCB-F	3	Bubbling	0,041	16,1	-	-	-	-	-	-
		5	Bubbling	0,026	15,9	-	-	-	-	-	-
		7	Bubbling	0,058	15,6	-	-	-	-	-	-
		10	Slugging	-	-	-	-	-	-	0,082	18,5
Sugar Cane Top	SCT-C	3	Jetting	-	-	-	-	0,047	13,1	-	-
		5	Segregation (F)	-	-	-	-	-	-	-	-
		7	Jetting	-	-	-	-	0,058	6,8	-	-
		10	Segregation (F)	-	-	-	-	-	-	-	-
	SCT-F	3	Bubbling	0,047	14,6	-	-	-	-	-	-
		5	Bubbling	0,026	13,7	-	-	-	-	-	-
		7	Channeling	-	-	0,058	12,9	-	-	-	-
		10	Channeling	-	-	0,047	8,8	-	-	-	-

5 Analysis of Results

The evaluation of the experimental ascertained results is divided into two parts. In the first part (5.1), the evaluation of the different applied experiments including the sieve analysis, the measurements of the bulk and particle density, the determination of the moisture content and the fluidization tests, is carried out. In the second part (5.2), the ascertained physical and fluid dynamical properties are summarized for each specific biomass sample in order to evaluate their availability for successful thermochemical conversion in a CFB-reactor.

5.1 Evaluation of the Applied Experiments to Determine the Biomass Properties

The sieve analysis was executed to determine the particle size distribution in order to calculate the mean particle diameter of the different biomass particles. During the sieving procedure, most of the biomass samples could be rapidly separated into fractions of different sizes, while a sieving time of 10 - 15 min was sufficient. For biomass samples with a higher amount of fine particles, especially for PL-R, longer sieving times have been necessary. Since the size and shape of the particles of some biomass samples vary within wide ranges, the following problem arose during experimentation.

The problem that had been identified was the tendency for longer and curlier particles to remain connected to each other resulting in a buildup of clusters. These clusters could not be separated by the motion of the sieve shaker. These particle collectives, shown in Figure 2.5, are retained in standard sieves with large aperture sizes, while single particles of the collectives could easily pass the sieves. This effect has an influence on the plot of the particle size distribution and the calculated mean particle diameter. This problem could be solved by separating the particle clusters by hand, which would result in a more precise particle size distribution. Even though the results would be more precise, the particle clusters also occur inside the reactor during the fluidization experiments and the exact results of the particle size distribution of the separated particle clusters would not represent the state of the particles as they will be fed into the reactor. Therefore, a pre-separation of the particles clusters was not carried out during the sieve analysis and the clusters of particles were considered as larger particles for the plot of the particle size distribution and the calculation of the mean particle diameter. The biomass samples in which clusters of particle could be observed are OPF-C, OPR-C and OPR-F.

Another problem noted during experimentation was that fragile particles disintegrate due to the motion of the sieve shaker, which resulted in the fact that the measured fractions of smaller

powder-like particles were higher than in the original sample. This problem only concerned PL-R particles. The plotted particle size distribution and the calculated mean particle diameter are therefore not precise. Since the PL-R particles are very fragile and break apart very easily, the physical characteristic of such samples changes permanently, due to the transportation, the pre-drying process, the feeding into the CFB-reactor through a screw feeder, etc. Therefore, the physical properties of the particles as they will be fed into the CFB-reactor cannot be predicted very precisely, which must be considered during the evaluation of the particle size distribution and the mean particle diameter in order to design a CFB-plant.

The calculated mean particle diameters of the different biomass samples are in a range between 201 μm (for OPF-F particles) and 2576 μm (for OPS-R particles). The evaluation of the mean particle diameter of each biomass sample is carried out in detail in section 5.2.

The experimental setup to determine the bulk density, as it is described in section 4.4, is applicable for most of the biomass samples. An even flow of the particles with the required flow rate of 1 ml/s could be reached due to the possibility of adjusting the angle of the particle reservoir. For biomass samples containing clusters of particles (OPF-C, OPF-F, OPR-C and OPR-F, as mentioned before), the particle flow was not as even as desired. The clusters clogged the particle reservoir while making it not possible for smaller particles to move forward; the angle of the reservoir therefore had to be increased to enable the flow of the particles. Also, when the clusters reach the end of the reservoir, the entire cluster fell freely into the graduated cylinder and the smaller particles that had been barricaded behind the clusters follow. In this case, the required flow rate of 1 ml/s had been sharply exceeded. Since the free fall of the particles was given and the three executed experiments of each biomass sample showed similar results, the ascertained bulk densities can be considered to be representative.

Another difficulty was encountered for the samples SCT-C and SCT-F. These samples contain small fractions of thin particles that have a length of up to 10 cm. The long particles do not move accurately within the vibrating reservoir and, to some extent, had to be manually filled into the graduated cylinder. Since this problem only occurred for a very low fraction of particles (about two or three single particles per experiment), the influence of this effect on the ascertained results can be neglected.

The determination of the particle density using the pycnometer worked without any remarkable problem. The investigated particles of each biomass sample do not have the same particle size distribution as the original sample due to the restricted opening size of the pycnometer. Since the investigated particles are taken from the major particle size fractions of each biomass sample and the entire original sample consists of the same material, the ascertained results are representative. Also, a notable influence on the results that is caused by any absorption of the test liquid by the particles could be excluded by the execution of the experiment as it is described in section 4.5.

During the determination of the moisture content, using a forced-convection oven, a constant mass could be reached for every biomass sample after a drying period of 24 h. The initial and terminal mass of each sample could be measured very accurately and the moisture content was calculated. Even though no problems occurred during the drying procedure, it must be considered that all biomass samples have been stored in not perfectly sealed plastic bags over a duration of approximately 3 months prior to the ascertainment of the moisture content. For the design of the thermochemical conversion process of the biomass samples through pyrolysis, gasification and combustion, the moisture content has a strong influence. Hence, the moisture content of the biomass samples as they are fed into the CFB-reactor can vary within the entire process, including the handling by the agricultural producer, the transport, the storage, etc. For the executed fluidization tests in the cold-flow fluidized bed riser, the influence that a variation of the moisture content would have, is neglectable.

Due to the difference in shape, size, internal structure and composition of the studied biomasses the bulk density varies between 35 kg/m³ for OPR-C and 707 kg/m³ for OPS-C, while the particle density varies between 579 kg/m³ for SCB-F and 1382 kg/m³ for OPR-F. The evaluation of the bulk and particle density of each biomass sample is carried out in detail in the following section 5.2.

The expected particle behavior of each tested biomass sample based on the Geldart classification could, only for some extend, be observed during the fluidization tests, which can be ascribed to two issues. The first issue is that the Geldart classification only considers the particle density and the mean particle diameter. Since most of the biomass samples contain particles within a wide range of sizes, the calculated mean particle diameter is not always representative of the entire biomass sample, especially when a sample consist of a combination

of very small and very large particles. The second issue is the fact that the form factor, which strongly influences the fluidization process, is also not considered and some biomass particles have very specific forms, such as sticks (sugar cane top), fibers (oil palm fibers) and flakes (coffee husk). Most of the biomass samples are classified as “Geldart B particles”, which are considered to be “sand-like” particles. By comparing the appearance of the different biomass samples, shown in the figures in section 2, it is notable that the description “sand-like” is not suitable for most of the samples.

In conclusion, the Geldart classification is not sufficient to predict the behavior of particles with such a large variation in form and size as those studied here. Therefore, practical fluidization experiments have been carried out in order to determine information that is essential for the design of a CFB-plant.

The different fluidization tests performed using the experimental setup depicted in section 4.7, resulted in a large quantity of results. During experimentation, the pressure difference through the bed was registered and plotted as a function of the superficial gas velocity and the occurring fluidization regimes were observed. In addition, the entire experimentation has been recorded on camera for a later comparison of the results.

The first fluidization experiments, in which only biomass particles without any bed material are fluidized, were carried out to determine if the different biomass samples could reach a homogeneous fluidization regime that result in an even mixing of the particles inside the reactor. The results show, that there are only three biomass samples that created a bubbling regime during the fluidization, namely OPS-C, OPS-F and PL-R. When the point of minimum fluidization is reached and the bubbling of the bed particles begins, the pressure drop through the bed and the gas velocity was noted. These values can, for instance, be used to calculate the void fraction of the bed at minimum fluidization velocity. The fluidization of the other biomass samples resulted either in channeling or slugging, which did not enable an even mixing of the particles. The critical velocities and the corresponding pressure differences are also registered.

Since most of the fluidization tests have not resulted in a fluidization regime that enables an even mixing of the particles, the second fluidization experiments were carried out to investigate whether or not a mixing of silica sand as a bed material with smaller amounts of biomass particles can improve the fluidization. For most of the biomass samples, the fluidization could

be improved. The pressure differences and the critical velocities were registered analogously to the first experiment.

In the following part, the ascertained results from the distinct experiments and especially the results of the second fluidization tests are summarized and evaluated for each specific biomass type.

5.2 Evaluation of the Determined Properties of each Biomass Type

The first investigated biomass type is coffee husk, which is available in two physical states: in "as-received condition" (CH-R) and "finely ground" (CH-F). The CH-R particles are in a large size range between 300 and 6300 µm. The calculated mean particle diameter is 1580 µm. Due to the grinding, the CH-F particles include a greater quantity of smaller sized particles, as shown in the diagrams in the appendix (A1). CH-R for instance, contains about 3 % of particles with a size of 300 µm or lower, while CH-F contains about 4 % with of particles with a size of 180 µm or lower. The calculated mean particle diameter of CH-F is 1032 µm.

A fixed bed of flake-like shaped coffee husk particles contains many void spaces. The ascertained bulk density of CH-R is 207 kg/m³. The smaller CH-F particles are packed more densely and therefore, the bulk density is about 50 % higher than the particles in "as-received condition". The determined value is 305 kg/m³. The particle density of both coffee husk samples is nearly equal with 1283 kg/m³ for CH-R and 1306 kg/m³ for CH-F.

According to the Geldart's classification, both coffee husk samples are classified as "Geldart D particles". It could be expected that a fluidized bed of these particles creates an erratic bubbling regime after exceeding the minimum fluidization velocity. On the contrary, the conducted fluidization tests with beds of both coffee husk samples showed the occurrence of channels, making not possible a homogeneous fluidization of the entire bed. Further fluidization experiments with bed mixtures of silica and coffee husk showed that the fluidization behavior could be improved and an even mixing of the bed in a bubbling regime could be reached. More exactly, bed mixtures with 3 % of CH-R particles and bed mixtures with 3 % and 5 % of CH-F particles exhibited a bubbling regime, while bed mixtures of larger amounts of coffee husk particles resulted in the creation of either slugging, jetting or the segregation of the bed.

By comparing the plotted fluidization curves, which can be found in the appendix (A3), it is notable that the fluidization curve of the 3 % mixtures of both coffee husk samples are nearly equal. The regular development of the 5 % mixture with CH-F particles is also notable while the other curves with higher percentages of coffee husk show an irregular development. In conclusion, the results of the fluidization experiments show that in a bed of silica sand, coffee husk particles can be successfully fluidized when the amount of particles does not exceed 3 % of the total mass of the bed, with no previous grinding of the particles. Also, it can be asserted that the process of grinding the particles into smaller sizes improves the fluidization of coffee husk particles when larger amounts, up to 5 %, are added to the bed.

The second investigated biomass type is the oil palm fiber, which is available in two physical states: “coarsely ground” (OPF-C) and “finely ground” (OPF-F). The particles of OPF-C are in a large size range between 106 and 9500 µm. The calculated mean particle diameter is 340 µm, while about 75 % of the particles are larger. It must be mentioned that about 25 % of the particles remained connected as cluster during the sieving procedure and therefore are classified in sizes between 2360 µm and 9500 µm while a single particle would rather be classified in sizes between 1000 µm and 2000 µm. In other words, the mean particle diameter of this samples is not absolutely representative. The appearance of clusters of OPF-F particles during the sieving process is only marginal (less than 1 %) and can therefore be neglected. The plotted particle size distribution shows a form similar to the Gaussian distribution curve. The mean particle diameter of 210 µm is representative since the fractions of small particles are large and have been screened precisely up to sizes of 45 µm.

As mentioned above, clusters of particles that remain connected only occur in the OPF-C sample and not in the OPF-F sample. Due to the fact that the clusters of particles contain large void spaces, the difference in the bulk density of both samples is large. Also, the clusters caused difficulties during the execution of the experiment to determine the bulk density, as mentioned earlier. The ascertained values are 43 kg/m³ for OPF-C and 300 kg/m³ for OPF-F. For the measurement of the particle density the clusters did not cause any problems. The measured particle density of both oil palm fiber samples is nearly equal with 1350 kg/m³ for the OPF-C sample and 1317 kg/m³ for the OPF-F sample.

As a result of the ascertained mean particle diameter and the particle density, OPF-C is classified as “Geldart B particles”, while OPF-F are classified as particles that are at the

transition between “Geldart B particles” and “Geldart D particles”. The occurrence of a bubbling regime, while reaching the minimum fluidization velocity can be expected during the fluidization process. However, the fluidization tests of beds of OPF-C and OPF-F particles resulted in slugging. The fluidization experiments with bed mixtures of silica sand and biomass particles is only carried out with weight fractions of 3 % and 5 % of biomass particles, due to the restricted amount of available oil palm fiber samples.

During experimentation, the OPF-C particle mixtures did not result in an even mixing of the bed due to the appearance of slugging and jetting. On the contrary, OPF-F particle mixtures fluidized well. The creation of a bubbling fluidization regime was observed and an even mixing of the bed particles was given for both mixtures with either 3 % or 5 % of OPF-F particles. Consequently, it can be asserted that the possibility of a successful fluidization of oil palm fiber is given when the particles are ground to smaller sizes.

The third investigated biomass type is the oil palm rachis that is available in two physical states: “coarsely ground” (OPR-C) and “finely ground” (OPR-F). The particles of the OPR-C sample are in a large size range between 106 and 9500 µm, containing about 50 % of particle clusters. The particles that remain in clusters are classified in sizes between 2360 µm and 9500 µm while a single particle would rather be classified in sizes less than 2000 µm. The calculated mean particle diameter is 709 µm. This value is strongly influenced by the large amount of clusters and therefore, not representative of the OPR-C sample. Since the OPR-F particles are ground into smaller sizes, the amount of clusters is smaller (less than 10 %), but the influence of the mean particle diameter calculation is still given. The calculated value of 354 µm is not representative.

Since the oil palm rachis samples contain clusters with a large content of void spaces, the determined values of the bulk density are low. During experimentation, the clusters of OPR-C particles clogged the particle reservoir of the experimental setup, therefore an even flow of the particles could not be reached. To achieve a result, the particles were helped manually to fall into the graduated cylinder. The clusters of OPR-F particles are smaller, which enabled the execution of the experiment while only slightly exceeding the required flow rate of 1 ml/s. The ascertained results are 35 kg/m³ for the OPR-C sample and 98 kg/m³ for the OPR-F sample. Even though the experimentation did not work out in an optimal way, the values can be considered to representative since the free fall of the particles was given and the three executed

experiments of each biomass sample showed similar results. In contrast to the determination of the bulk density, the ascertainment of the particle density could be carried out as planned. The results are 1073 kg/m³ for the OPR-C sample and 1382 kg/m³ for the OPR-F sample. The significant difference of the values could be ascribed to the fact that the empty fruit bunch of the oil palm plant (oil palm rachis) consists of different components (section 2.2) with different internal structures. The particles used for the density measurement were taken from the most representative particle size fractions of each biomass sample, which are particles classified in sizes between than 6300 µm and 9500 µm for OPR-C and particles classified in sizes between 300 µm and 425 µm for OPR-F. Since the particles size fractions, where the particles were taken, are very different, the possibility is given that the particles size fractions contain different amounts of the different components of the empty fruit bunch, which influences the results.

Both samples of oil palm rachis are classified as “Geldart B particles”. The expected bubbling regime of beds of OPR-C and OPR-F particles did not appear during experimentation. Also, further experimentation with bed mixtures of silica sand and oil palm rachis could not show that the fluidization behavior of oil palm rachis could be improved. All executed fluidization tests resulted in either channeling, jetting or in the segregation of the bed mixtures. Thus, the fluidization of a bed of particles that contains oil palm rachis was not successful and the process of grinding did not improve the fluidization behavior of the particles.

The fourth investigated biomass type is oil palm stone particles that are available in two physical states, namely in “as-received condition” (OPS-R) and “coarsely ground” (OPS-C). OPS-R particles have sizes between 1000 and 9500 µm and the calculated mean particle diameter is 2576 µm. OPS-C particles are in a size range between 710 and 4760 µm, with a mean particle diameter of 1781 µm. Since both samples contain very low fractions of small powder-like particles, the screening could be executed very precisely.

Since oil palm stone particles are larger and irregular in shape, a fixed bed of these particles contains several void spaces. The measured bulk density OPS-R is 595 kg/m³. Due to the grinding, a bed of OPS-C particles is packed more densely, which increases the bulk density. The ascertained value for OPS-C is 707 kg/m³. The determined particle density of both samples is similar, with 1375 kg/m³ for OPS-R and 1276 kg/m³ for OPS-C. During the ascertainment of the bulk and particle density, no mentionable problems arose.

Due to the larger mean particle diameter, both samples of oil palm stone particles are classified as “Geldart D particles” and the behavior of a bed of these particles, as it can be expected, could be observed during the fluidization experiments. Since the fluidization of the oil palm stone samples resulted in an erratic bubbling regime, a constant mixing of the particles was given. Further fluidization experiments were conducted to observe the fluidization behavior of the material in a bed of silica sand. The experiments showed that a bed of silica sand with a weight fraction of up to 10 % of OPS-R and OPS-C particles can be successfully fluidized.

By comparing the plotted fluidization curves found in the appendix (A3), it can be noted that the curves of the 3 % mixtures of both samples are nearly equal. The curves of 5 %, 7 % and 10 % mixtures of OPS-C are more regular than the curves of the OPS-R mixtures. Consequently, it can be inferred that a bed of silica sand that contains up to 10 % of oil palm stone particles can be successfully fluidized, while a grinding of the particles to smaller sizes improves the regularity of the bubbling regime.

The fifth investigated biomass type is poultry litter. It is the only biomass type available in a single physical state; in “as-received condition” (PL-R). Poultry litter is a very fragile material that disintegrates during the sieving procedure. Therefore, the particles are in a large size range between less than 45 and 4760 µm. As mentioned earlier, the calculated mean particle diameter of 258 is only representative of the sieved sample that had been used for the fluidization experiments but not for the poultry litter as it can be received from the agricultural producer.

Also, the determined bulk density is only valid for the sieved sample since smaller sized particles are packed more densely, which affects the bulk density. The ascertained value is 544 kg/m³. Since poultry litter is a porous material, it is taken into consideration that air or gas inclusions inside the particles are broken up within the sieving procedure, which influences the value of the particle density. The measure value is 1367 kg/m³.

According to Geldart classification, PL-R is classified as “Geldart B particles” and the creation of a bubbling regime can be expected and could be verified by the practical fluidization of a bed of PL-R. Fluidization tests with bed mixtures of silica sand and particles of poultry litter showed that a bed of silica sand can be successfully fluidized with a content of PL-R up to 10 %, while providing an excellent mixing behavior within a bubbling regime.

The sixth biomass type investigated is the rice husk, which is available in two physical states, namely “as-received condition” (RH-R) and “finely ground” (RH-F). RH-R particles are in a size range of 180 µm to 2360 µm and have a mean particle diameter of 1040 µm. Due to the grinding, RH-F particles include a larger fraction of small particles. The size range is between 53 µm and 2000 µm and the calculated mean particle diameter is 395 µm.

During the ascertainment of the bulk and particle density of the two rice husk samples, no mentionable problems arose. The determined value of RH-R particles is 154 kg/m³. The bulk density of the more densely packed RH-F particles is about twice as high, with a value of 292 kg/m³. The particle density of both samples is similar, with a value of 1092 kg/m³ for RH-R and 1277 kg/m³ for RH-F.

According to the ascertained mean particle diameter and the particle density, RH-R are classified as particles that are in transition between “Geldart B particles” and “Geldart D particles”, while RH-F are clearly classified as “Geldart B particles”. Therefore, the creation of a bubbling regime within a bed of both kinds of rice husk particles can be expected during fluidization. However, during experimentation, channels occurred and a fluidization of the entire bed of both rice husk samples was not given. Further fluidization tests with bed mixtures of silica sand and rice husk showed that the fluidization could be improved. In detail, bed mixtures with 3 % and 5 % of RH-R and RH-F particles fluidized well, while creating a bubbling regime that supports an even mixing of the particles. The experimentation with larger contents of rice husk particles resulted in channeling or in the segregation of the bed.

By comparing the fluidization curves, it can be seen that the development of the 3 % and 5 % curves of RH-F particles is more regular than the curves of RH-R bed mixtures. As a result, it can be asserted that a bed of silica sand can be successfully fluidized as long as the content of rice husk particles does not exceed 5 % of the total mass of the bed. Furthermore, it is noted that the process of grinding the rice husk particles, improves the mixing behavior.

The seventh biomass type that was available for investigation is sugar cane bagasse in two different physical states: coarsely ground (SCB-C) and “finely ground” (SCB-F). Even though the sugar cane bagasse also included clusters of particles, the motion of the sieve shaker was strong enough to separate the particles rapidly. SCB-C particles are in a size range between

300 µm and 3350 µm with a calculated mean particle diameter of 888 µm. The finely ground particles have sizes of 180 µm to 2000 µm and the mean particle diameter is 545 µm.

Due to the large variation of different formed particles, a fixed bed of sugar cane bagasse contains several void spaces. The measured bulk density of SCB-C is 75 kg/m³, while the value of the smaller and more densely packed SCB-F particles is 153 kg/m³. Sugar cane bagasse is a very light material with many pores. When the particles are ground, large pores are broken up with the result that finely ground particles have a lower content of air inclusions in relation to coarsely ground particles. Hence, the particle density of different sized particles of the same material can vary. The measured particle density of SCB-C is 579 kg/m³. The smaller SCB-F particles have a higher particle density with a value of 814 kg/m³.

Even though the mean particle diameter and the particle density varies between SCB-C and SCB-F particles, both samples are classified as "Geldart B particles". Since slugging occurred during the fluidization of both kinds of sugar cane bagasse, the expected behavior based on the Geldart classification could not be verified. The fluidization test of silica sand mixtures showed that SCB-C does not fluidize well. On the contrary, the mixtures with up to 7 % of SCB-F particles create a bubbling regime. Thus, it can be stated that only finely ground particles of sugar cane bagasse can be successfully fluidized, as long as the quantity of SCB-F particles does not exceed 7 % of the total mass of the bed.

The last investigated biomass type is sugar cane top, which is available in two physical states: "coarsely ground" (SCT-C) and "finely ground" (SCT-F). The SCT-C particles are in a large size range between 300 µm and 9500 µm and have a mean particle diameter of 912 µm. The finely ground particles are in a smaller size range between 180 µm and 2000 µm and the ascertained particle diameter of 623 µm is about 50 % smaller.

The sugar cane top samples, especially SCT-C, contain some particles that are larger than 10 cm. During the determination of the bulk density, these long particles were manually inserted into the graduated cylinder in order to measure the bulk density. Since this problem only concerned a very small fraction of particles (about 3 %), the influence on the results can be neglected. The ascertained bulk density for SCT-C is 109 kg/m³. Since the smaller particles of SCT-F are packed more densely the bulk density is higher. The measured value is 171 kg/m³. While measuring the particle density, it must be considered that sugar cane top particles contain,

similar to particles of sugar cane bagasse, large air inclusions, which results in different particle densities of differently ground particles. The measured particle density of SCT-C is 662 kg/m³, while the particle density of SCT-F particles is about 50 % higher. The determined value is 993 kg/m³.

According to the determined mean particle diameter and the low particle density, the samples of the sugar cane top are classified as “Geldart B particles”. Since slugging occurred during the fluidization tests of the beds of both kinds of sugar cane top, the expectation of an arising bubbling regime could not be fulfilled. Further fluidization experiments showed that SCT-C particles are not able to fluidize well in with a bed of silica sand either. During experimentation, jetting and the segregation of every bed mixture was observed. On the contrary, bed mixtures of silica sand with 3 % and 5 % of SCT-F particles fluidized well, while creating a bubbling regime that enables an even mixing of the particles inside the bed. Fluidization experiments with larger quantities of SCT-F particles resulted in slugging. In conclusion, it can be asserted that sugar cane top particles can be successfully fluidized in a bed of silica sand when the particles are ground into smaller sizes and when the content of sugar cane top particles does not exceed 5 % of the total mass of the bed.

6 Conclusion

In the present work, 15 different samples of eight residual biomass types from five different agricultural sectors of Colombia had been investigated. The aim was the experimental ascertainment of the physical and fluid dynamical properties of the biomass samples in order to assess the possibility of a thermochemical conversion within a CFB-reactor.

The evaluation of the experimental determined results has shown that the most suitable residual biomass types are oil palm stones and poultry litter. In a commonly used bed of silica sand with a mean particle diameter of 200 µm, mass fractions of up to 10 % of these types of biomass, fluidize well while displaying an excellent mixing behavior.

Coffee husk and rice husk particles could also be successfully fluidized in a bed of silica sand when smaller quantities of these biomass types, up to 5 % of the total weight, are used. Thereby, it could be shown that the process of grinding and the resulting reduction of the particle sizes improves the fluidization behavior of the biomass samples. The fluidization tests of oil palm fiber, sugar cane bagasse and sugar can top samples also indicated the improvement of fluidization due to the reduction of the particles since only finely ground samples resulted in an even fluidization while using beds with a biomass content between 5 % and 7 %. The only biomass type that could not be successfully fluidized was the oil palm rachis.

Within this thesis, the characteristic properties of the different biomass types, such as the particle size distribution, the mean particle diameter, the bulk and particle density and the moisture content, are ascertained and can be utilized for the design of a CFB-plant and the modelling of the thermochemical conversion process.

As it could be shown, the Geldart classification of particles is, only for some extent, able to provide reliable information about the fluidization behavior of the biomass samples studied here, due to a large variation in form and size of the particles. Therefore, further investigations will be carried out by the research group “BIOT” in order to determine the form factor of each biomass sample and to analyze its influence on the fluidization process.

7 References

[1] Kunii, D., Levenspiel, O., *Fluidization Engineering*, Butterworth-Heinemann, 1991, p. 10.

[2] Guío-Peréz, D.C., Rincón-Prat, S.L., Cáceres-Martínez, L.E., Tibocha-Guzmán, D.A., *Suitability Analysis of Residual Biomass in Colombia for Gasification in Fluidized Bed – Theoretical and Technical Energy Potential*, Universidad Nacional de Colombia, Bogotá D.C., Colombia, 2016.

[3] Wintgens, J.N., *Coffee: Growing, Processing, Sustainable Production*, Wiley-VCH, 2004, p. 4.

[4] Food and Agriculture Organization of the United States, *Modern Oil Palm Cultivation*, http://www.fao.org/docrep/006/t0309e/T0309E01.htm., 2017, March 3.

[5] Alexander, A.G., Food and Agriculture Organization of the United States, *Sugarcane as a Source of Biomass*, http://www.fao.org/docrep/003/s8850e/S8850E04.htm., 2017, March 16.

[6] Polato, N. Gramene: A Resource for Comparative Grass Genomics, *Introduction to Rice*, http://archive.gramene.org/species/oryza/rice_illustrations.html., 2017, March 22.

[7] Basu, P., *Combustion and Gasification in Fluidized Beds*, Taylor & Francis Group LLC, 2006, pp. 21-25.

[8] Stieß, M., *Mechanische Verfahrenstechnik 2*, Springer-Verlag, 1993, pp. 346-348.

[9] Kunii, D., Levenspiel, O., *Fluidization Engineering,* Butterworth-Heinemann, 1991, pp. 71-72.

[10] Kunii, D., Levenspiel, O., *Fluidization Engineering,* Butterworth-Heinemann, 1991, pp. 1-4.

[11] Basu, P., *Combustion and Gasification in Fluidized Beds*, Taylor & Francis Group LLC, 2006, pp. 25-29.

[12] Kunii, D., Levenspiel, O., *Fluidization Engineering,* Butterworth-Heinemann, 1991, pp. 223-224.

[13] Basu, P., *Combustion and Gasification in Fluidized Beds*, Taylor & Francis Group LLC, 2006, pp. 88-90.

[14] Grace, J.R., Avidan, A.A., Knowlton, T.M., *Circulating Fluidized Beds*, Blackie Academic & Professional, 1997, p. 215.

[15] Basu, P., *Combustion and Gasification in Fluidized Beds*, Taylor & Francis Group LLC, 2006, p. 197.

[16] Yang, W.C., *Handbook of Fluidization and Fluid-Particle Systems*, Taylor & Francis Group LLC, 2003, section 3.11.

[17] Stieß, M., *Mechanische Verfahrenstechnik 2*, Springer-Verlag, 1993, pp. 8-9.

[18] Grace, J.R., Avidan, A.A., Knowlton, T.M., *Circulating Fluidized Beds*, Blackie Academic & Professional, 1997, pp. 114-118.

[19] Grace, J.R., Avidan, A.A., Knowlton, T.M., *Circulating Fluidized Beds*, Blackie Academic & Professional, 1997, pp. 249-254.

[20] Kunii, D., Levenspiel, O., *Fluidization Engineering,* Butterworth-Heinemann, 1991, pp. 64-70.

[21] Kunii, D., Levenspiel, O., *Fluidization Engineering,* Butterworth-Heinemann, 1991, p. 89.

[22] Stieß, M., *Mechanische Verfahrenstechnik 1*, Springer-Verlag, 1991, pp. 91-92.

[23] Grzechnik, E., Pitch, H., Retsch GmbH & Co. KG, *The Basic Principles of Sieve Analysis*.

[24] Basu, P., *Combustion and Gasification in Fluidized Beds*, Taylor & Francis Group LLC, 2006, p. 422.

[25] Oka, S.N., *Fluidized Bed Combustion*, Marcel Dekker INC, 2004. p. 39.

[26] Gupta, S.V., *Practical Density Measurement and Hydrometry*, Institute of Physics Publishing, 2002, pp. 126-127.

[27] Lal, R., *Encyclopedia of Soil Science*, Taylor & Francis Group, 2006, p. 1243.

[28] Kunii, D., Levenspiel, O., *Fluidization Engineering,* Butterworth-Heinemann, 1991, pp. 77-79.

[29] Basu, P., *Combustion and Gasification in Fluidized Beds*, Taylor & Francis Group LLC, 2006, pp. 422-444.

[30] Norm, DIN 51718:2002:06, *Prüfung fester Brennstoffe - Bestimmung des Wassergehaltes und der Analysenfeuchtigkeit*.

[31] Norm, ASTM D 4442-07, *Standard Test Methods for Direct Moisture Content Measurement of Wood and Wood-Base Materials*.

[32] Norm, ASTM D2854-09, *Standard Test Method for Apparent Density of Activated Carbon*.

[33] Norm, UNE-EN 993-1, *Métodos de ensayo para productos refractarios conformados densos – Parte 1: Determinación de la densidad aparente, de la porosidad abierta y de la porosidad total*.

[34] Kunii, D., Levenspiel, O., *Fluidization Engineering,* Butterworth-Heinemann, 1991, p. 324.

8 Appendix

A.1 Particle Size Distribution

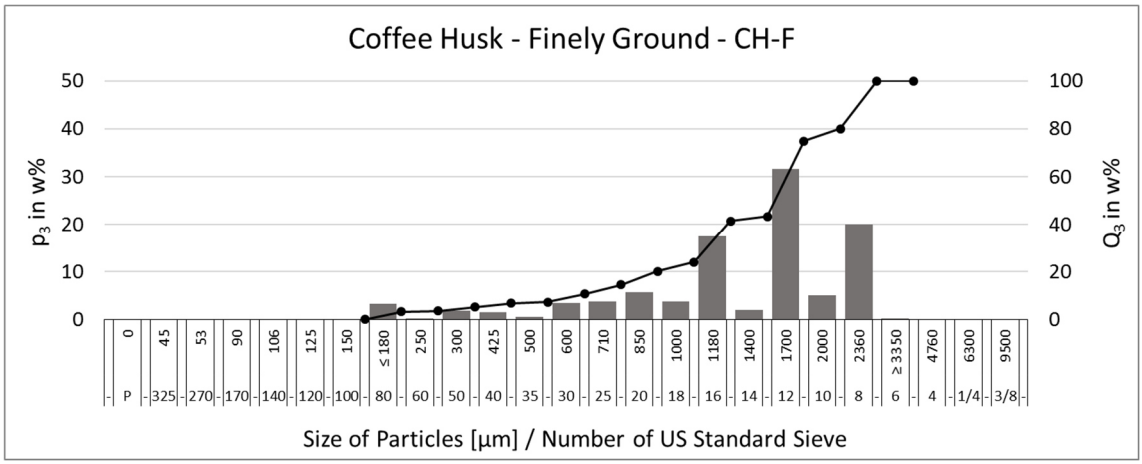

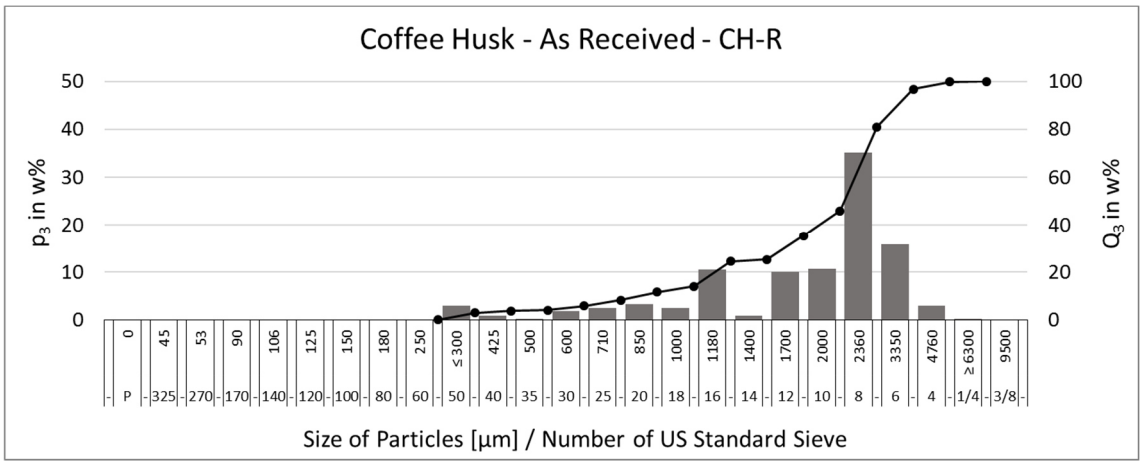

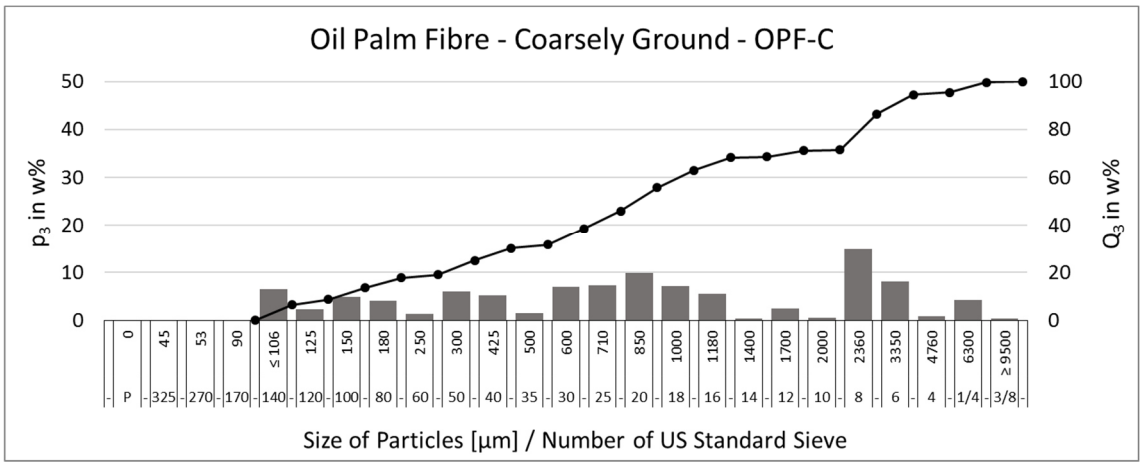

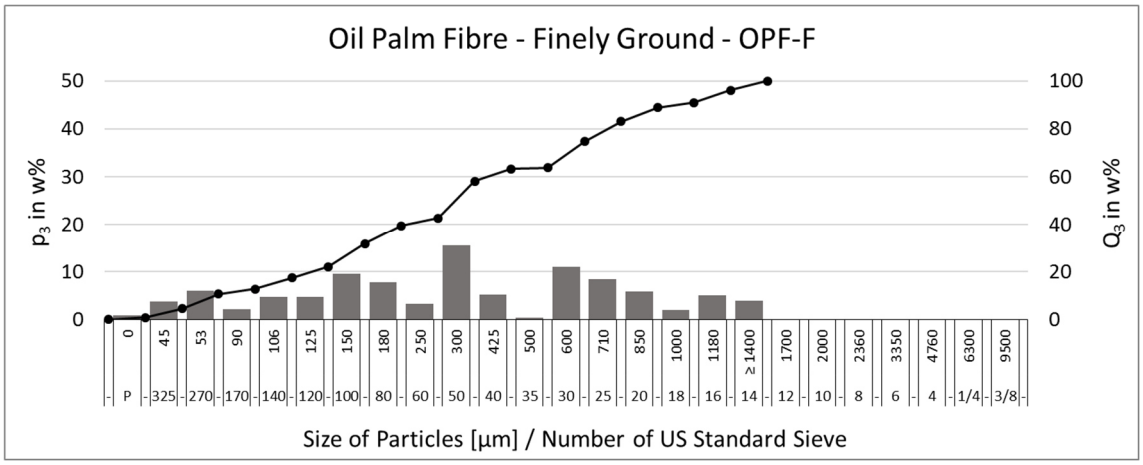
Oil Palm Fibre - Finely Ground - OPF-F
p3 in w%
Q3 in w%
0 10 20 30 40 50
0 20 40 60 80 100
0 P 45 325 53 270 90 170 106 140 125 120 150 100 180 80 250 60 300 50 425 40 500 35 600 30 710 25 850 20 1000 18 1180 16 ≥ 1400 14 1700 12 2000 10 2360 8 3350 6 4760 4 6300 1/4 9500 3/8
Size of Particles [µm] / Number of US Standard Sieve

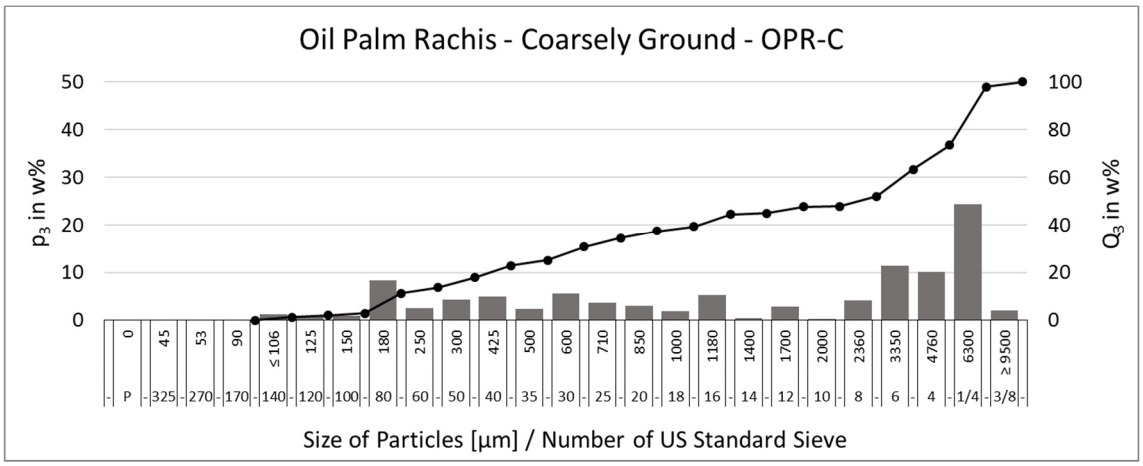
Oil Palm Rachis - Coarsely Ground - OPR-C
p3 in w%
Q3 in w%
0 10 20 30 40 50
0 20 40 60 80 100
0 P 45 325 53 270 90 170 ≤ 106 140 125 120 150 100 180 80 250 60 300 50 425 40 500 35 600 30 710 25 850 20 1000 18 1180 16 1400 14 1700 12 2000 10 2360 8 3350 6 4760 4 6300 1/4 ≥ 9500 3/8
Size of Particles [µm] / Number of US Standard Sieve

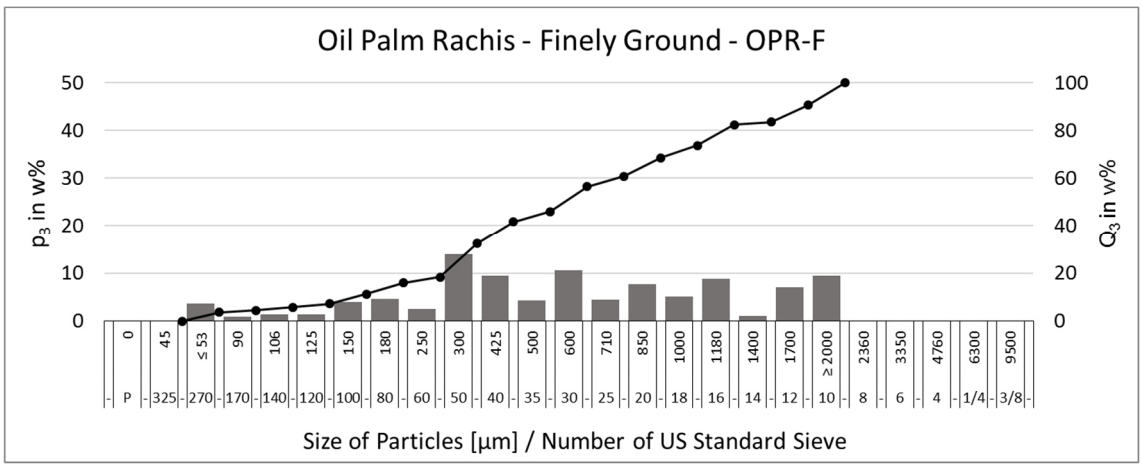
Oil Palm Rachis - Finely Ground - OPR-F
p3 in w%
Q3 in w%
0 10 20 30 40 50
0 20 40 60 80 100
0 P 45 325 ≤ 53 270 90 170 106 140 125 120 150 100 180 80 250 60 300 50 425 40 500 35 600 30 710 25 850 20 1000 18 1180 16 1400 14 1700 12 ≥ 2000 10 2360 8 3350 6 4760 4 6300 1/4 9500 3/8
Size of Particles [µm] / Number of US Standard Sieve

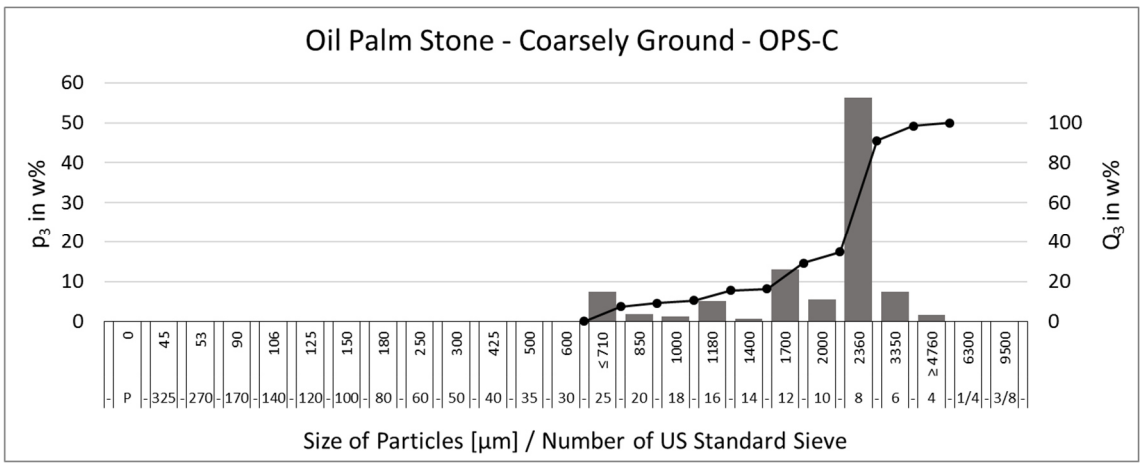
Oil Palm Stone - Coarsely Ground - OPS-C
p3 in w%
Q3 in w%
0 10 20 30 40 50 60
0 20 40 60 80 100
0 P 45 325 53 270 90 170 106 140 125 120 150 100 180 80 250 60 300 50 425 40 500 35 600 30 ≤ 710 25 850 20 1000 18 1180 16 1400 14 1700 12 2000 10 2360 8 3350 6 ≥ 4760 4 6300 1/4 9500 3/8
Size of Particles [µm] / Number of US Standard Sieve

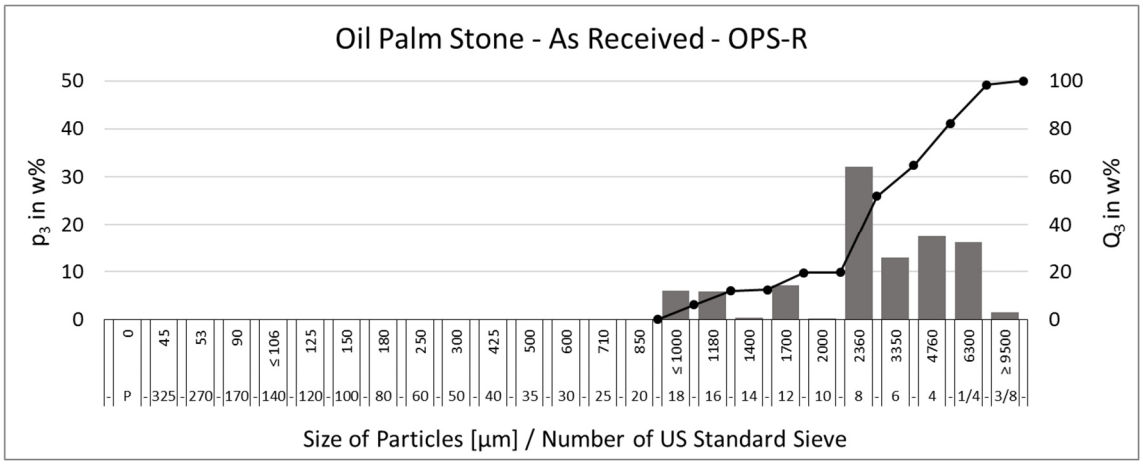
Oil Palm Stone - As Received - OPS-R
p3 in w%
Q3 in w%
Size of Particles [µm] / Number of US Standard Sieve

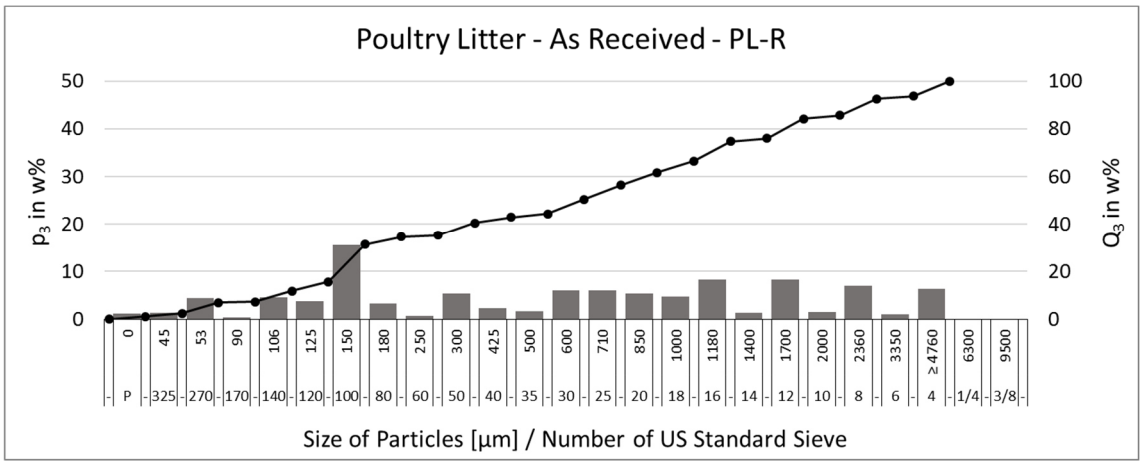
Poultry Litter - As Received - PL-R
p3 in w%
Q3 in w%
Size of Particles [µm] / Number of US Standard Sieve

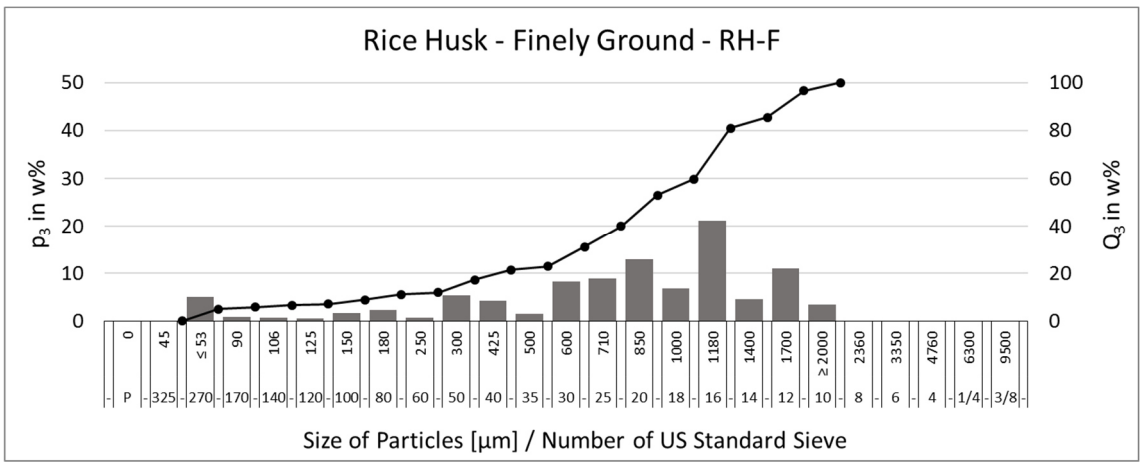
Rice Husk - Finely Ground - RH-F
p3 in w%
Q3 in w%
Size of Particles [µm] / Number of US Standard Sieve

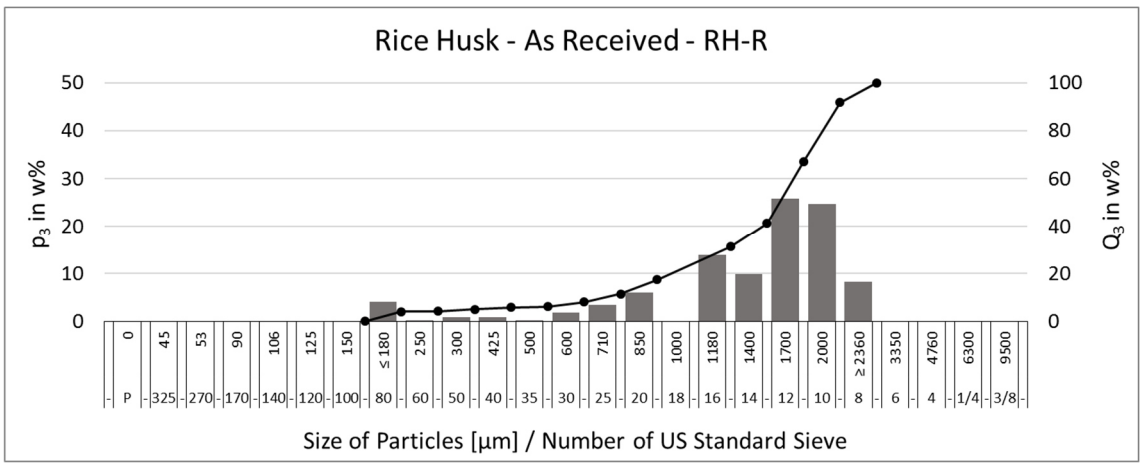
Rice Husk - As Received - RH-R
p3 in w%
Q3 in w%
Size of Particles [µm] / Number of US Standard Sieve

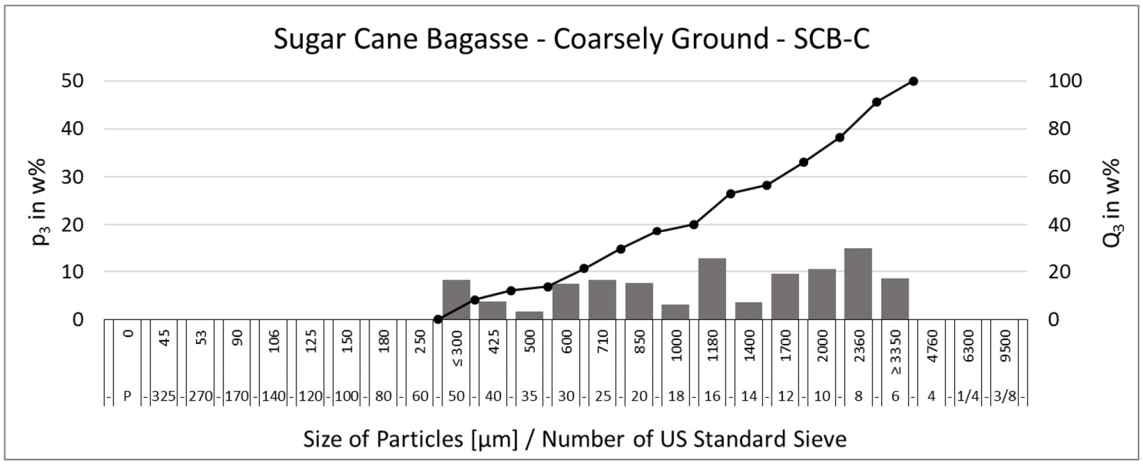
Sugar Cane Bagasse - Coarsely Ground - SCB-C
p3 in w%
Q3 in w%
0 10 20 30 40 50
0 20 40 60 80 100
0 45 53 90 106 125 150 180 250 ≤ 300 425 500 600 710 850 1000 1180 1400 1700 2000 2360 ≥ 3350 4760 6300 9500
- P - 325 - 270 - 170 - 140 - 120 - 100 - 80 - 60 - 50 - 40 - 35 - 30 - 25 - 20 - 18 - 16 - 14 - 12 - 10 - 8 - 6 - 4 - 1/4 - 3/8 -
Size of Particles [µm] / Number of US Standard Sieve

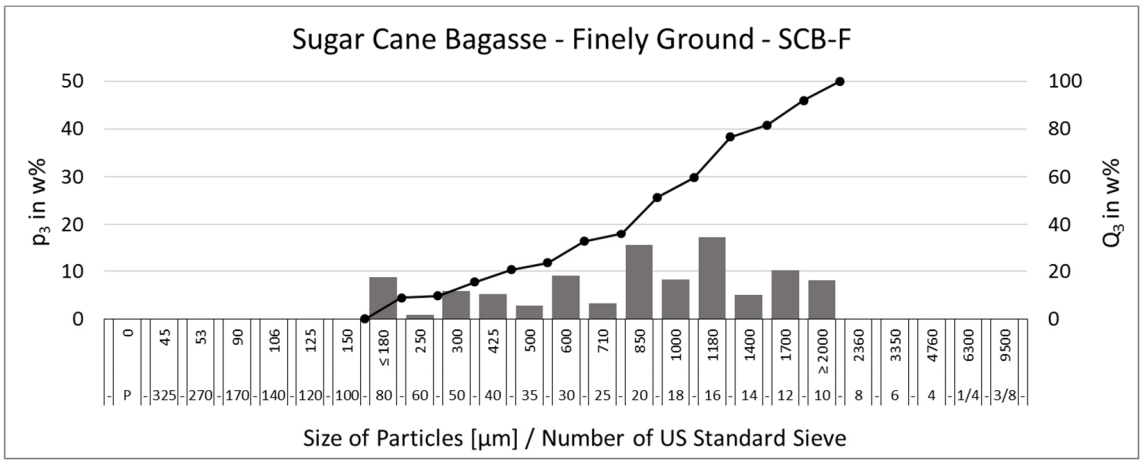
Sugar Cane Bagasse - Finely Ground - SCB-F
p3 in w%
Q3 in w%
0 10 20 30 40 50
0 20 40 60 80 100
0 45 53 90 106 125 150 ≤ 180 250 300 425 500 600 710 850 1000 1180 1400 1700 ≥ 2000 2360 3350 4760 6300 9500
- P - 325 - 270 - 170 - 140 - 120 - 100 - 80 - 60 - 50 - 40 - 35 - 30 - 25 - 20 - 18 - 16 - 14 - 12 - 10 - 8 - 6 - 4 - 1/4 - 3/8 -
Size of Particles [µm] / Number of US Standard Sieve

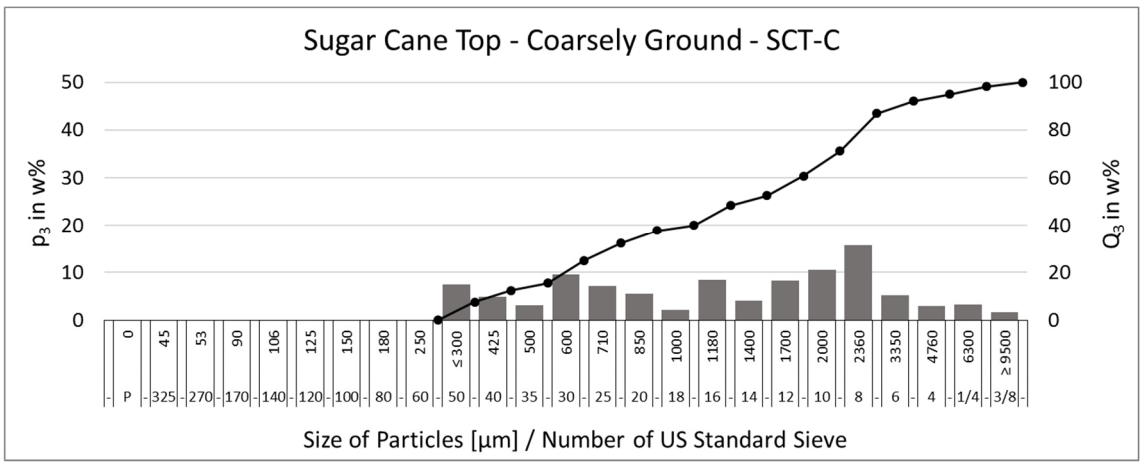
Sugar Cane Top - Coarsely Ground - SCT-C
p3 in w%
Q3 in w%
0 10 20 30 40 50
0 20 40 60 80 100
0 45 53 90 106 125 150 180 250 ≤ 300 425 500 600 710 850 1000 1180 1400 1700 2000 2360 3350 4760 6300 ≥ 9500
- P - 325 - 270 - 170 - 140 - 120 - 100 - 80 - 60 - 50 - 40 - 35 - 30 - 25 - 20 - 18 - 16 - 14 - 12 - 10 - 8 - 6 - 4 - 1/4 - 3/8 -
Size of Particles [µm] / Number of US Standard Sieve

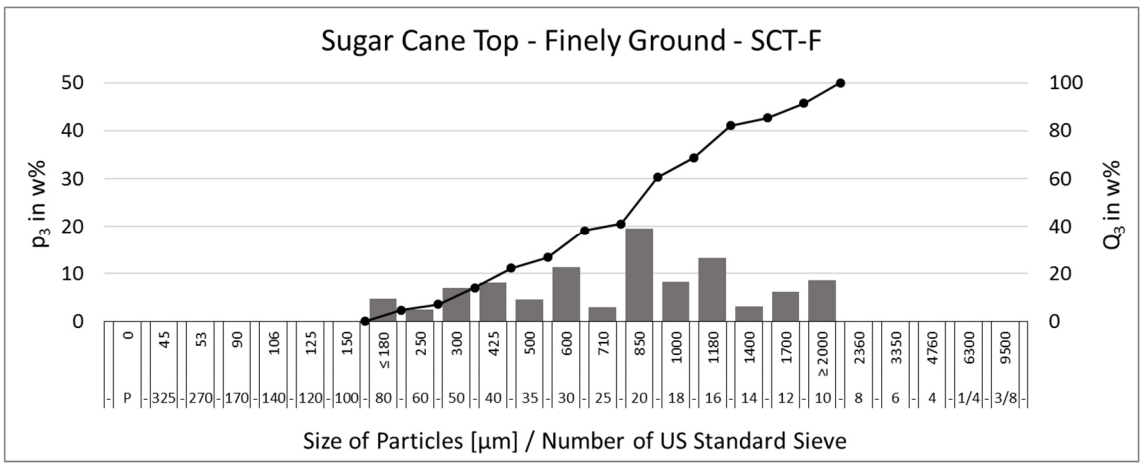
Sugar Cane Top - Finely Ground - SCT-F
p3 in w%
Q3 in w%
0 10 20 30 40 50
0 20 40 60 80 100
0 45 53 90 106 125 150 ≤ 180 250 300 425 500 600 710 850 1000 1180 1400 1700 ≥ 2000 2360 3350 4760 6300 9500
- P - 325 - 270 - 170 - 140 - 120 - 100 - 80 - 60 - 50 - 40 - 35 - 30 - 25 - 20 - 18 - 16 - 14 - 12 - 10 - 8 - 6 - 4 - 1/4 - 3/8 -
Size of Particles [µm] / Number of US Standard Sieve

A.2 Fluidization Curves of Biomass Samples

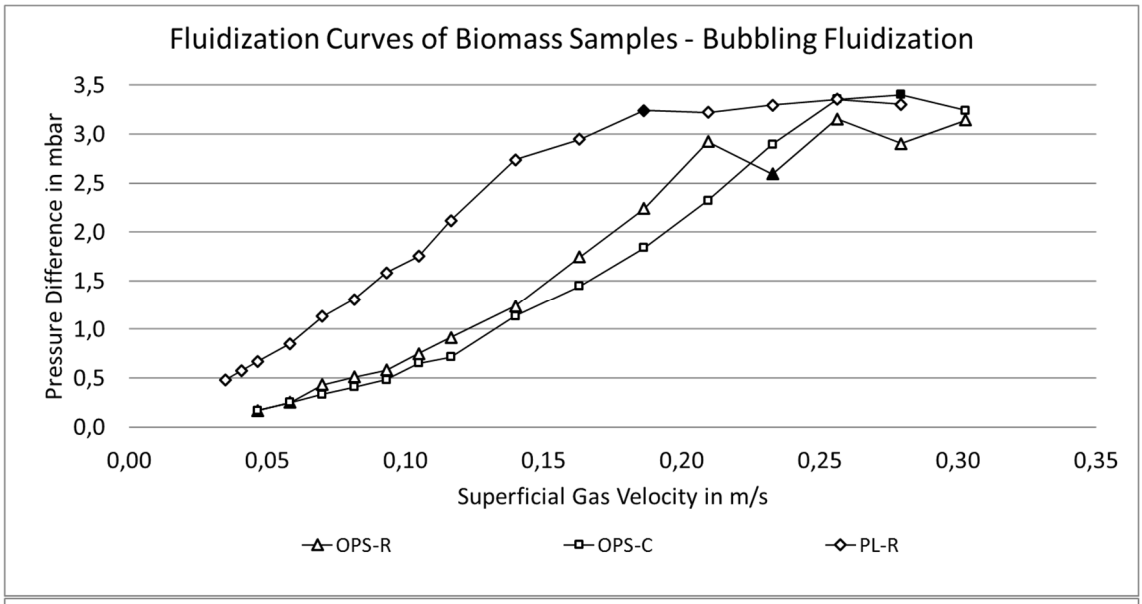

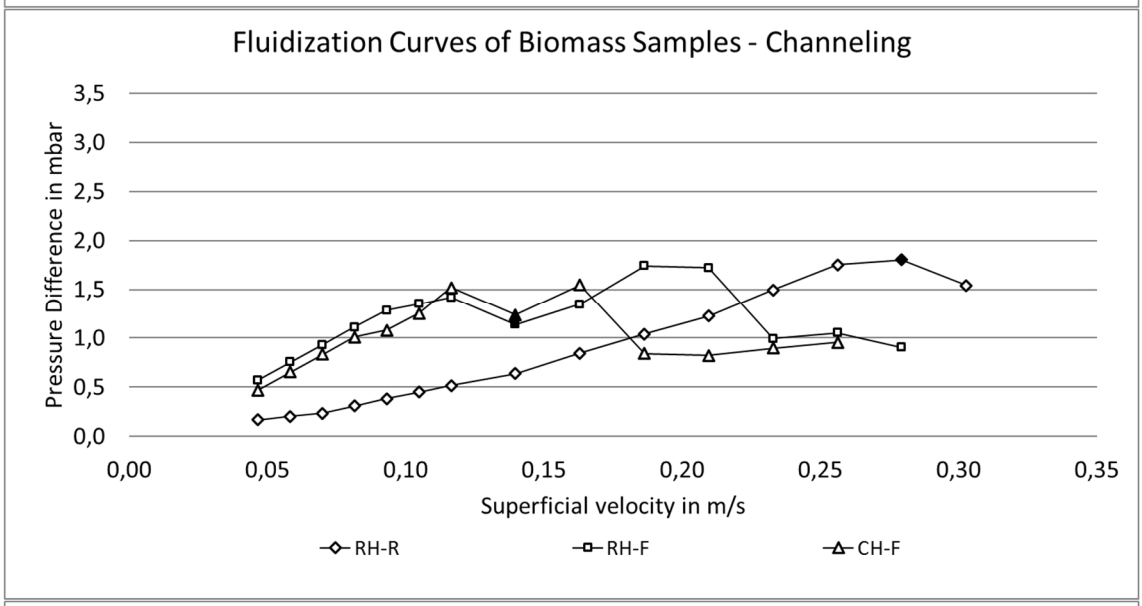

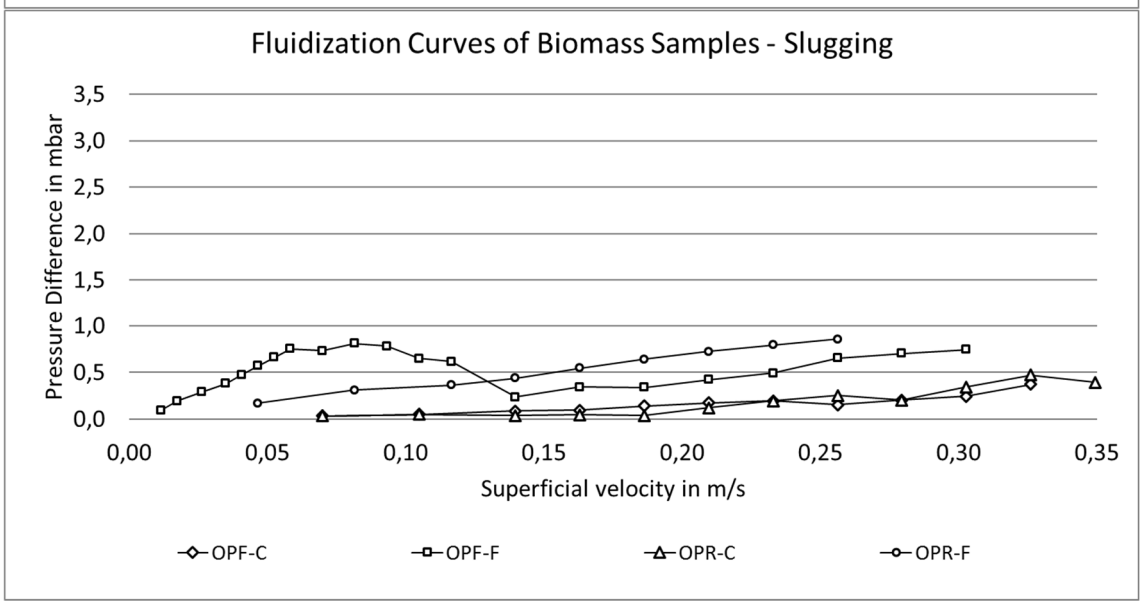

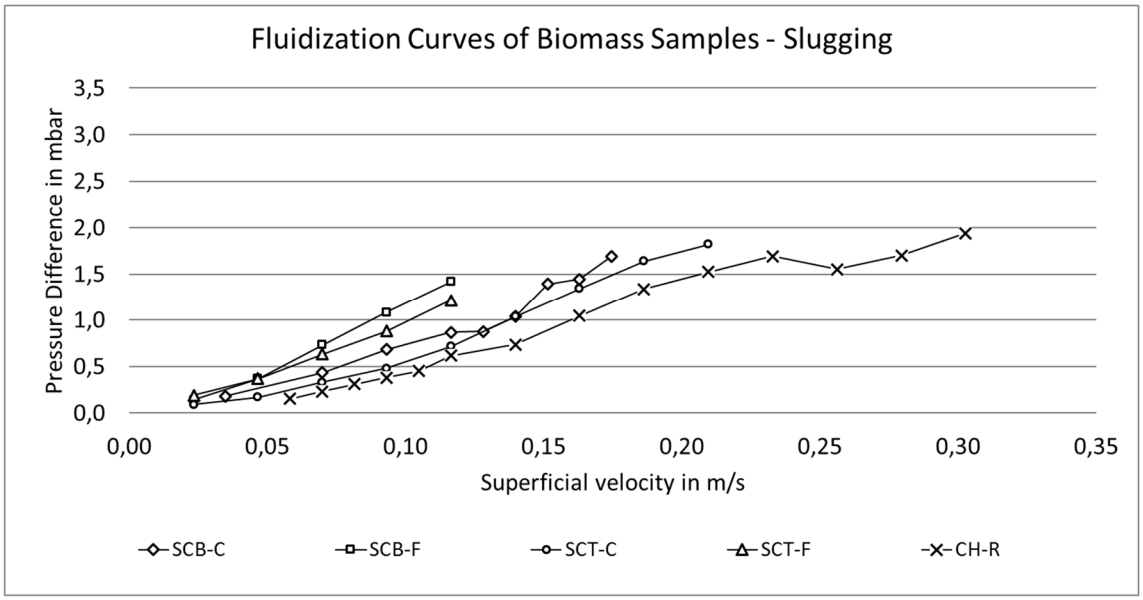
Fluidization Curves of Biomass Samples - Slugging
Pressure Difference in mbar
3,5
3,0
2,5
2,0
1,5
1,0
0,5
0,0
0,00
0,05
0,10
0,15
0,20
0,25
0,30
0,35
Superficial velocity in m/s
SCB-C
SCB-F
SCT-C
SCT-F
CH-R

A.3 Fluidization Curves of Mixtures of Bed Material and Biomass Particles

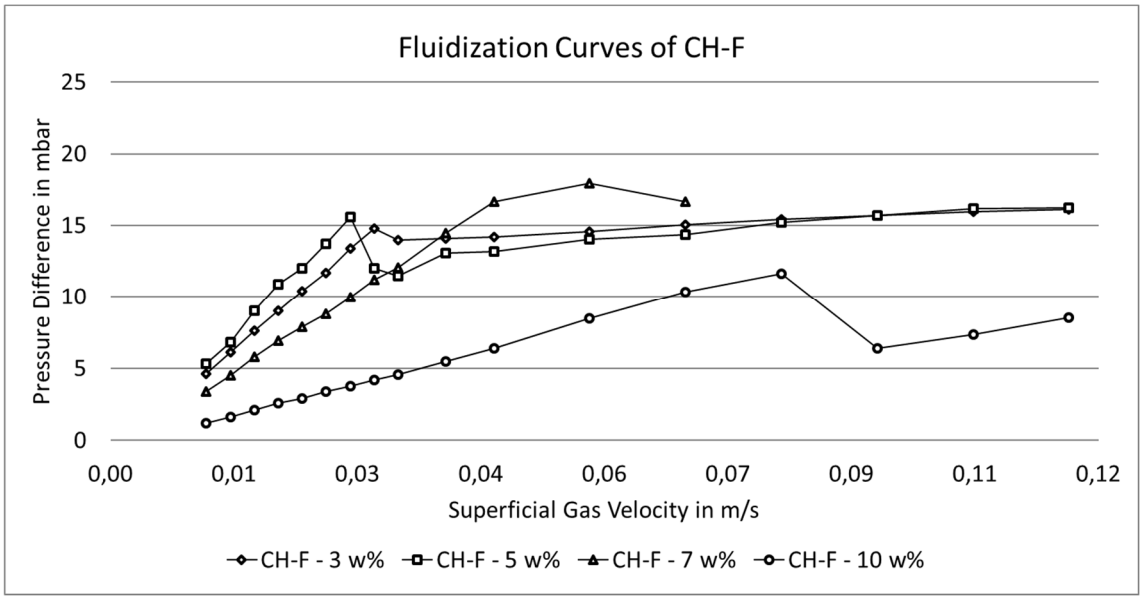

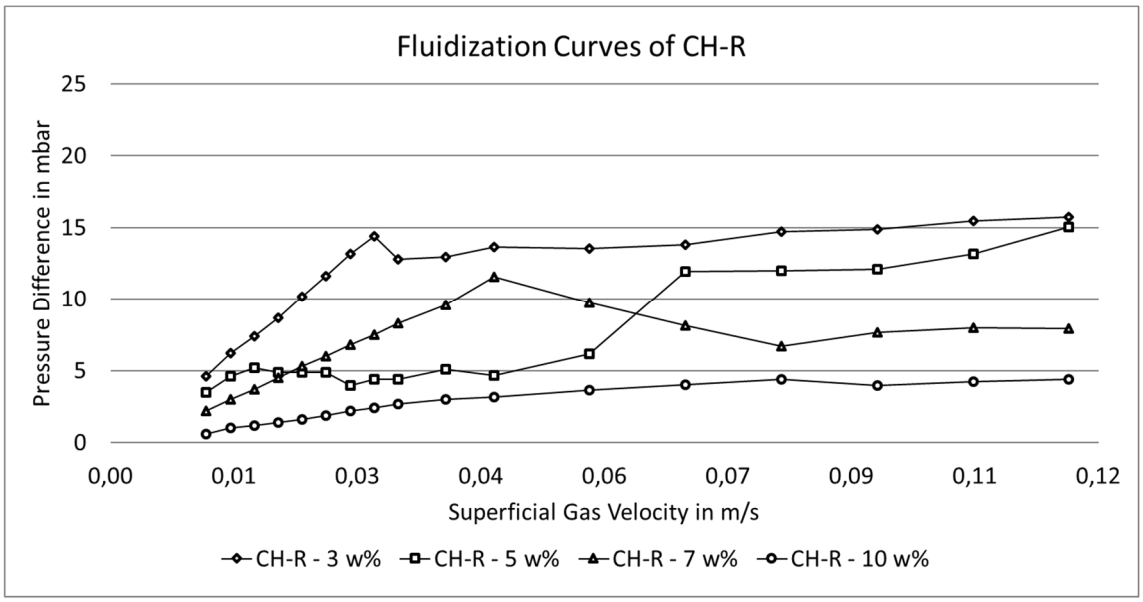

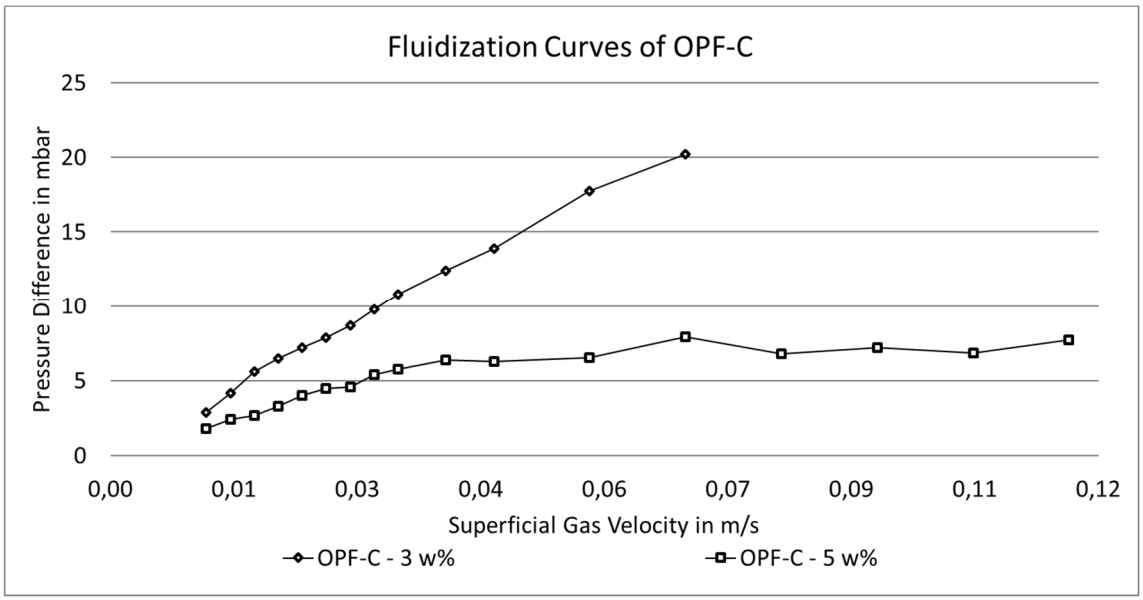

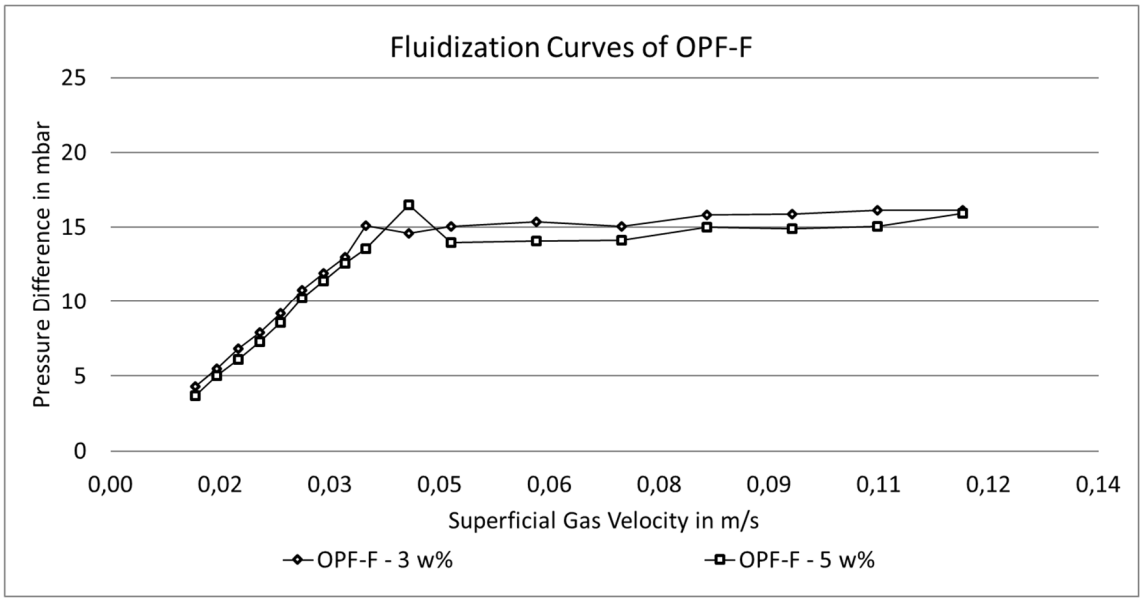
Fluidization Curves of OPF-F
Pressure Difference in mbar
25
20
15
10
5
0
0,00
0,02
0,03
0,05
0,06
0,08
0,09
0,11
0,12
0,14
Superficial Gas Velocity in m/s
OPF-F - 3 w%
OPF-F - 5 w%

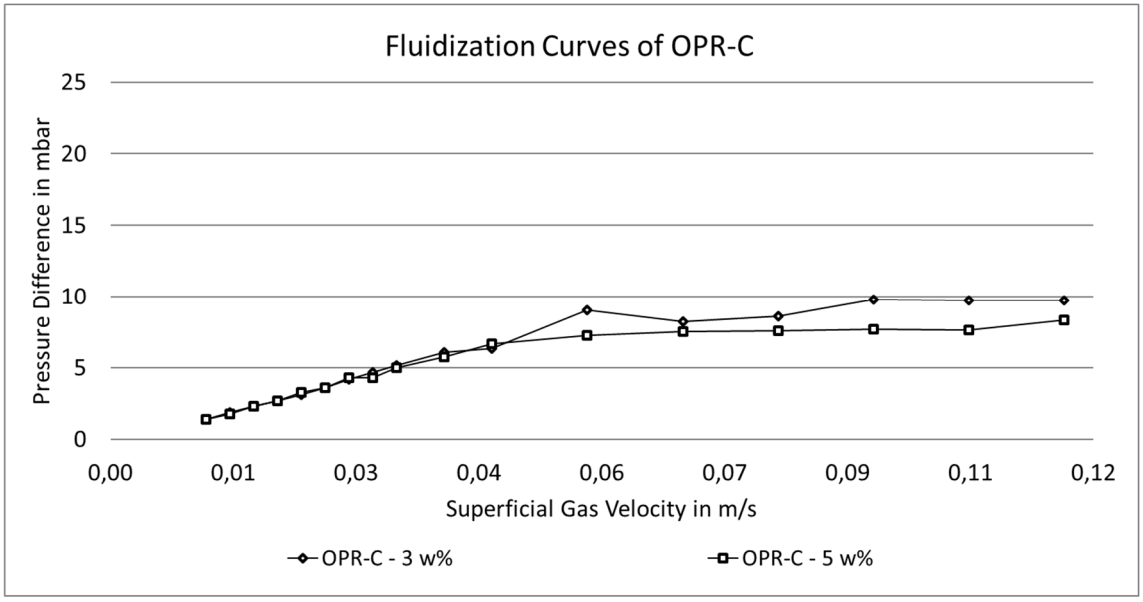
Fluidization Curves of OPR-C
Pressure Difference in mbar
25
20
15
10
5
0
0,00
0,01
0,03
0,04
0,06
0,07
0,09
0,11
0,12
Superficial Gas Velocity in m/s
OPR-C - 3 w%
OPR-C - 5 w%

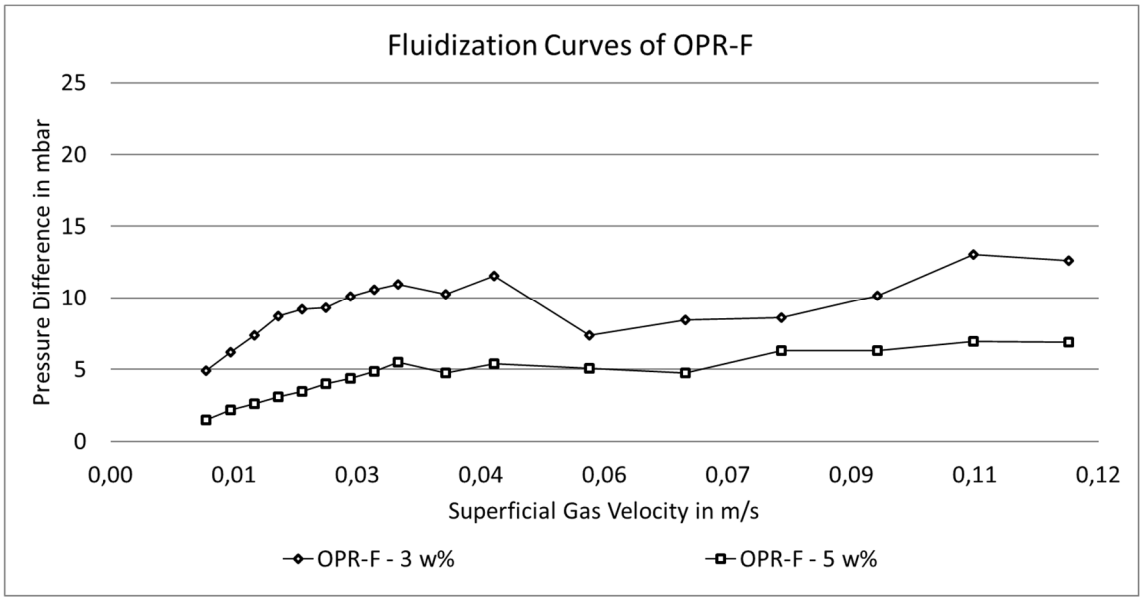
Fluidization Curves of OPR-F
Pressure Difference in mbar
25
20
15
10
5
0
0,00
0,01
0,03
0,04
0,06
0,07
0,09
0,11
0,12
Superficial Gas Velocity in m/s
OPR-F - 3 w%
OPR-F - 5 w%

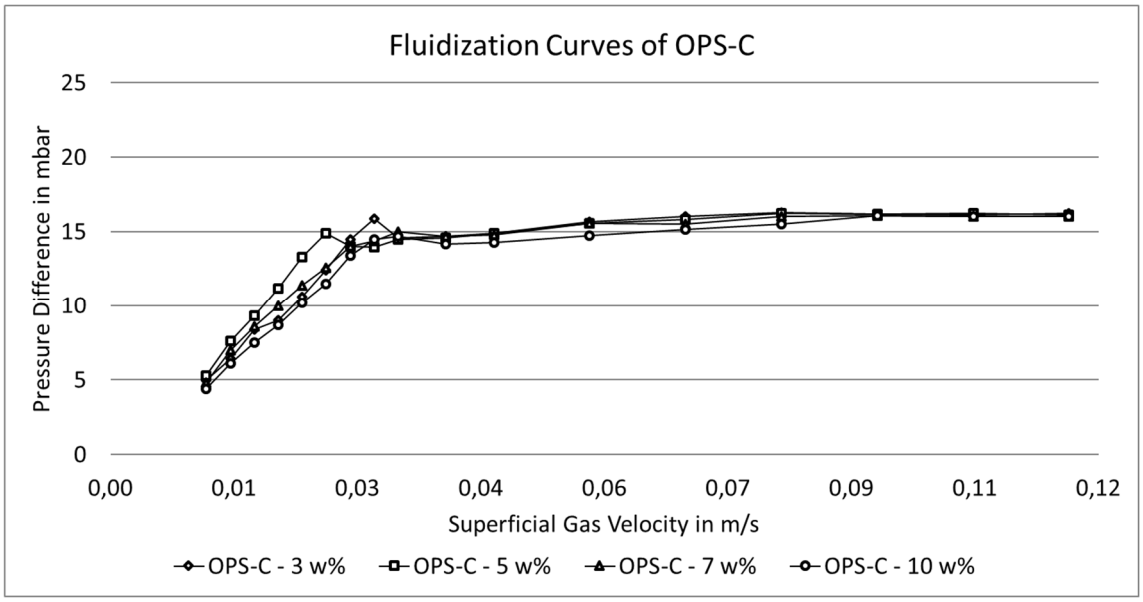
Fluidization Curves of OPS-C
Pressure Difference in mbar
25
20
15
10
5
0
0,00
0,01
0,03
0,04
0,06
0,07
0,09
0,11
0,12
Superficial Gas Velocity in m/s
OPS-C - 3 w%
OPS-C - 5 w%
OPS-C - 7 w%
OPS-C - 10 w%

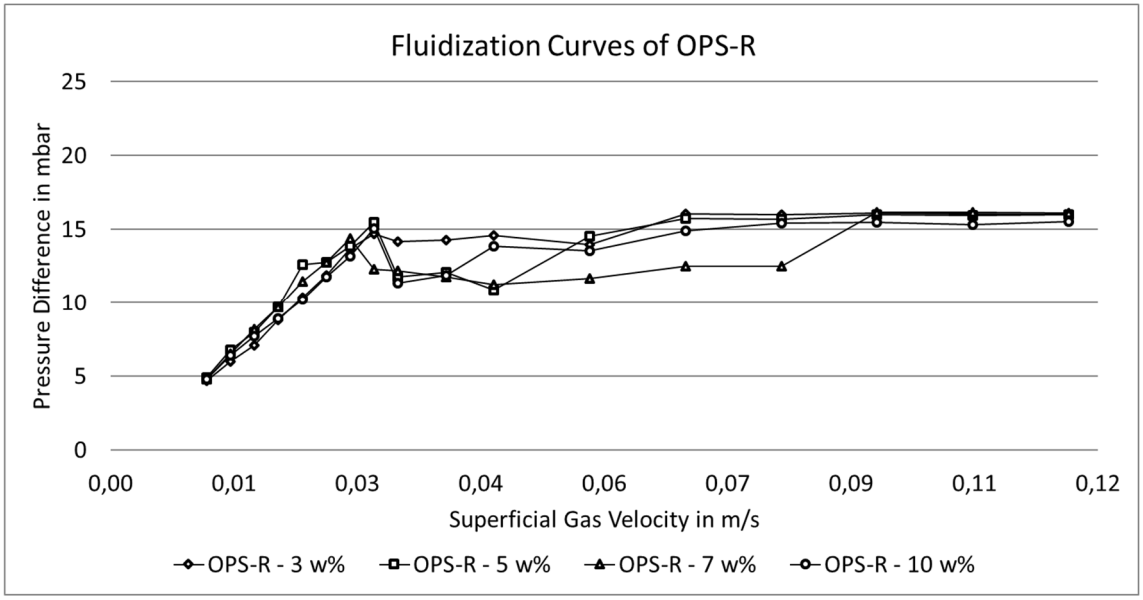
Fluidization Curves of OPS-R
Pressure Difference in mbar
25
20
15
10
5
0
0,00
0,01
0,03
0,04
0,06
0,07
0,09
0,11
0,12
Superficial Gas Velocity in m/s
OPS-R - 3 w%
OPS-R - 5 w%
OPS-R - 7 w%
OPS-R - 10 w%

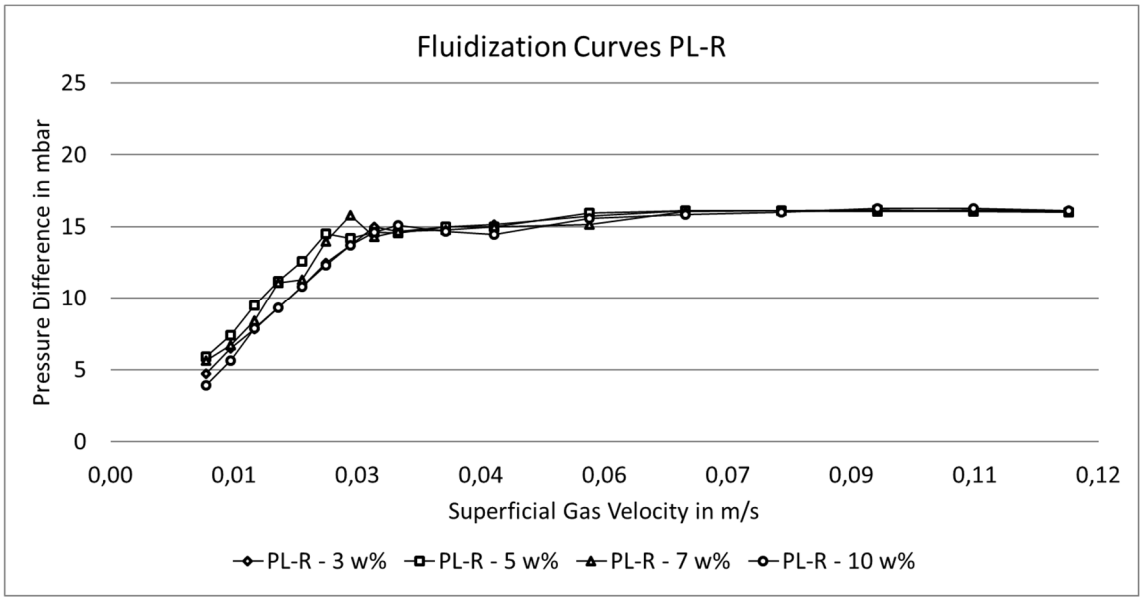
Fluidization Curves PL-R
Pressure Difference in mbar
25
20
15
10
5
0
0,00
0,01
0,03
0,04
0,06
0,07
0,09
0,11
0,12
Superficial Gas Velocity in m/s
PL-R - 3 w%
PL-R - 5 w%
PL-R - 7 w%
PL-R - 10 w%

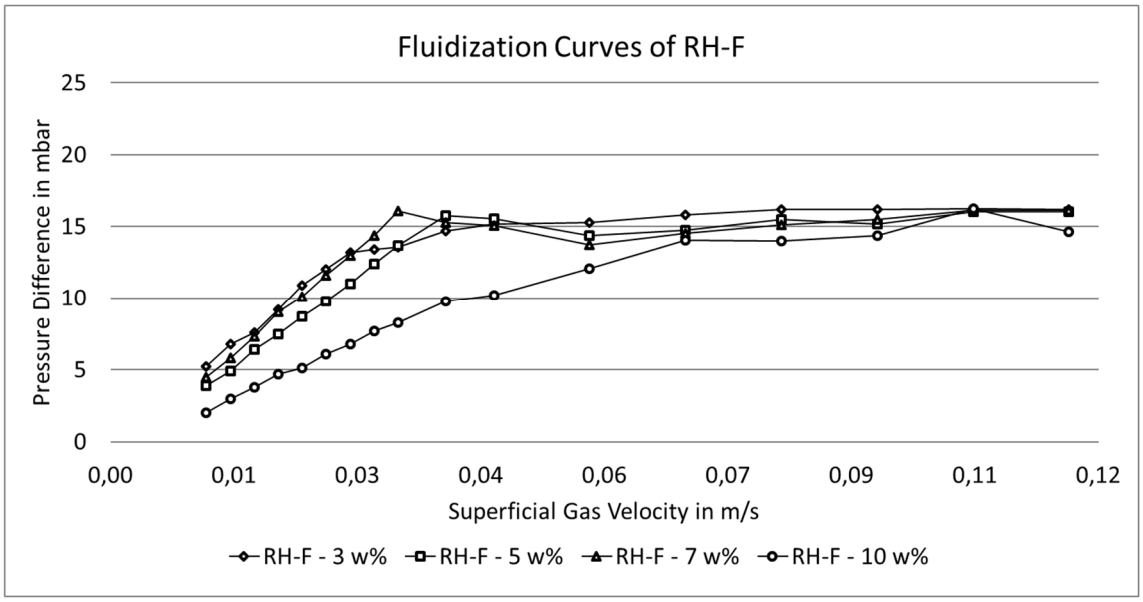
Fluidization Curves of RH-F
Pressure Difference in mbar
25
20
15
10
5
0
0,00
0,01
0,03
0,04
0,06
0,07
0,09
0,11
0,12
Superficial Gas Velocity in m/s
RH-F - 3 w%
RH-F - 5 w%
RH-F - 7 w%
RH-F - 10 w%

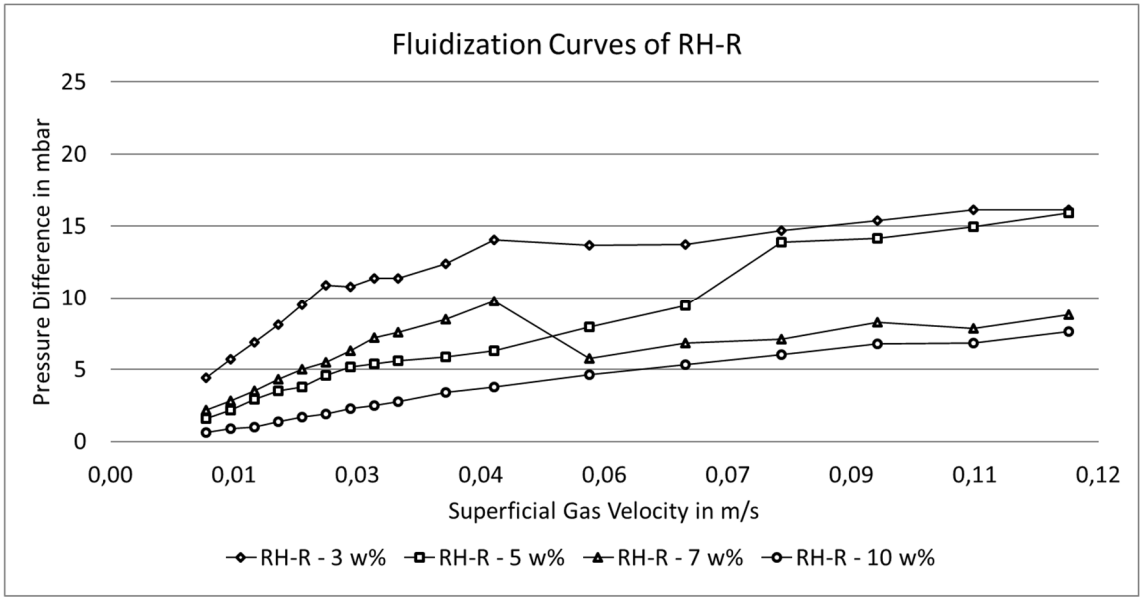
Fluidization Curves of RH-R
Pressure Difference in mbar
25
20
15
10
5
0
0,00
0,01
0,03
0,04
0,06
0,07
0,09
0,11
0,12
Superficial Gas Velocity in m/s
RH-R - 3 w%
RH-R - 5 w%
RH-R - 7 w%
RH-R - 10 w%

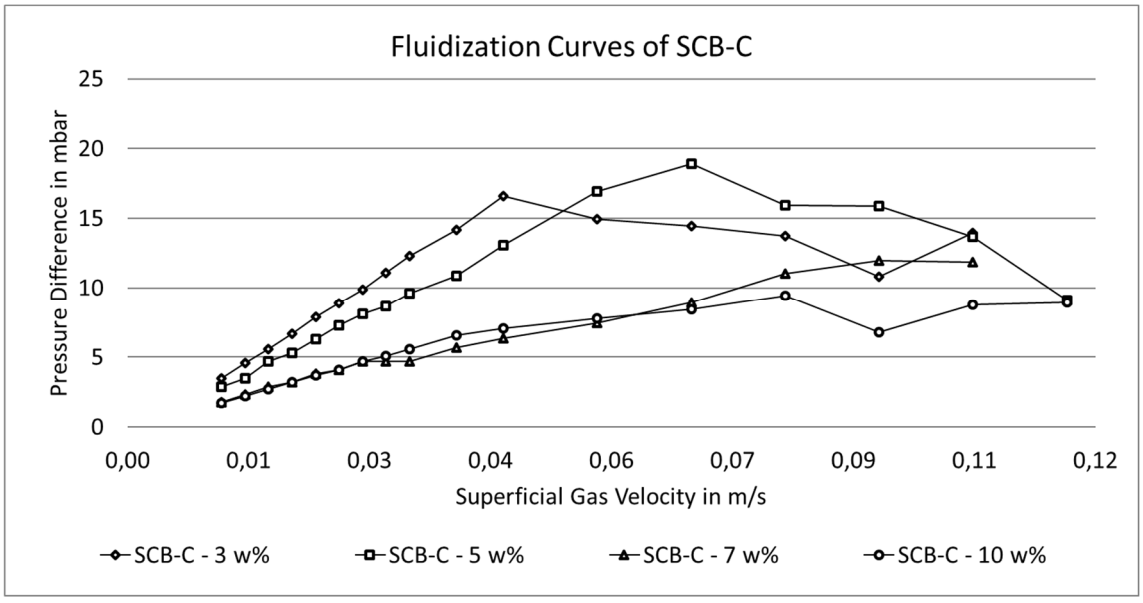
Fluidization Curves of SCB-C
Pressure Difference in mbar
25
20
15
10
5
0
0,00
0,01
0,03
0,04
0,06
0,07
0,09
0,11
0,12
Superficial Gas Velocity in m/s
SCB-C - 3 w%
SCB-C - 5 w%
SCB-C - 7 w%
SCB-C - 10 w%

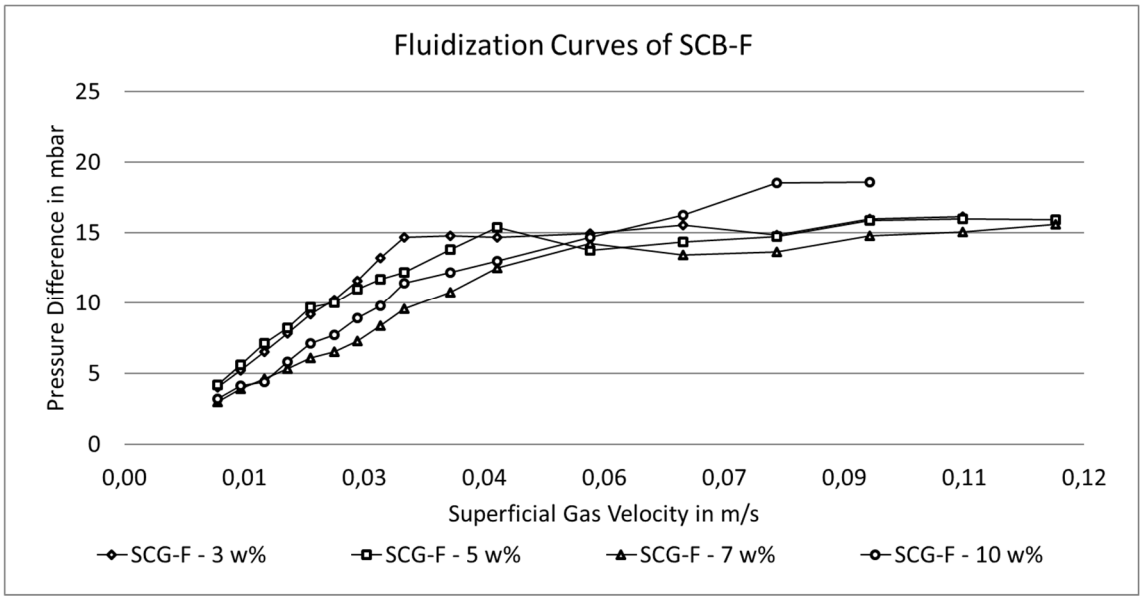
Fluidization Curves of SCB-F
Pressure Difference in mbar
25
20
15
10
5
0
0,00
0,01
0,03
0,04
0,06
0,07
0,09
0,11
0,12
Superficial Gas Velocity in m/s
SCG-F - 3 w%
SCG-F - 5 w%
SCG-F - 7 w%
SCG-F - 10 w%

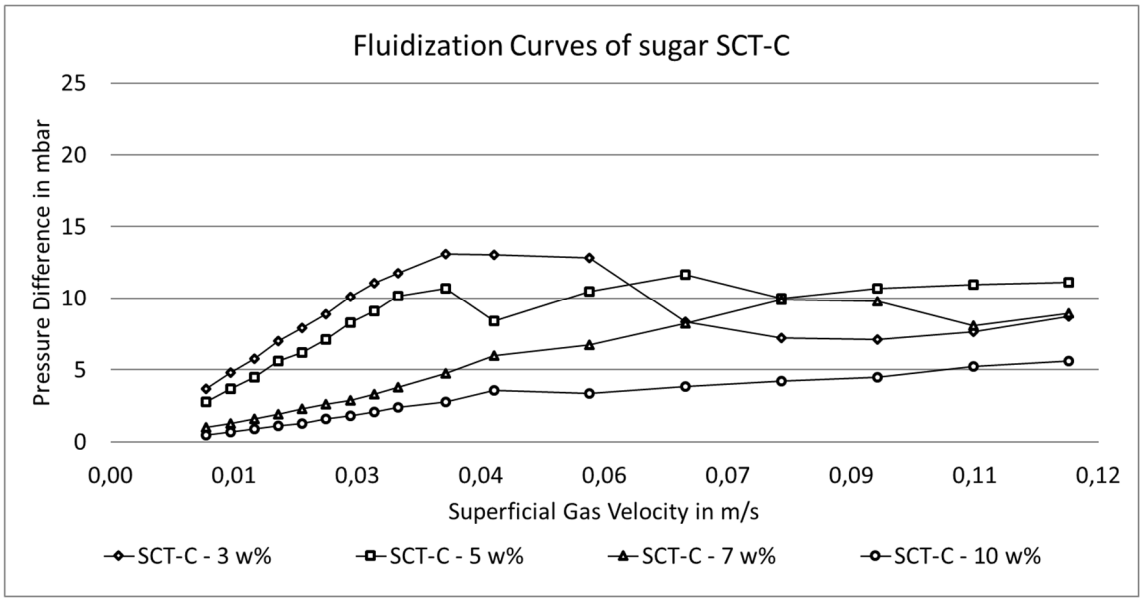
Fluidization Curves of sugar SCT-C
Pressure Difference in mbar
25
20
15
10
5
0
0,00
0,01
0,03
0,04
0,06
0,07
0,09
0,11
0,12
Superficial Gas Velocity in m/s
SCT-C - 3 w%
SCT-C - 5 w%
SCT-C - 7 w%
SCT-C - 10 w%

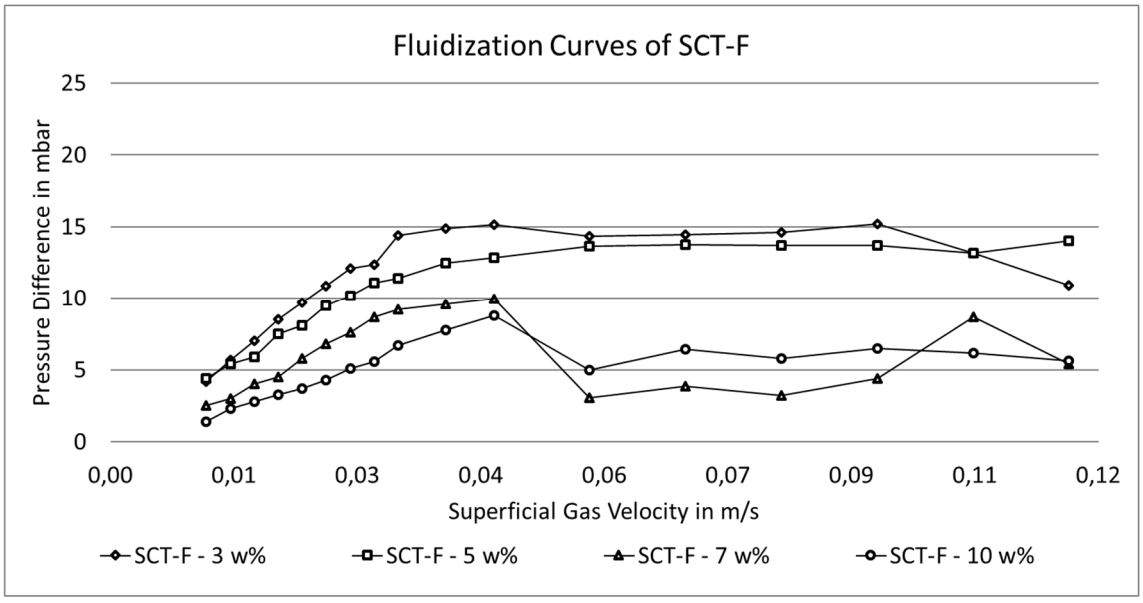
Fluidization Curves of SCT-F
Pressure Difference in mbar
25
20
15
10
5
0
0,00
0,01
0,03
0,04
0,06
0,07
0,09
0,11
0,12
Superficial Gas Velocity in m/s
SCT-F - 3 w%
SCT-F - 5 w%
SCT-F - 7 w%
SCT-F - 10 w%